CONTROL AND PERFORMANCE ANALYSIS OF RES BASED MICROGRID

Thesis submitted to
DELHI TECHNOLOGICAL UNIVERSITY

FOR
THE AWARD OF THE DEGREE OF
DOCTOR OF PHILOSOPHY

by

AVDHESH KUMAR
(2K17/Ph.D./EE/04)

Under the Supervision of

Prof. Rachana Garg and Prof. Priya Mahajan
Department of Electrical Engineering
Delhi Technological University
Delhi-110042

DEPARTMENT OF ELECTRICAL ENGINEERING
DELHI TECHNOLOGICAL UNIVERSITY
DELHI-110042

NOVEMBER 2023

DECLARATION

This is to certify that the thesis titled **"Control and Performance Analysis of RES Based Microgrid"** was carried out by Mr. Avdhesh Kumar under the supervision of Prof. Rachana Garg and Prof. Priya Mahajan, Delhi Technological University, Delhi, India.

The interpretations put forth are based on my reading and understanding of the original texts and they are not published anywhere in the form of books, monographs or articles. The other books, articles and websites, which I have referred are acknowledged at the respective place in the text.

For the present thesis, which I am submitting to the university, no degree or diploma has been conferred on me before, either in this or in any other university.

Date: 09/11/2023
Place: New Delhi

Mr. Avdhesh Kumar
2K17/Ph.D./EE/04
Department of Electrical Engineering
Delhi Technological University
Shahbad Daulatpur, Delhi-110042, India

CERTIFICATE

This is to certify that the thesis titled **"Control and Performance Analysis of RES Based Microgrid"** submitted for the award of the Doctor of Philosophy is original to the best of our knowledge. The work was carried out by Mr. Avdhesh Kumar under our guidance and has not been submitted in parts or full to this or any other University for the award of any degree or diploma. All the assistance and help received during the course of study have been duly acknowledged.

Prof. Rachana Garg
Department of Electrical Engineering
Delhi Technological University
Shahbad Daulatpur, Delhi-110042, India

Prof. Priya Mahajan
Department of Electrical Engineering
Delhi Technological University
Shahbad Daulatpur, Delhi-110042, India

ACKNOWLEDGEMENT

Writing this thesis has been fascinating and extremely rewarding. First of all, I am thankful to God, who has blessed me strength and support throughout my life and always provides me with a path to acquire knowledge and learning.

I would like to express my sincere gratitude to my supervisors, **Prof. Rachana Garg** and **Prof. Priya Mahajan**, for all their help, guidance, valuable suggestions, explanation, advices and above all, their support for carrying out this thesis work. Throughout my thesis-writing period, they were highly supportive and encouraging.

I would like to express my deepest thanks to **Prof. Uma Nangia** (DRC Chairman), **Prof. Rachana Garg**, HOD (Electrical Engineering), and **Prof. Rinku Sharma**, Dean (Academic-PG), Delhi Technological University (formerly Delhi College of Engineering) for their immense support and valuable guidance during the entire work of this thesis.

I extend my gratitude to **Prof. Jai Prakash Saini** (Vice-Chancellor) for his co-operation and support for providing a supportive environment to complete my research at Delhi Technological University. My sincere thanks and deep gratitude are to **Prof. Madhusudan Singh**, (Registrar, Delhi Technological University) for his consistent support during my research work.

I would like to express my deepest thanks to **Prof. Prerna Gaur and all SRC members**, for their immense support and valuable guidance during the entire work of this thesis.

Sincere thanks to Delhi Technological University authorities for providing me necessary facilities for the smooth completion of my work. I would like to give special thanks **Mr. Mukesh Kumar** of Project and Research Lab, **Mr. Vickey** of UEE Lab, DTU Delhi for providing me with the facilities and assistance during this work. I would like to thank the office staff of EED, Central Library and Central Computer Centre for their valuable co-operation and support.

I would like to thank all my seniors, **Dr. Nikita Gupta**, and **Dr. Pallavi Verma,** to motivate and guide me in the starting of my research work. I would like to use this opportunity to thank my fellow researchers, and juniors I would like to use this opportunity to thank my fellow researchers and juniors, **Issak Abdow Hassan, Aakash Seth, Saket Gupta, Sirish Rayzada, Pankhuri Asthana, Snigdha Sharma, Mo. Bilal, Monika Verma,** and **Arvind Goswami** for their co-operation and informal support in pursuing this research work.

I am thankful to those who have directly or indirectly helped me to finish my dissertation study. It is not possible to mention all of them; nonetheless, I wish to acknowledge their contribution to this work.

Last but not least, I am always indebted to my parents **Smt. & Sh. Ramkesh Ram**, and **all other family members** for supporting me during all the ups and down throughout my research work.

Avdhesh Kumar
(2k17/Ph.D./EE/04)

Date: ____/____/___

ABSTRACT

Energy is one of the most important, indicative parameters for the economic and industrial development of a country. It is expected that in coming years world energy consumption will be significantly higher than at present. Most of the power produced across the world is from conventional sources. The adverse effect of power generation from these conventional sources has led to alternative renewable energy sources (RES) of power generation. Therefore, the role of RES has increased considerably in current years due to increasing energy demand with minimum ecological impact. Renewable energy sources (RES) such as solar, wind, geothermal, tidal, and hydrogen energy etc. are progressively emerging as a sustainable and cost-effective way to satisfy power demand. Furthermore, due to technological improvements, abundant availability, and satisfactory performance, solar energy is emerging as one of the most popular renewable energy source. For the SPV system to operate reliably and effectively, other energy sources such as wind, fuel cells, batteries, etc., can be integrated with it.

The power generated by the SPV system can either be integrated into the utility grid or used by the local loads in the microgrid. Microgrid is a collection of distributed generation (DG), renewable energy sources, and local loads connected to the utility grid. Since the SPV power generation is near to the load, the microgrid offers various advantages, viz. efficiency, lower transmission losses, as well as increased stability.

A grid-integrated microgrid offers a way to manage local loads and generation. It could increase the system's overall effectiveness, power quality, and availability of energy for vital loads. Therefore, for developing efficient and cost-effective SPV systems, the study, analysis and control of SPV-based microgrids need to be performed.

In the present work, “Control and performance analysis of RES based microgrid”, a system approach is considered for efficient design, development and control of microgrid to provide reliable and good quality.

A 10.25 kW, two-stage, three-phase grid integrated SPV based microgrid is designed and developed. In the developed, grid-connected SPV-based microgrid, the output power of the SPV array is governed by a maximum power point tracking (MPPT)

algorithm by controlling the switching of DC-DC boost converter. The output of the boost converter is coupled to DC link voltage of the voltage source converter (VSC), which is interfaced to the grid at the point of common coupling (PCC). The voltage source converters (VSC), supplies the power produced from the SPV system to the appropriate voltage and frequency, as well as maintain the power balance between the SPV system, load, and grid.

Grid integration/synchronization of SPV system is accomplished using the VSC control algorithm, which regulates the operation of VSC to ensure efficient performance. Furthermore, VSC, operating under unity power factor (UPF) mode of operation, control the output of the VSC thus improve the power quality at the PCC by compensating the reactive power, harmonics, and load unbalancing along with the overall efficiency.

In this work, various VSC control algorithms viz. conventional synchronous reference frame (SRF) theory, instantaneous reactive power theory (IRPT), unit template and adaptive least mean logarithmic (LMS) based control algorithm have been implemented. Furthermore, it has been observed that overshoots/undershooting, settling time, and oscillations under the dynamic condition in their responses are inevitable with these conventional control algorithms while regulating the DC-link voltage and estimating the fundamental active component of the load current. Additionally power quality issues that affect the distribution grid and consumers viz. unbalance load, low power factor, and excessive reactive power demand are power quality related issues that are observed due to power electronics-based technology. A rise in power electronics-based loads leads to poor power quality at the power distribution. These nonlinear loads produce a harmonic current that circulates to other coupled loads at the point of interconnection (PCC). To address the aforementioned issues, an intelligence-based novel modified SRF control algorithm, and adaptive-filter based variable step size least mean logarithmic (VSSLMS), and robust least mean logarithmic square (RLMLS) control algorithms for VSC are designed and developed. The simulation studies for the considered system have been carried out using proposed algorithms, under different operating conditions to validate the feasibility of the proposed control algorithm.

All the above-aforementioned control algorithms have been designed and developed in MATLAB /Simulink environment. The performance of the proposed control algorithms has been thoroughly investigated using simulation studies and experimentally on the prototype hardware developed in the laboratory. Due to laboratory resource limitations, adaptive control algorithms of VSC are tested in real time on the prototype hardware set-up of DSTATCOM developed in the laboratory using a Micro-Lab box(dSPACE-1202). The various performance parameters are measured and analysed using FLUKE PQ Analyzer. Furthermore, the design and selection of various components viz. interfacing inductors, DC link capacitor, voltage sensing circuits, current sensing circuits, linear, reactive and nonlinear loads to be compensated, are also required for the prototype hardware set-up in the laboratory.

Despite the benefits of solar PV power generation, they also pose some risks, such as unintended islanding, safety concerns, reverse power flow, etc. As a result, the grid integration of DG necessitates protection and safety concerns in the distribution network.

The detection of the island operations of distributed generators has become very important, in order to ensure the safety of service personnel and electrical components. Microgrid islanding arises as a consequence of faults, breakers accidentally tripping, resulting in a significant threat to the safety of staff, damage to the equipment of utilities, consumers, loss of control over voltage and frequency, etc. Islanding refers to a situation where energized DGs are disconnected from the bulk power grid, providing power only to the local loads for the time being. A comprehensive review, analysis and study of the various islanding detection techniques that have been described and are divided into the following categories: remote, passive, active, signal processing is presented. An active islanding identification based on disturbance injection through the quadrature axis controller has been studied and analysed. Analysis of different islanding detection scheme along with the advantages, disadvantages and limitations are evaluated and summarized.

The thesis research work is designed to give good exposure to the design, and development of a solar PV-based microgrid.

CONTENTS

LIST OF FIGURES

LIST OF TABLES

LIST OF ABBREVIATIONS

RES	Renewable Energy Sources
SPV	Solar Photovoltaic
MPPT	Maximum Power Point Tracking
VSC	Voltage Source Converter
PCC	Common Coupling Point
DG	Distributed Generation
PQ	Power Quality
IGBTs	Insulated Gate Bipolar Transistors
SRFT	Synchronous Reference Frame Theory
IRPT	Instantaneous Reactive Power Theory
LMS	Least Mean Square
VSSLMS	Variable Step Size Least Mean Square
RLMLS	Robust Least Mean Logarithmic Square
PFC	Power Factor Correction
LPF	Low Pass Filter
DSTATCOM	Distribution Static Compensator
OCV	Open Circuit Voltage
SCC	Short Circuit Current
PLL	Phase Locked Loop
SOGI -PLL	Second-Order Generalized Integrator-PLL
QPLL	Quadrature PLL
EPLL	Enhanced PLL
FLC	Fuzzy Logic Controller
IT-2 FLC	Interval Type-2 Fuzzy Logic Controller
MPP	Maximum Power Point
MPPT	Maximum Power Point Tracking
STC	Standard Test Condition
P&O	Perturb And observe
Inc	Incremental Conductance

DSO	Digital Storage Oscilloscope
PI	Proportional Integral
THD	Total Harmonic Distortion
PQ	Power Quality
HCC	Hysteresis Current Control
UPF	Unity Power Factor
PWM	Pulse Width Modulation

LIST OF SYMBOLS

V_{grid}, I_{grid}	Voltage and current of grid respectively
P_{grid}, Q_{grid}	Grid active and reactive power respectively
P_{load}, Q_{load}	Active and reactive power of load respectively
P_{inv}, Q_{inv}	Inverter active and reactive power respectively
I_{load}, I_{inv}	Load and inverter current respectively
C.B.	Circuit breaker
R_s, L_s	Source resistance and inductance
R_f, L_f	Resistance and inductance of interfacing inductor
Δi_1	ripple current in inductor of the boost converter
I_D	Current through the diode
I_S	Saturation current
I	Output current of solar cell
V	Output voltage of solar cell
R_{sh}	Shunt resistance
R_s	Series resistance
q	Electron charge ($1.6 * 10^{-16}\ C$)
K	Boltzmann constant ($1.381 * 10^{-23}\ \frac{Joule}{\text{kelvin}}$)
L	Inductor of boost converter
C	Capacitor of boost converter
D	Diode of boost converter
R	Load resistance of boost converter
V_{in}	Input voltage of boost converter
V_O	Output voltage of boost converter
I_{in}	Input current of boost converter
I_O	Output current of boost converter
f_{sw}	Switching frequency
k	Duty ratio of the boost converter
dI, dV	Derivative of current and voltage of PV cells respectively

e	Error in DC link voltage
Δe	Change in error
e(k)	Error in DC link voltage at k_{th} instant
$\Delta e(k)$	Change in error at k_{th} instant
W/m^2	Solar irradiance
P_{pv}, V_{pv}, I_{pv}	power, voltage and current of SPV respectively
V_{dc}	DC-link voltage
V_{dc}^*	Reference DC-link Voltage
m	Modulation index
h	Overloading factor
$V_{dcripple}$	Ripple voltage in dc link voltage
I_{dc}	DC-link current
Δi	Current ripple in the interfacing inductor
P_{dc}	Power transfer through DC link capacitor
i_{dloss}	Output of PI controller
p_L, q_L	Fundamental active and reactive power of load respectively
i_d^*	Reference active component of load current
i_d	Fundamental DC current component of load current
$\mathcal{U}_{qa}, \mathcal{U}_{qb}, \mathcal{U}_{qc}$	Quadrature unit templates of voltages
e_{pa}, e_{pb}, e_{pc}	Estimation error of a, b, and c phases
w_{pa}, w_{pb}, w_{pc}	Fundamental active weights component of load current in a, b, and c phase
w_{qa}, w_{qb}, w_{qc}	Fundamental reactive weights component of load current in a, b, and c phase
w_{lp}	Average of the fundamental active component of load current of a, b, and c phase
w_{lq}	Average of the fundamental reactive component of load current of a, b, and c phase
$v_{dc(e)}(n)$	Error in DC link voltage with respect to reference DC link voltage at n^{th} sampling
K_{pd}, K_{id}	Gains of PI controller of DC link

K_{pa}, K_{ia}	Gains of PI controller of AC side
w_{dc}	DC loss weight component
w_{ac}	AC loss weight component
w_{ps}	Total active weight component
w_{qs}	Total reactive weight component
α, and β	Scaling factor are positive scalar constant
ΔP ; ΔQ	Active and reactive Power shared by grid
P_{DG} ; Q_{DG}	Active and reactive Power shared by DG
P_{load} ; Q_{load}	Load demand
Q_f	Quality factor

CHAPTER-I
INTRODUCTION

1.1 INTRODUCTION

Energy is one of the most important indicative parameters for the economic and industrial development of a country. It is expected that in coming years the world energy consumption will increase exponentially. Presently most of the power produced across the world is from conventional sources. The adverse effect of power generation from these conventional sources has led to alternative renewable energy sources (RES) of power generation. The role of RES has increased considerably in coming years due to increasing energy demand with minimum ecological impact. Renewable energy such as solar, wind, geothermal, tidal, and hydrogen energy etc. are progressively emerging as a sustainable and cost-effective way to satisfy power demand.

Sources of sustainable and green energy such as renewable energy sources (RES) are ecologically friendly and can be harnessed for microgrids [1]-[3]. Among all the renewable energy sources (RES), solar energy is the most abundant source of energy which leads to photovoltaic (PV) based microgrids gaining much interest as a source of power generation. Additionally, solar photovoltaic (SPV) power generation is becoming eminent due to ease of installation, low maintenance cost, an adequate amount of resources etc. [4]-[6]. Furthermore, SPV based power generation, resolves ecological issues like global warming, greenhouse effect etc. Therefore, for developing efficient and cost-effective systems, the study, analysis and control of SPV-based microgrids need to be performed.

The power generated by the SPV system can either be integrated into the distribution grid or used by the local loads in the microgrid. Since the SPV power generation is near to the load, the microgrid offers various advantages, viz. efficiency, lower transmission losses, as well as increased stability. Furthermore, due to technological improvements, abundant availability, and satisfactory performance, solar energy is the most popular renewable energy source. For the SPV system to operate reliably and effectively, other energy sources such as wind power, fuel cells, batteries, etc., can be connected in parallel.

A grid-integrated microgrid offers a way to manage local loads and generation. It could increase the system's overall effectiveness, power quality, and availability of energy for vital loads.

1.2 RENEWABLE ENERGY SOURCES BASED MICROGRID

A microgrid is a group of distributed energy resources and interconnected loads within clearly defined electrical boundaries with respect to the grid. Microgrid expresses the concept of integrating RESs (PV, wind, biomass, etc.) to take use of their potential as a way to fulfil the rising energy demands. Microgrids can be run in grid-connected or autonomous modes. A microgrid system based on SPV is going to be an alternative source of power generation in the future. However, for a microgrid to be reliable and efficient network, it needs an operational mechanism and an advanced control system. Single line diagram of RES based microgrid is shown in figure 1.1. In the present work, control and performance analysis of SPV based microgrid has been performed.

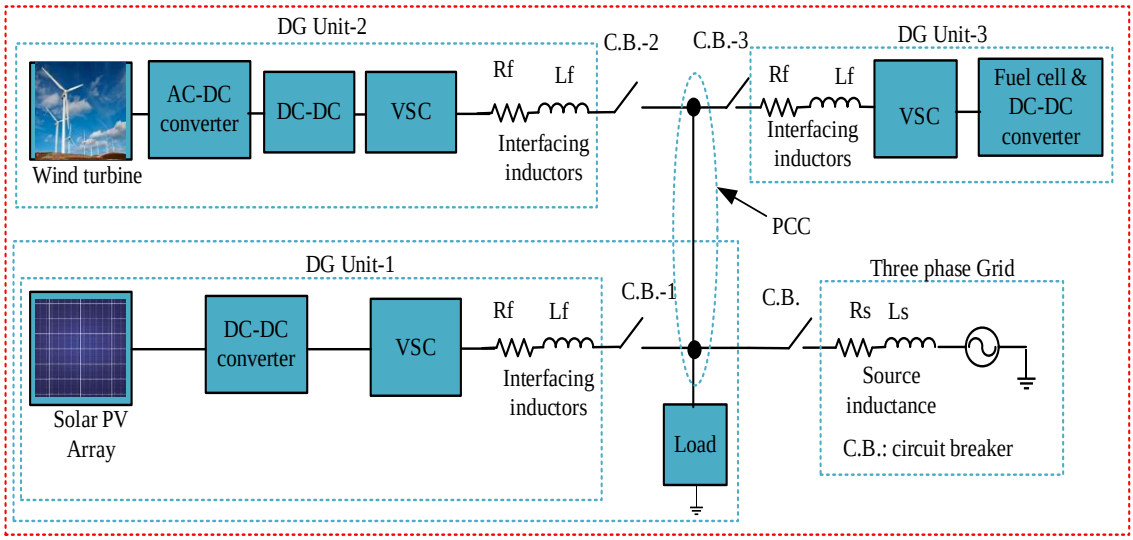

Fig.1.1 Single line diagram of RES based microgrid

1.2.1 Grid Connected Solar PV Based Microgrid

Figure 1.2 shows, the block diagram of the SPV based micro grid. Main components of SPV based microgrid are PV array, DC-DC converter, MPPT, voltage source converter (VSC). The system is two stage power conversion system. In the first stage, converter is used to convert the voltage that is obtained from PV array to get the required voltage level. As power from PV array is not constant and changes with environmental conditions, therefore to track the maximum power, MPPT algorithm is used. In second stage of conversion, dc link voltage obtained after first stage conversion is converted to ac voltage of required magnitude and frequency using VSC. VSC is an IGBT based three leg converter used to feed power to the load and utility grid.

VSC serves the active and reactive power demand of load and maintains unity factor at grid side. Furthermore, under nonlinear and unbalance load, VSC maintains the grid current to be sinusoidal and balanced by compensating the harmonics and unbalancing of the load.

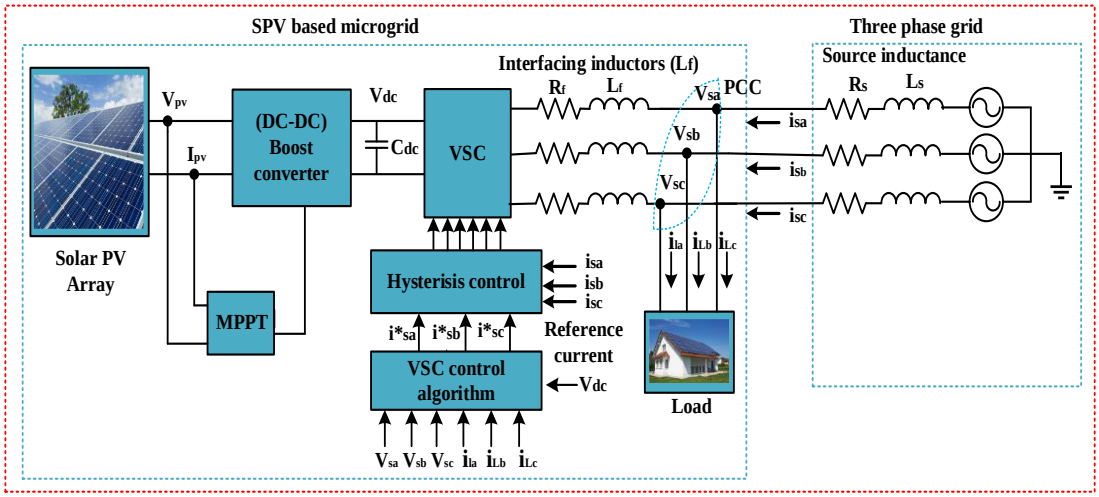

Fig.1.2. Block diagram of grid integrated SPV based microgrid

1.2.2 Maximum Power Point Tracking (MPPT) Techniques

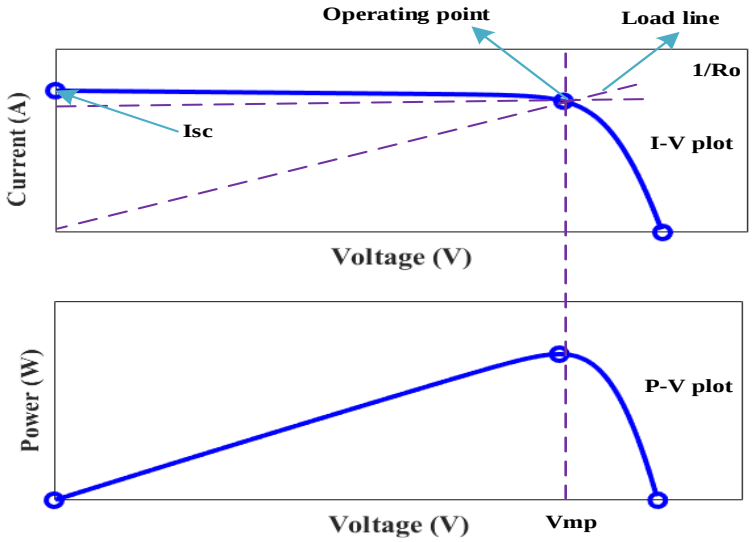

Fig.1.3. I-V and P-V characteristics of PV array

The SPV power generation emerges as a hopeful among the RES due to it being ubiquitous, cost-effective, ecological, and abundant in nature. In the SPV power generation, the amount of power supplied by SPV system depends upon the available solar energy. The available solar energy is depend on environmental conditions viz. temperature, irradiance etc. [7]-[10]

However, the output power is primarily influenced by factors such as the cell's temperature, and irradiation [11]. To maximise the power extraction from the SPV array, maximum power tracking technique (MPPT) have been embedded along with the boost converter. I-V and P-V characteristics of the PV array can be seen from the figure 1.3 [12]-[13].

In the present work, a 10.25 kW, two-stage, three-phase grid integrated SPV based microgrid has been design, developed and analysed. The power point tracking (MPPT) algorithms are used to track the optimal power from the PV array. The DC link voltage is transformed into three phase AC of 415V, 50Hz using the VSC (PV inverter), which is connected to the grid. Interfacing inductors are designed properly to produce a sinusoidal voltage waveform. The SPV based microgrid system is to grid through connected to voltage source converter (VSC) at the point of common coupling (PCC). VSC control algorithm is used to convert generated DC power into AC of required voltage level and frequency for grid synchronization and also to regulate the DC link voltage. Furthermore, VSC supplies the power produced from the SPV system, as well as maintain the power balance between the SPV system, load, and grid.

The mathematical modelling and design of a grid-connected PV system along with the simulation investigations are carried out using MATLAB/Simulink. The various design and developed parameters for the proposed system is given in the appendix: A.

1.3 VSC CONTROL ALGORITHMS FOR GRID INTEGRATION OF MICROGRID

The increasing penetration of solar photovoltaic (SPV) system in utility grids, degrades power quality (PQ) at the point of common coupling (PCC) and it's becoming a major concern. Harmonics are generated either by nonlinear local loads or power electronics converter used in the PV based microgrid system [14]-[17]. To successfully mitigate power quality concerns and comply with IEEE standards, an efficient control for optimal operation of VSC is necessary. Grid integration techniques are used to control VSC output for its efficient operation. Furthermore, to improve power quality at PCC by providing reactive power and harmonic compensation, and maintaining the grid current to be sinusoidal and balanced under unbalanced load.

In the present work, various VSC control algorithms viz. conventional synchronous reference frame (SRF) theory, instantaneous reactive power theory (IRPT), unit template and adaptive least mean logarithmic (LMS) based control algorithm have been implemented. Furthermore, it has been observed that overshoots/undershooting, settling time, and oscillations under the dynamic condition in their responses are inevitable with these conventional control algorithms

while regulating the DC-link voltage and estimating the fundamental active component of the load current. To address the aforementioned issues, an intelligent-based novel modified SRF control algorithm, and adaptive-filter based variable step size least mean logarithmic (VSSLMS), and robust least mean logarithmic square (RLMLS) control algorithm of VSC are designed and developed.

Furthermore, in the adaptive theory-based control algorithms, the calculation of fundamental active and reactive power components of load currents is based on input signals, which can be constant or variable. The benefit of adopting fixed parameters is low complexity, which reduces the burden of computation on the DSP processor. An adaptive theory based VSC control algorithms has been presented for grid integration of microgrid.

The simulation studies have been carried out using proposed VSC algorithms, for the developed system under different operating conditions and results have been presented to prove the feasibility of the proposed VSC control algorithm.

The efficiency of the proposed VSC control algorithms has been evaluated in MATLAB /SIMULINK and Sim-power system (SPS) toolboxes.

1.4 DEVELOPMENT OF PROTOTYPE HARDWARE FOR THE GRID CONNECTED PV SYSTEM

To test the efficacy of the developed VSC control algorithms in the real time, a prototype model of DSTATCOM is developed in the laboratory. This requires the design, development and selection of three phase VSC, DC bus capacitor, voltage sensing circuits, current sensing circuits, interfacing inductors, linear, reactive and nonlinear loads to be compensated.

The VSC (Semikron make), insulated gate bipolar transistors (IGBTs) and antiparallel diodes has been used to develop the DSTATCOM prototype in the laboratory. The simulation model of the system is developed in MATLAB environment using SIMULINK and Sim Power System (SPS) tool boxes. VSC is used to feed power to the load and operate at UPF mode thus maintain unity power factor at grid side along with harmonics compensation.

The prototype hardware set- up is designed and developed at a voltage rating of 110V, 50Hz in the laboratory. Figure 1.4 shows, block diagram of three phase DSTATCOM that has been developed in the laboratory. The developed VSC control algorithm in MATLAB/ Simulink is validated in real-time on the hardware(prototype) developed in the laboratory.

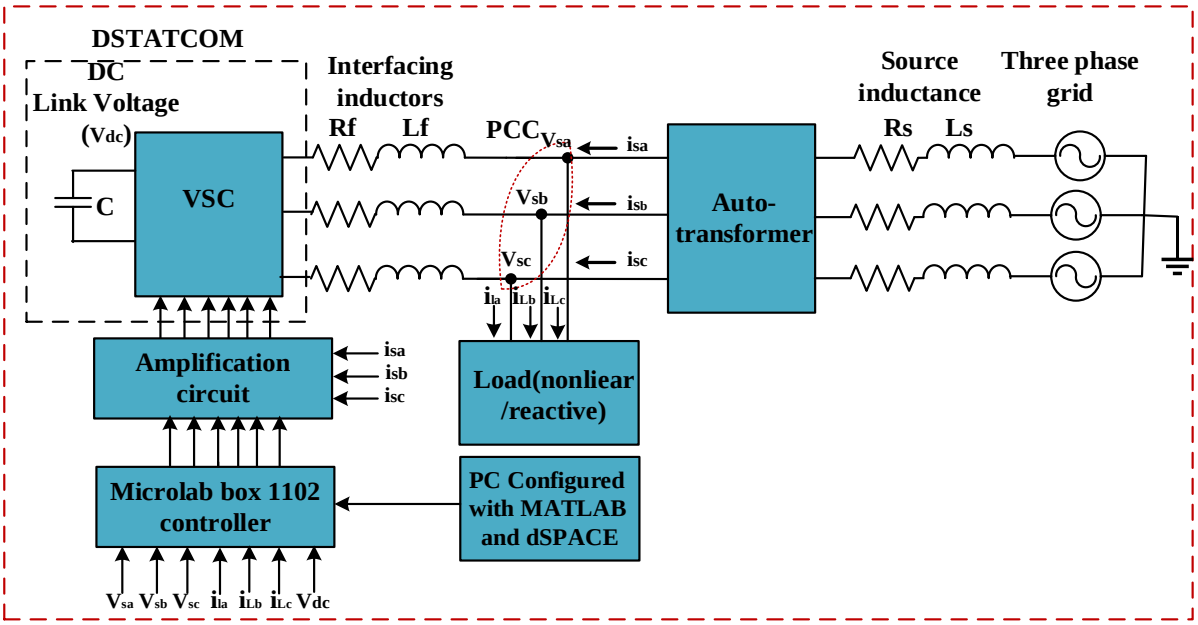

Fig.1.4. Block diagram of layout of three phase DSTATCOM connected to grid

The DSP (Microlab box/dSPACE 1102) embeded in the personal computer is used to perform the real- time control operation of the VSC. Figure 1.5 shows, the layout of three phase prototype hardware set-up developed in the laboratory. The various design and developed parameters for the prototype hardware are given in the appendix: B.

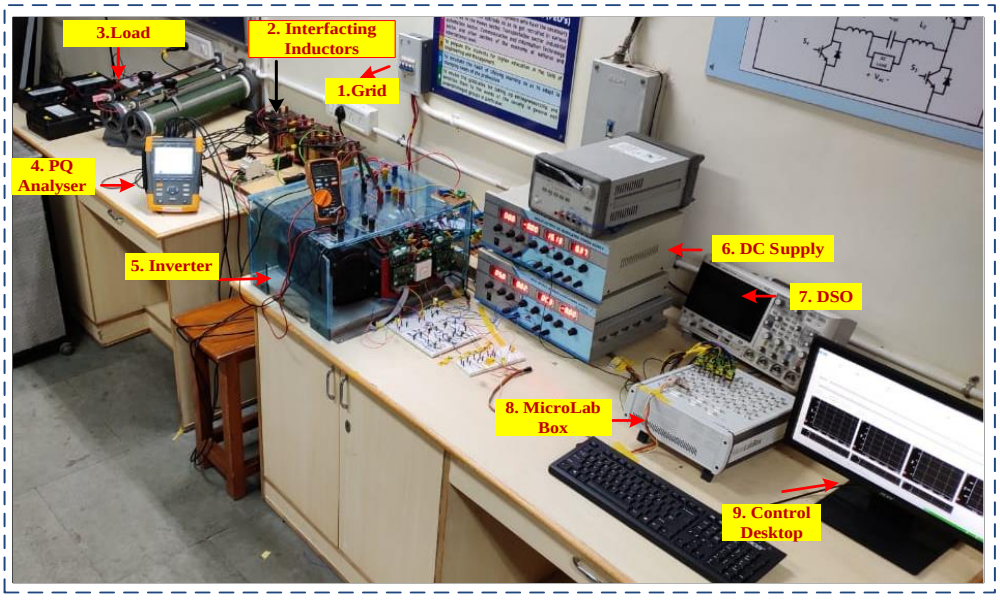

Fig.1.5. Layout of three phase Prototype Hardware set-up

1.5 COMPREHENSIVE REVIEW ANALYSIS OF ISLANDING DETECTION TECHNIQUES IN MICROGRID

Nowadays, the renewable energy sources (RES) based distributed generator (DG) has been increased substantially in the distribution grid. The most practical DG technology has been grid-connected photovoltaic systems, which have advantages in terms of technology, economical, and the environmentally clean and green. Despite the benefits of RES, they also pose some risks, such as unintended islanding, safety concerns, reverse power flow, etc. As a result, the grid integration of DG necessitates protection and safety concerns in the distribution network [18]. Islanding occurs when a section of the utility system that comprises both load and distributed resources remains energised while disconnected from the rest of the utility system. Islanding refers to a situation where energized DGs are disconnected from the bulk power grid, providing power only to the local loads during that power [19]-[20].

Figure1.6 depicts the single line diagram for islanding detection schemes.

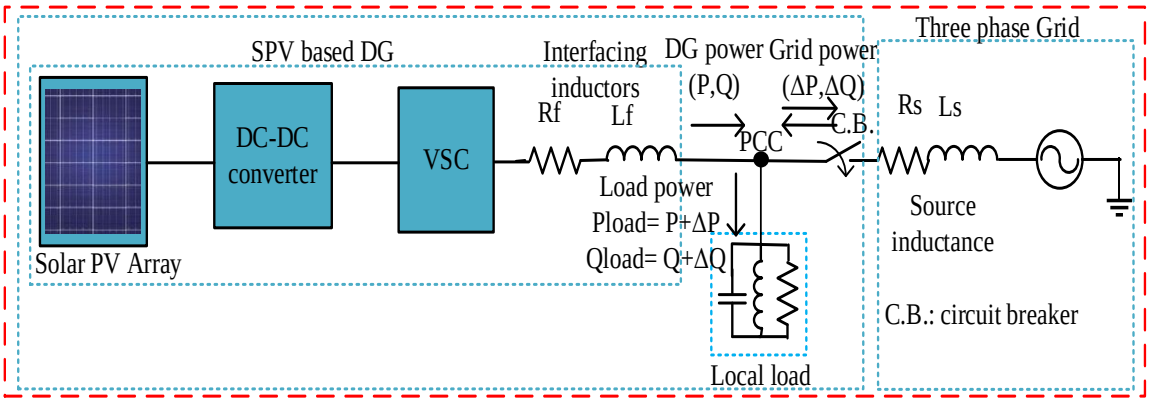

Fig.1.6 Single line diagram for islanding detection

1.6 MOTIVATION AND RESEARCH OBJECTIVES

RES based micro grid are gaining much interest as a source of renewable energy. For developing efficient and cost-effective systems, the study, analysis and control of RES based microgrid need to be performed. Furthermore, among all RES, solar energy is the most abundant source of energy and also resolves the ecological issues like the global warming, greenhouse effect etc. The SPV generation is becoming eminent due to ease of installation, low maintenance cost, and an adequate amount of resources.

Power generated using SPV system can be utilized locally and can be integrated with grid also. SPV integration to the utility grid faces challenges related to power quality like distortion in voltage/current, voltage fluctuations and harmonics [21]-[23]. Due to grid integration of SPV

system, harmonics are generated on both sides viz. SPV (source) and common coupling point (PCC) of the system. However, harmonics injection from SPV system to grid is mainly due to switching of power electronics based converter, degrading power quality of supply system [21], [24]-[30].

All these advantages and limitations [4]-[6],[31]-[36] of PV based microgrid motivated and led to the following research objectives:

1. Design and development of control algorithms for tracking of Maximum Power Point in solar PV based microgrid.
2. Design and development of VSC (inverter) control algorithms for microgrid.
3. Design and development of prototype hardware of grid connected SPV system.
4. Islanding detection techniques for the microgrid.

1.7 PROBLEM IDENTIFICATION

The following issues have been observed in order to accomplish the defined objectives:

- The design and development of the SPV-based microgrid and its components, including the dc-dc boost converter, VSC, DC link capacitor, and interface inductors, needs to be carried out along-with the simulation studies. The output of SPV are non-linear in nature and depend on environmental conditions viz. temperature, irradiance etc. Therefore, special techniques known as MPPT are employed to extract the maximum available power from the PV source. Thus, efficient MPPT techniques needs to be developed.
- In grid integrated PV system, VSC control algorithms regulates the active and reactive power sharing between the load, grid and PV system. As a result, a controller capable of maintaining constant dc link voltage during system transients needs to be developed and implemented. The grid interfacing control algorithms are used to regulate the output of the VSC, and to improve power quality at PCC. An efficient control for efficient functioning of VSC is essential to successfully minimise power quality concerns and to comply with the relevant IEEE standards.
- Developed VSC control needs to be efficient, under dynamic and nonlinear load and also under distorted grid voltage conditions viz. harmonics, unbalanced and voltage fluctuations.
- The prototype hardware model of the grid connected PV system, needs to be developed in the laboratory for the real-time validation of the developed VSC control algorithms.

- Despite the benefits of solar PV power generation, they also pose some risks, such as unintended islanding, safety concerns, reverse power flow, etc. As a result, the grid integration of DG necessitates protection and safety concerns in the distribution network. The detection of the island operations of distributed generators has become very important, in order to ensure the safety of service personnel and electrical components.

1.8 THESIS ORGANIZATION

Chapter-I Includes the research work's introduction, motivation, objectives, and problem identification. This chapter also contains information on how to organise your thesis.

Chapter-II This chapter presents an overview of the literature on grid-connected SPV-based microgrids and its related aspects. A literature review of the MPPT control technique for grid-integrated PV based microgrid have been presented. Furthermore, literature survey on conventional VSC control, adaptive theory based VSC control algorithms and comprehensive review of islanding detection techniques for the microgrid have been carried out.

Chapter-III This chapter presents the design and development of a 10.25kW grid integrated solar PV-based microgrid. The mathematical modelling, and parameter selection/design of grid-integrated solar PV-based microgrid systems have been presented in the subsequent sections.

The design and modelling of conventional VSC control algorithm for grid integration viz. synchronous reference frame theory-based conventional control algorithm, instantaneous reactive power theory (IRPT), unit template-based convention control algorithm also has been presented.

Furthermore, novel intelligence-based VSC control algorithm is presented. Modelling and simulation of the two-stage, three-phase grid-interfaced SPV system has been carried out using conventional and proposed VSC control algorithm both in the MATLAB/SIMULINK environment. The simulation studies have been carried for the developed system using these developed VSC control algorithms under different operating conditions and results have been presented to prove the feasibility of the proposed control algorithm.

Chapter-IV This chapter presents adaptive theory-based PV inverter (VSC) control algorithms for three-phase grid interfaced two stage PV system. Adaptive filters-based novel variable step

size LMS (VSSLMS), and robust least mean logarithmic square control algorithm (RLMLS), VSC control algorithms along with the conventional LMS are developed and presented for the PV based microgrid. The efficiency of the proposed control algorithms has been tested for different condition such as insolation variation, load variation, load unbalancing, nonlinear load, reactive load, grid voltage unbalancing, and distorted grid voltage etc. The performance of the proposed control algorithms is verified on MATLAB/ Simulink. Furthermore, the performance of the proposed algorithms is compared with conventional SRF and LMS control in terms of THD and weight convergence has also been presented to validate the superiority of the proposed VSC control algorithms.

Chapter-V In this chapter, the development of prototype hardware for the grid connected PV system has been presented. The developed VSC control algorithm in MATLAB/ Simulink is validated/ tested in real-time on the prototype hardware set-up developed in the laboratory. The DSP (Microlab box/dSPACE 1102) embeded in the personal computer is used to perform the real- time control operation of the VSC. Due to laboratory limitations the developed algorithms are tested on a prototype hardware of grid-connected VSC, acting as a DSTATCOM.
The performance of developed control algorithms is evaluated on prototype hardware setup developed in the laboratory using dSPACE1202.
The efficiency of the proposed adaptive control algorithms has been tested under different condition such as load variation, load unbalancing, nonlinear load, reactive load, grid voltage unbalancing etc. Furthermore, the performance of the proposed algorithms are compared with conventional SRF and LMS control.

Chapter-VI This chapter provides a comprehensive analysis and study of the various islanding detection techniques. The various islanding detection techniques are categorised as, remote, passive, active, and signal processing-based schemes. An active islanding identification based on disturbance injection through the quadrature axis controller has been studied and analysed.

Chapter-VII The key summary and conclusions of the proposed work are highlighted in this chapter. At the end of this chapter, the scope for future study in this area is also stated.
The list of references and appendices is given at the end of the thesis.

1.9 CONCLUDING REMARKS

This chapter provides an overview of the completed and included research work in this dissertation. The research work challenges are outlined, along with the purpose and main objectives of the research work. The research work completed in each chapter is summarised.

CHAPTER-II
LITERATURE REVIEW

2.1 INTRODUCTION

In chapter-I, the motivation, and problem identification for the proposed research work are derived. A literature review has been carried out in the associated domains of the research problems in order to get the right perspective on research work. This chapter provides the brief review on the (i) renewable energy sources based microgrid (ii) design and development of grid connected SPV based microgrid along with the Maximum Power Point Tracking (MPPT) Techniques (iii) Conventional and intelligent based novel VSC control algorithm (iv) Adaptive theory-based VSC control algorithms (v) development of prototype hardware for the grid connected PV system (vi) Islanding detection techniques in microgrid. Each issue is briefly explored and examined in the present chapter.

2.2 RENEWABLE ENERGY SOURCES BASED MICROGRID

Nowadays, the sources of sustainable and green energy such as renewable energy sources (RES) are ecological friendly and can be harnessed for distributed generation (DG). Furthermore, with increase in electrical demand and harmful effect of conventional sources, the future of energy generation is moving towards distributed generation (DG) using renewable energy sources (RES) [29],[30],[31],[32]. Amongst different RES (Photovoltaic, wind, biomass, etc.), solar photovoltaic (SPV) based power generation, resolves the ecological issues like the global warming, greenhouse effect etc [33]-[34]. The SPV generation is becoming eminent due to ease of installation, low maintenance cost, and an adequate amount of resources and also its cost continues to decrease in the recent years [35]-[36]. Solar photovoltaic (SPV) is a source of green energy SPV system has been installed worldwide at a massive scale for power generation. Power generated using SPV system can be utilized locally and can be integrated with grid also.

2.2.1 Grid Connected SPV Based Microgrid

PV array, dc-dc converter, VSC, interface inductors, loads, and grid comprise an SPV-based microgrid. The output characteristics of a PV array are determined by meteorological factors such as solar irradiation and temperature. Therefore, power from PV array is not constant and changes with environmental conditions, hence to get the maximum efficiency of SPV array,

MPPT algorithm is used. DC link voltage maintained at certain level and converted to ac voltage of required magnitude and frequency using VSC.

SPV based Microgrid can be either grid connected or stand alone system. The development of a microgrid system gives several benefits to both the consumer and utility grid. The application of a grid connected microgrid is improves the power quality, reduce the emissions, and cost of electricity.

From the view point of the electric utility grid, the goal is to minimise power flow on transmission and distribution lines, hence lowering losses and network construction costs. Micro grids can also lower network load to fulfil power demand and assist in network repair if a malfunction arises.

DGs are often located near to the customer and necessitate power electronic devices for grid connection. The synchronization of a solar PV system to the grid poses several issues, including efficient performance and power quality [1],[21],[23] [37]-[38]. Appropriately designed power electronics and controls guarantee that the microgrid satisfies both its customers' and the utility's challenges [39]-[41].

Before making an investment, it is consequently necessary to model the entire system, including control techniques, in order to forecast the system's behaviour in both steady and dynamic states [42]-[43].

2.2.2 Maximum Power Point Tracking (MPPT) Techniques

Solar PV arrays possess nonlinear current-voltage characteristics that are irradiance and temperature dependent, and hence it is very challenging to get the maximum efficiency of a PV array. To maximise the power extraction from the SPV array, solar PV systems are being regulated utilising a maximum power tracking technique (MPPT). For maximising the amount of power available from SPV systems, MPP techniques are fitted with the appropriate controller. To get maximum power from PV array, various maximum power point tracking algorithm (MPPT) algorithm has been discussed precisely [44]-[50].

Bidyadhar Subudhi et al. [44] presented, a comprehensive review of the maximum power point tracking (MPPT) techniques applied to photovoltaic (PV) power system. A detailed description and classification of the MPPT techniques have been carried out. Comparison of Photovoltaic Array Maximum Power Point Tracking Techniques has been presented by Trishan et al. [47]. M. A. G. de Brito et al. [51], have presented the different techniques of the conventional MPPT, viz. incremental conductance (InC), hill climbing (HC), open circuit voltage (OCV), short circuit current (SCC), perturb and observe (P&O), improved P&O

method. The MPPT problem has been addressed in the literature, however P&O is the most commonly employed technique due to its low cost and ease of implementation. The simplicity and general character of the P&O approach, which includes trade-offs between response rate and steady-state oscillations, is one of its advantages [52]-[54]. Further research is being carried out to improve the existing MPPT algorithm to handle temperature and irradiance variations.

2.2.3 VSC Control Algorithm

The design and development of the VSC control algorithm for grid integration of SPV based microgrid, has been reported in various literature along with the various conventional, intelligent and adaptive theory based VSC control algorithms for reference current generation.

Synchronous reference frame (SRF), instantaneous reactive power theory (IRPT), unit template, and power balance theory (PBT) have been developed in the various literature [14]-[17], [55]-[59]. In SRF-based control [55], a phase locked loop (PLL) is necessary to convert three phase quantities to two phase, however it sometimes shows computational delay and must be tuned prior to operation. Conventional SRF is one of the most practically applicable method. Although due to conventional PLL, it exhibits poor performance under distorted and unbalance grid [60],[61]. In the literature [21], [61], it has been observed that performance of PLL is easily affected by distortions and noise, to overcome these drawbacks SOGI PLL has been proposed by H. K. Yada et al. [62]. F. Xiao, et al. [63], presented second-order generalized integrator (SOGI) based phase-locked loops (PLLs) are widely used for grid synchronization in single-phase grid-connected power converters. However, it also suffers from poor dynamic response and uses generalized integrator thus requiring tuning of gains. Furthermore, second-order generalized integrator-PLL [64], quadrature PLL (QPLL) and enhanced PLL (EPLL) [65] and synchronous PLL(SRF-PLL) [66] have been presented. The main drawbacks of PLL-based approaches include more complexity, the presence of a low-pass filter in SRF-PLL, which reduces dynamic response, and higher computational burden. Furthermore, it has been observed that sometimes implementation of PLL, exhibit computational delay and must be tuned before use. In the literature, Deo et al. [66] has presented an adaptive PLL-less approach, demonstrating that the operation of a system utilising a PLL-less method is less appropriate for real-time applications since it is more sensitive to parameter fluctuations. N.Beniwal at al.[21],[67], sentenced that in the implementation of IRPT, in which reference current is estimated using voltage and current of

the PCC, so fluctuation in voltage is reflected in the reference current. Furthermore, in the literature, S. B. Pandu et al. [59], presented power quality enhancement in distribution grid using intelligent based Interval Type-II Fuzzy Logic Controlled (FLC) in DSTATCOM. P.K. Bharik et al.in [60] evaluated the power quality of distribution static compensator system (DSTATCOM) using type-1 FLC. DC-link voltage regulation and reduction in its settling time are realized by either PI or FLC or fuzzy-PI controller schemes in SRF based designed control for shunt active filter. Karuppanan P. et.al in [61] proposed, FLC based control algorithm for estimating reference current using shunt active power filter for PQ improvement. THD (%) in grid current and DC link settling time are small using FLC. H. K. Yada et al. [62], presented power quality enhancement using FLC based control. D. Pullaguram et al. [69], authors have proposed Takagi Sugeno Fuzzy to maintain voltage across DC link for enhance performance of standalone PV system connected to single phase grid. In the literature, M. Farhat et al. [70] PI genetic algorithm-based control of grid integrated to PV system has been proposed to reduce the harmonics in UPF mode of operation. The genetic algorithm has been compared with PI controller and genetic algorithm found to be better than PI controller.

Gupta N. et al in [71]-[72] presented asymmetrical fuzzy logic control (FLC) for reference generation, showing type-1 FLC is superior than conventional PI controller for the control of DC link voltage. However, type-1 FLC may not handle dynamic environment having linguistic and numerical uncertainties. FLCs exhibit obvious limitations such as their requirement on the user's knowledge about the system and complicated rules. The higher number of rules will increase the difficulty of FLC design and implementation [73]. Type-1 FLC is very challenging when these uncertainties are related to input, output which leads to uncertainties in the optimization of fuzzy set membership functions. The limitations of type-1 FLC can be overcome by interval type (IT-2) FLCs which have the potential to optimize the fuzzy set membership function and give more efficient performance for grid integration of RES based micro grid applications [74].

2.3 ADAPTIVE THEORY-BASED VSC CONTROL ALGORITHMS FOR GRID INTEGRATION OF MICROGRID

Adaptive control methods have been implemented for a variety of applications throughout the last several decades. Among these, the least mean square (LMS) algorithm distinguished one, with its stability and optimality being studied in several literature. Conventional LMS, adaptive control has been widely used because to its simplicity, however the

performance is frequently unsatisfactory due to poor dynamic performance caused by a trade-off between tracking capacity and precision in fixed step size [75]-[77].

Agarwal et al. [78] developed the least mean fourth (LMF) control algorithm which has a poor steady-state response due to fourth-order optimisation and lacks precision in terms of fundamental extraction capabilities. Z. Li et al. [79] and M. O. Sayin et al. [80] have presented, LMS and LMF respectively whereas the adaptive LMS control is a distinguished one, which is widely used due to its simplicity. LMS and LMF, are subject to oscillations and have lower accuracy in estimating mean square error (MSE). However, LMF offer better performance than LMS, in terms of trade-off point between steady state and transient performance. The performance of conventional adaptive LMS controls is frequently inadequate due to poor dynamic performance as a result of there is a trade-off between tracking capabilities and accuracy related to fixed step size. As a result, an optimal control approach is required to provide good transient, dynamic and steady-state performance, which can be overcome the aforementioned issues. Y. Tsuda et al.[81] have presented an improved NLMS algorithm. A. Chaturvedi, et al. [82] have presented, a comparative analysis of LMS and NLMS algorithms for adaptive filter. J. Dhiman, et al. [83], discussed about comparative analysis between adaptive filter algorithms LMS, NLMS and RLS. K. Xiong et al. [84], and Z. Yuan et al.[85] have presented the various adaptive filter alongwith the robust least mean logarithmic square and new LMS adaptive filtering algorithm with variable step size for different application respectively.

B. Fan et al. [86] presented, a lyapunov-based nonlinear power control algorithm for grid-connected VSC. A. A. S. Mohamed et al. [87], presented predictive neural network controller (PNNC) with aim to improve the PQ issues like harmonics within IEEE norms and DC link voltage regulation along with reactive power compensation.

2.4 ISLANDING DETECTION TECHNIQUES IN MICROGRID

Despite the benefits of solar PV, they also pose some risks, such as unintended islanding, safety concerns, reverse power flow, etc. As a result, the grid integration of DG necessitates protection and safety concerns in the distribution network [18],[29]-[30],[88].

In order to ensure the safety of service personnel and electrical components, the detection of the island operations of distributed generators has become very important. Microgrid islanding arises as a consequence of breakers accidentally tripping, resulting in a significant threat to the safety of staff, damage to the equipment of utilities, consumers, loss of control over voltage and frequency, etc. Islanding refers to a situation where energized DGs are

disconnected from the bulk power grid, providing power only to the local loads for the time being. The islanding operation is detrimental to the maintenance crew that provided a de-energized line [88]-[90]. The rapid detection of an islanding activity is a compulsory requirement, for microgrid for seamless reconnection to preserve the stability of the procedure and supplying likewise, critical demand of loads. Furthermore, several islanding detection techniques for the microgrid have been described in the literature, Z. Lin et al. [91] and R. Sun et al. [92] have discussed and presented remote island detection investigations based on the Phasor Measurement Unit (PMU). In the literature, G. Bayrak et al. [93]-[94], presented the remote islanding detection method in which, the frequency, real power, and current in the circuit breaker are used as criteria for the detection of islands. Whereas, remote IDTs (islanding detection techniques) are not suitable for small microgrids because of the increased investment due to communication system. It is possible to apply these reliable and fast schemes to synchronous as well as inverter-based DGs. However, the increased burden due to expense is recognised as the key constraint. N. Liu et al. [95], presented, a magnitude of frequency-dependent impedance-related data for the Passive IDTs in the literature. B. Guha et al. [96], presented, voltage ripple-based passive islanding detection technique for grid-connected photovoltaic inverters and furthermore, to identify islanding, the inverter's ripple content output voltage's content of ripple is analysed in the time domain. J. Merino et al. [97] also presented islanding detection in microgrids using harmonic signatures.

K. Colombage et al. [98], and D. Reigosa et al. [99], have presented the Local islanding detection technique (IDTs) which are usually limited to the different parameters at common coupling point (PCC) such as voltage, current, frequency is monitored for evaluation, and decision making. There are three kinds of local IDTs: passive, active and hybrid techniques. Recent passive approaches are illustrated in the literature. Y. M. Makwana et al. [100], R. Haider et al. [101], and M. Bakhshi et al. [102] presented the criteria for island detection are voltage and PCC harmonic characteristics. Although these passive solutions in the literature can be applied easily and cheaply. However, they have a large non-detection zone (NDZ), or circumstances where power generation and consumption are nearly matched but not detected by islanding. Another difficulty is choosing a threshold which trade- off between false tripping and minimum NDZ. To extract features from the frequency-domain, a number of mathematical approaches have been employed in the literature. In the literature, H. Pourbabak et al. [103], which includes positive feedback different inverter control parameters, such as voltage, frequency, and phase angle, consequences an unstable system when the inverter is controlled and the grid is disconnected. To enhance the NDZ and PQ

degradation, hybrid method including two local IDTs have been developed in the literature Q. Sun, et al. [104]. Under standard operating circumstances, the standard of power has not been impacted [105]. Nevertheless, difficulty and costs are still regarded as the biggest disadvantages in the Hybrid methods of IDT's. For the purpose of detecting islands depending on reactive power and load control approach, Laghari et al. have presented a hybrid strategy [106],[107].

2.5 IDENTIFIED RESEARCH GAPS

Despite the fact that lots of studies have been carried out in the field of solar PV-based microgrids, many challenges still remain unsolved. Based on the extensive literature review indicated above, the following research gaps were identified:

- It is very challenging to get the maximum efficiency of a PV array. To maximise the power extraction from the SPV array, it is required to be regulated utilising a maximum power tracking technique (MPPT).
- Existing control algorithms for inverter are sometimes plagued by slow convergence, higher complexity and harmonics in the reference current.
- The VSC control schemes developed, have scope for improvement in terms of convergence speed, inintal/ dynamic transients in their estimation of fundamental components and their ability to operate under unbalanced and distorted grid circumstances.
- Despite the benefits of solar PV, they also pose some risks, such as unintended islanding, safety concerns, reverse power flow, etc. As a result, the grid integration of DG necessitates protection and safety concerns in the distribution network. In order to ensure the safety of service personnel and electrical components, the detection of the island operations of distributed generators needs to be studied.

2.6 CONCLUDING REMARKS

This chapter provides a review of the literature on grid connected solar PV-based microgrid and related areas. The contribution of research in the area of design and development of SPVs connected to utility grids with their VSC control algorithms has been outlined. It is offered a review of the work of many researchers in the area of control of grid connected SPV based microgrid. The research gaps in the solar PV-based microgrid are identified based on the literature review.

CHAPTER-III
DESIGN AND DEVELOPMENT OF GRID CONNECTED SPV BASED MICROGRID

3.1 INTRODUCTION

The sources of sustainable and green energy such as renewable energy sources (RES) are ecological friendly and can be harnessed for distributed generation (DG). Amongst different RES, solar photovoltaic (SPV) based power generation, resolves the ecological issues like global warming, greenhouse effect etc. The SPV generation is becoming eminent due to ease of installation, low maintenance cost, learning skill, an adequate amount of resources, and emerging technologies. SPV system has been installed worldwide at a massive scale for power generation. Power generated using SPV system can be utilized locally and can be integrated with grid also.

This chapter contributes towards the design and development of grid integrated solar PV based microgrid. MATLAB/SIMULINK environment is used for the simulation of the solar PV based microgrid system. The mathematical modelling and parameter design of grid integrated solar PV based microgrid systems have been presented in the subsequent sections. Also, a novel intelligence based modified synchronous reference frame-based voltage source converter (VSC) control algorithm has been developed. To establish the superiority of the developed algorithm, it is compared with the conventional algorithm of VSC control.

3.2 DESIGN AND MODELLING OF GRID CONNECTED SOLAR PV SYSTEM

In this chapter, a 10.25kW, two stage solar photovoltaic (SPV system) has been designed and integrated to the grid. The power point tracking (MPPT) algorithms are used to track the maximum power of the PV array. The PV array's DC output voltage is transformed into three-phase, 415V,50Hz AC by the PV inverter, which is connected to the distribution grid.

Figure 3.1 depicts the schematic diagram of the grid-connected SPV system, and its primary components including a solar PV panel/array, a boost converter, a MPPT control technique for maximum power point tracking, VSC, and a load.

In the first stage, DC-DC converter is used to convert the voltage that is obtained from PV array to the required voltage level. As power from PV array is not constant and changes with environmental conditions, therefore to track the maximum power, MPPT algorithm is used.

In the second stage, three phase VSC is used to achieve the DC-AC conversion. On the DC side, the VSC comprises of insulated gate bipolar transistors (IGBTs) with antiparallel diodes based three leg (six switch) and DC link capacitor (C_{dc}). Interfacing inductors (L_f) are used on the AC side of the VSC to connect it to the grid. An uncontrolled bridge rectifier with a series R-L branch is used to simulate the nonlinear load. The control algorithm receives voltages signal at the PCC (V_{sa}, V_{sb}, V_{sc}), grid current (i_{sa}, i_{sb}, i_{sc}), load current (i_{la}, i_{lb}, i_{lc}), and DC bus voltage (V_{dc}). This section goes on to discuss the design and selection of SPV arrays, DC-DC boost converter characteristics, DC bus voltage, and interface inductors. The mathematical modelling and design of a grid-connected PV system along-with the simulation investigations are carried out using the MATLAB/Simulink.

The design parameters of SPV system are given in Appendix: A. The detailed design of components used for grid connected SPV system is discussed as follows.

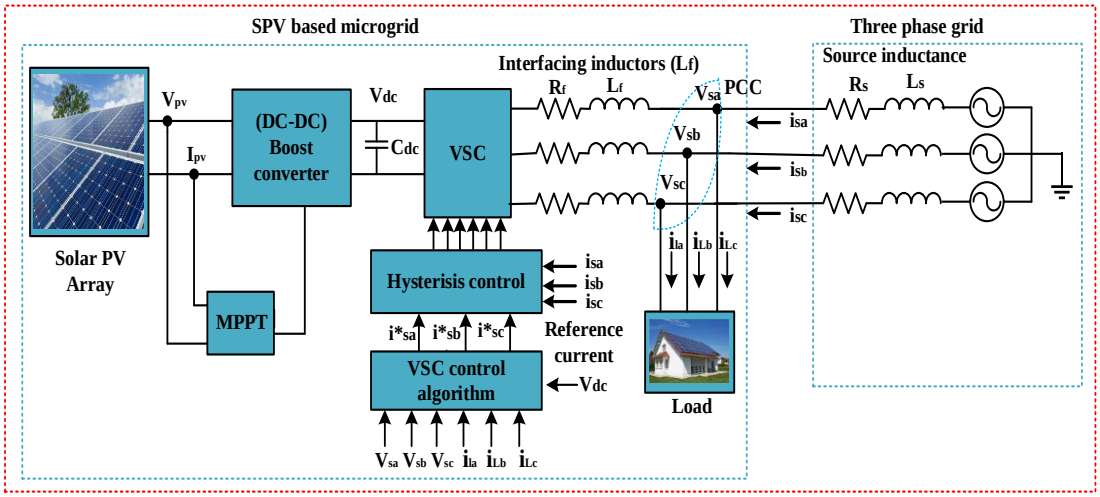

Fig.3.1. Schematic diagram of the grid-connected SPV system

3.2.1 Design of PV Array Configuration

PV cells, an active transducer that transforms light energy (photons) into electricity, are the fundamental building block of a photovoltaic array. To create PV modules, PV cells are connected in parallel and /or series. PV modules may then be combined in series or parallel

to create PV arrays with the specified output voltage and current. A Typical cell, module and array can be seen from the figure 3.2.

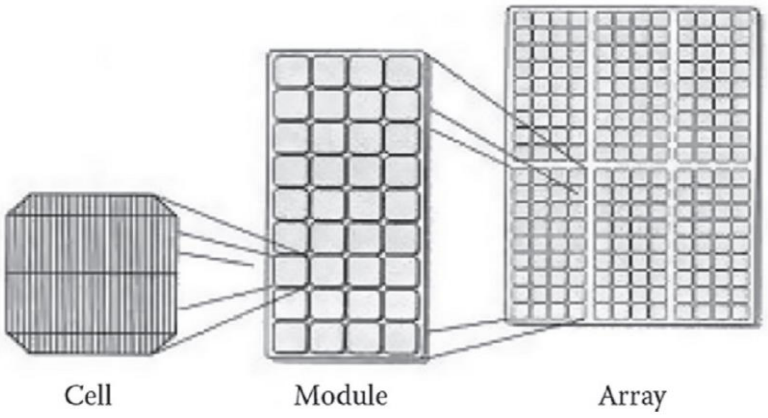

Fig.3.2. Typical PV cell, module and array

3.2.1.1 *Modelling of PV cell*

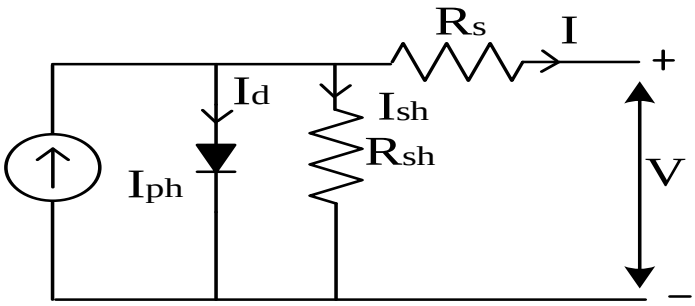

Fig. 3.3 Equivalent circuit of a PV cell

The photovoltaic cell is the basic element of a PV array, that transforms sunlight into electricity when its p-n junction is exposed to light and provides an open circuit output voltage of 0.5V to 0.7V. If a solar cell is short-circuited, the incident light generates a charge carrier, which causes an electric current to flow.

Photo voltaic generator is neither a constant voltage source nor constant current source. A dc current is generated if solar irradiance falls on it. Approximate circuit of PV cell consist of current source (I_{ph}), diode, shunt (R_{sh}) and series (R_s) resistance. figure 3.3 depicts the approximate equivalent circuit of PV cell from which nonlinear characteristics can be derived. Depending on the application, required voltage and power level can be derived from the PV cell by connecting them in series or parallel combination and forming a PV array. The PV cell can be presented by equation (3.1) to (3.3):

$$I_D = I_S\left[e^{\left(q\left(\frac{V+IR_S}{KT}\right)\right)} - 1\right] \quad (3.1)$$

Output current of solar cell:

$$I = I_{ph} - I_D - I_{sh} \quad (3.2)$$

By putting the value of I_D and I_{ph} in the above equation (3.2), output current Equation can be written as:

$$I = I_{ph} - I_S\left[e^{\left(q\left(\frac{V+IR_S}{KT}\right)\right)} - 1\right] - (V + IR_S)/R_{sh} \quad (3.3)$$

Where I is output current (A), I_D is current through the diode, I_{ph} is photon current generated by PV cell, V is output voltage (V), I_S is saturation current, q is electron charge ($1.6 * 10^{-16}\ C$), K is Boltzmann constant ($1.381 * 10^{-23}\ \frac{Joule}{\text{kelvin}}$) and T is operating temperature (K), R_{sh} is shunt resistance and R_s is series resistance.

3.2.1.2 *I-V and P-V Curve of PV Array*

To obtain a peak power capacity of 10.25kW, 10 such modules in series and 5 such modules in parallel are required. Thus, a 10.25 kW PV array was developed and simulated in the MATLAB/ Simulink. Each module has an open circuit voltage of 47.8V and a short circuit current of 5.53A. Furthermore, the modules' voltage at maximum power point (V_{mp}) and current at maximum power point I_{mp} (A) are 40V and 5.13A, respectively. The SPV array is developed by connecting these modules in the combination of series and parallel as needed. I-V and P-V curve of PV array is shown in the figure 3.5(a) and 3.5(b).

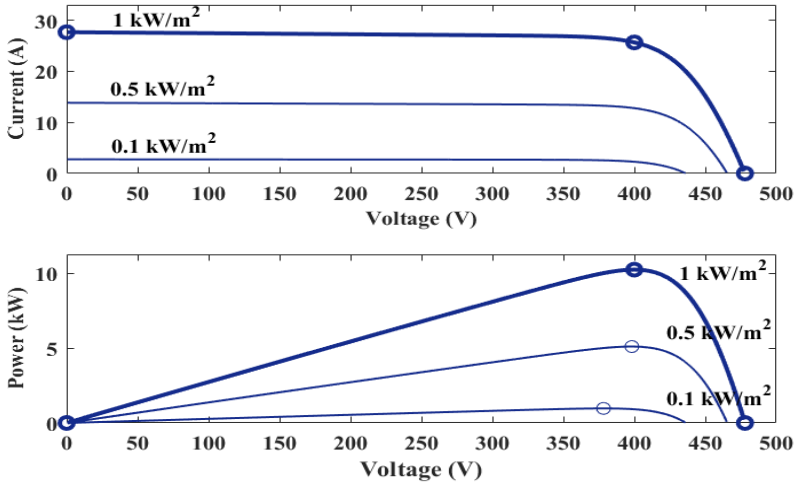

Fig.3. 4(a). I-V and P-V curve of PV array at variable insolation

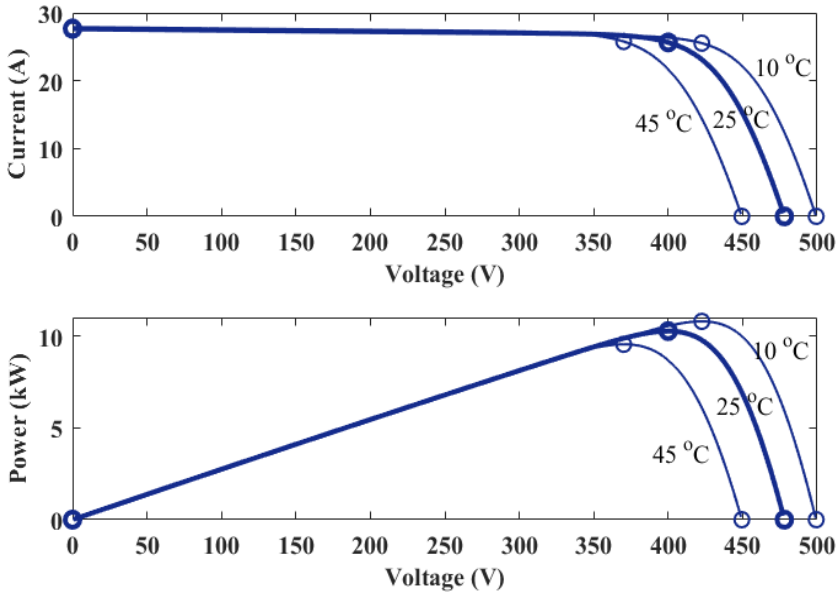

Fig. 3.4(b). I-V and P-V curve of PVarray at variable temperature

3.2.2 Design of Boost Converter

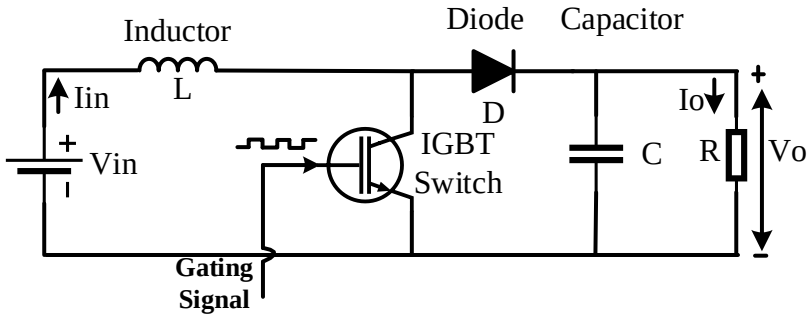

Fig.3.5. Schematic diagram of Boost converter

DC-DC converters are commonly employed for a regulated voltage output from a source which could be effectively controlled. DC-DC converters are buck converter, boost converter and buck-boost converter etc. In the present work, the output voltage of the PV array is 400V and output of the DC-DC converters is required to be 750V, hence, a boost converter is needed. Figure 3.5 depicts the boost converter (dc-dc) having output voltage more than its input voltage. The output voltage and current equations for above converter along with the design parameters are given below [58],[108]-[110],[55].

The output voltage and current equations for above converter are given below:

$$V_O = V_{in}/(1-k) \quad (3.4)$$

$$I_O = I_{in}/(1-k) \quad (3.5)$$

k= 1- ($\frac{V_{in}}{V_O}$)

Where k is duty ratio, V_O is output voltage, I_O is output current, f_{sw} is switching frequency (10 kHz), L is the inductance of the boost converter respectively. Maximum power is tracked by P&O control algorithm. SPV array voltage (Vpv) has been boosted to 750V, by using DC-DC boost converter.

Design parameters of the DC-DC converter are given as:

$$L = k * V_{pv}/(2\Delta i_1 * f_{sw}) \quad (3.6)$$

Calculated value of duty cycle (k)= 1- ($\frac{V_{in}}{V_O}$), is 0.46.

This converter boosts the voltage of SPV array from $V_{pv} = V_{in} =$ 400 V to Vdc=750 V.

The calculated value of k is between 0.46. Δi_1 is the ripple current and taken as 10% of input current ($i_1 = Ppv/V_{in}$ =25.65) of the converter. The calculated value of Δi_1 is 2. 565A. The estimated value of inductance (L) using the equation (3.6) is 3.58mH.

3.3 MAXIMUM POWER POINT TRACKING

PV systems are not linear in nature and depend on environmental conditions viz. temperature, irradiance etc. The nonlinear characteristic of the I-V curve of P-V module has a unique single point of maximum power as shown in figure 3.4. Therefore, special techniques known as MPPT are used to extract the maximum available power from the PV source. The MPPT technique is used to control of these power electronic converters. Several techniques for locating the MPP have been developed over time. These methods differ in a variety of ways, including the number of sensors used, their complexity, price, efficacy range, speed of convergence, how well they detect changes in temperature and/or radiation, the hardware required for implementation, and their general popularity.

3.3.1 Perturb and Observe (P&O) Algorithm

This P&O MPPT is user-friendly, has the simplest algorithm and is simple to implement on any microcontroller, making it ideal for most researcher, to utilise in their applications. P&O involves changing the DC-DC converter's duty cycle as well as the operating voltage of the DC-link connecting the SPV system and the DC-DC converter. Changing the duty cycle of the converter means changing the voltage of the DC-link connecting the converter and SPV system. The sign of

the most recent perturbation and the most recent power increment also determine the direction of the next perturbation.

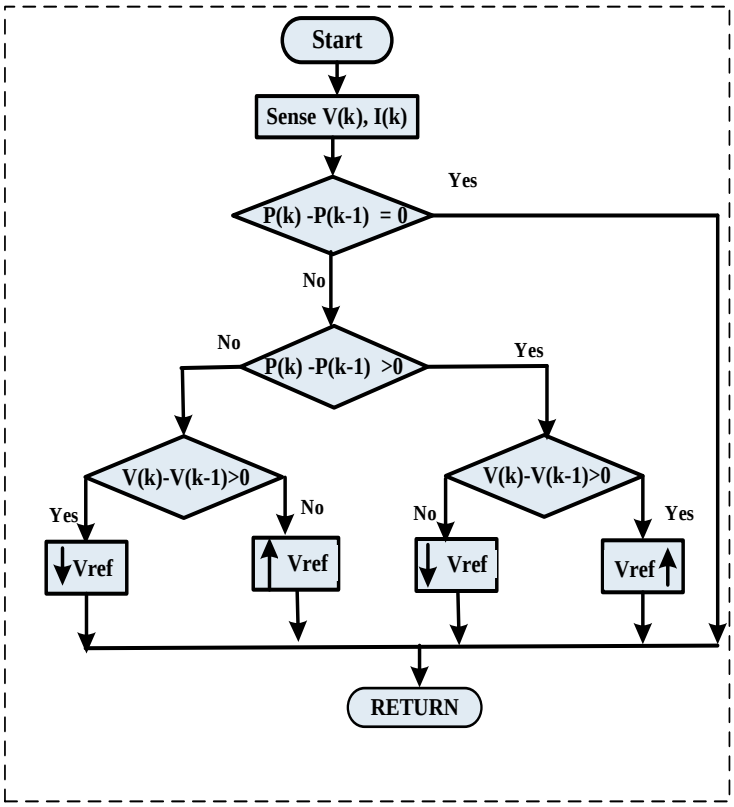

Fig. 3.6. Flowschart of P&O algorithm for MPPT

According to figure 3.8, increasing the voltage on the left of the MPP causes the power to increase, while decreasing the voltage on the right causes the power to decrease. The perturbation should remain in the same direction if the power increases, and if the power decreases, the next perturbation should be in the opposite direction [108]. P&O calculations compare the voltage position after comparing, with obtained power at two places on a P-V curve. The voltage is then changed appropriately to follow the MPP (either to the left or right of the P-V curve). based on aforesaid facts algorithm is implemented and shown in flowchart in figure 3.6.

3.3.2 Incremental Conductance (InC) Algorithm

This approach largely follows the same path from P&O to MPP, but makes use of the special relationship between the I-V curve.

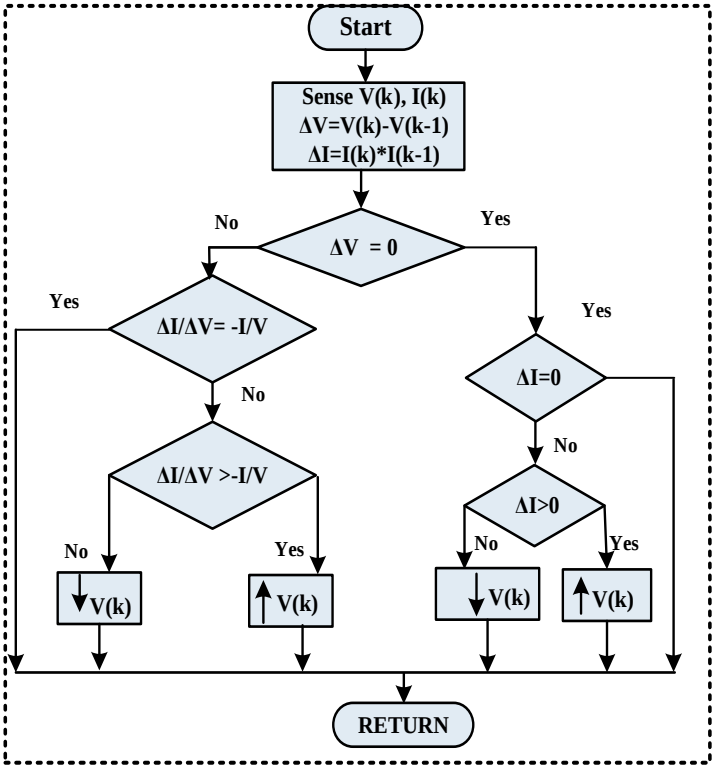

Fig.3.7. Flow chart of InC algorithm for MPPT

In the incremental conductance method, which is based on the incremental and instantaneous conductance of the PV module, the array terminal voltage is always adjusted in accordance with the MPP voltage. According to figure 3.8, the slope of the P-V array power curve is zero at the MPP and increases to a greater extent on the left and decreases to a greater extent on the right side of the MPP.

Following are the fundamental equations for this method.

At MPP, $\frac{dI}{dV} = -\frac{I}{V}$ (3.7)

$Left\ of\ MPP, \frac{dI}{dV} > -\frac{I}{V}$ (3.8)

Right of MPP, $\frac{dI}{dV} < -\frac{I}{V}$ (3.9)

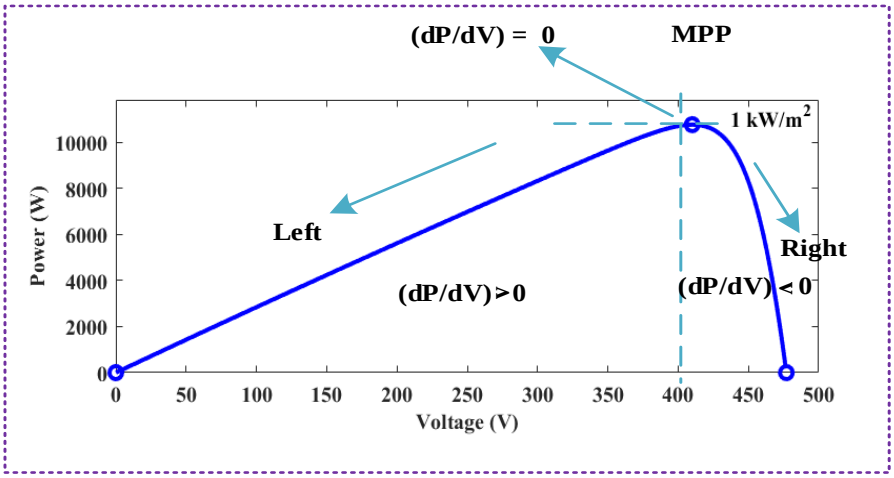

Fig.3.8. P-V curve of the array

Equations' left side denotes the P-V module's incremental conductance, while their right side denotes the instantaneous conductance. The solar array will function at its peak power point when the ratio of change in output conductance equals the negative output conductance. The theory behind this method assumes that the ratio of output conductance change to negative output instantaneous conductance is equal. [108]-[109].

In the present work, Perturb and Observe (P &O) MPPT has been used.

3.4 DESIGN AND SELECTION OF VOLTAGE SOURCE CONVERTER PARAMETER [55],[58]

VSC is an IGBT based three leg converters used to feed power to the load and utility grid. VSC supplies, power to the load/grid and operate at UPF mode thus maintain grid power factor at unity.

3.4.1 DC Link Voltage

Minimum required voltage across dc link capacitor must be more than two times of the voltage per phase of the system.

$$V_{dc} = 2\sqrt{2} * \frac{V_{LL}}{(\sqrt{3}*m)} = (2\sqrt{2}) * 415 / (\sqrt{3} * 1) \quad (3.10)$$

V_{dc}= 677 V

Modulation index (m) is taken as 1, Voltage across dc link obtained from equation (3.10), is 677V for V_{LL} of 415 V and is chosen as 750V.

3.4.2 DC Link Capacitor

$$C_{dc} = I_{dc}/(2 * \omega * V_{dcripple}) \quad (3.11)$$

Where C_{dc} is dc link capacitor, V_{pv} and P_{dc} are PV voltage and power respectively. DC link current ($I_{dc} = P_{dc}/V_{pv}$), when load on one phase is removed DC current is (2/3) of the original current. Considering, $V_{dcripple}$ as 5% of V_{dc}, P_{dc} as 10.25 kW and V_{pv} as 400 V and ω is angular frequency.

C_{dc}= 644.8 μF, calculated value using the equation (3.11), corresponding to load unbalancing of one phase. Selected value of C_{dc} is 1000 μF.

3.4.3 Interfacing Inductors

Interfacing inductor rating of VSC depends on switching frequency (f_{sw}), current ripple (Δi) and dc link voltage (V_{dc}). Interfacing inductor (L_f) is given as follows:

$$L_f = \sqrt{3} * m * V_{dc}/(12 * h * f_{sw} * \Delta i) \quad (3.12)$$

$$L_f = 3.35\ mH$$

Where h is overloading factor, m is modulation index and Δi is current ripple. Assuming,

$m = 1, V_{dc} = 750\ V, h = 1.2, f_{sw} = 10\ kHz\ and\ \Delta i = 10\%$.

The calculated value of L_f is 3.35 mH. In the proposed system L_f of 4 mH is taken. Table 3.1, shows the system parameters considered in this system.

TABLE 3.1. System parameters

Design parameter of boost converter	Values	Unit
Inductor (L)	3.58	mH
Capacitor (C)	1000	μF
Switchign frequency (fsw)	10	kHz
Input voltage of boost converter	400	V
Output voltage of boost converter	750	V
Duty cycle	46	%
Interfacing inductor (L_f)	4	mH
Grid voltage	415	V

3.5 SYSTEM DESCRIPTION AND OPERATING PRINCIPLE

In this section, Solar PV based microgrid has been integrated to the grid using inverter control algorithms. A two-stage three-phase grid-interfaced PV system has been demonstrated. Interfacing inductors (L_f) link the VSC at the point of common connection. The integration of PV system requires voltage source converter (VSC), switching of this converter generates harmonics at the output of microgrid. Control algorithms are used to control the VSC for the grid integration for efficient utilization of power. VSC control algorithms compensates harmonics and reactive power of the local loads.

A PV system's main objective is to transmit power to loads and the grid while mitigating the power quality issues such as reactive power, unbalanced currents, and load harmonics present in the load (if any) and supplying sinusoidal balanced grid currents. In the present work, various VSC's conventional control algorithm and a novel intelligence based modified synchronous reference frame-based control algorithms are developed and proposed for grid connected PV system. The proposed control algorithms are evaluated and compared with conventional control algorithms, by conducting simulation studies using MATLAB-Simulink.

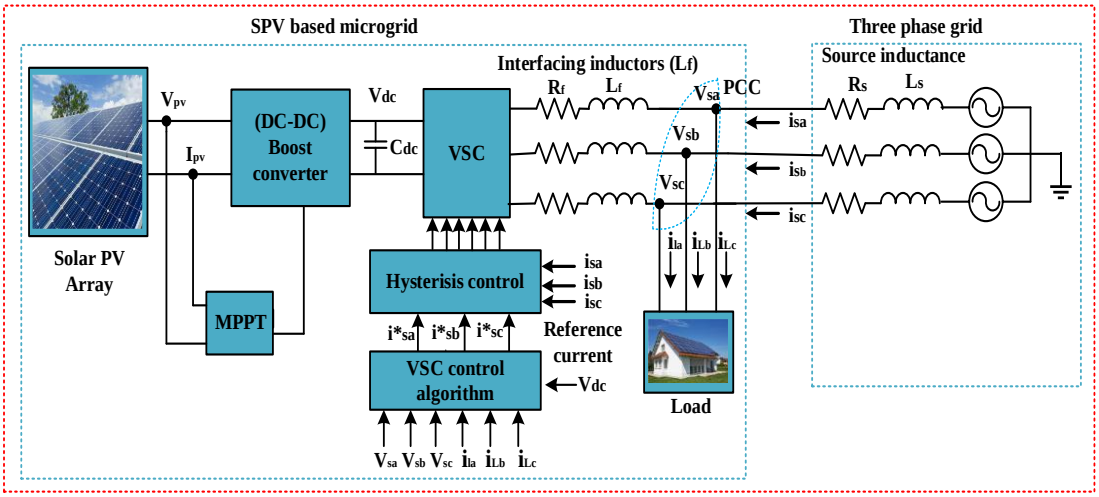

Fig.3.9. Proposed model of grid integrated PV system

Figure 3.9, depicts a two-stage three-phase grid-interfaced SPV system with a 10.25 kW SPV array. The MPPT (P&O) is utilised to get the maximum power out of a PV array under a range of scenarios of environmental conditions. VSC control algorithms are developed to generate reference current, which is subsequently utilised to produce inverter (VSC) switching pulses.

3.6 VSC (PV INVERTER) CONTROL ALGORITHMS

For the voltage source converter, a variety of control algorithms viz. Conventional, adaptive theory and intelligence based are available to estimate reference currents. In the section, conventional and intelligence-based VSC control algorithm has been modelled and simulated along with the design, and modelling of grid connected Solar PV system. The following are the VSC control algorithms used in the current work:

- Conventional Control Algorithms
  - Synchronous reference frame theory (SRFT)
  - Instantaneous reactive power theory (IRPT)
  - Unit Template based conventional control algorithm
- Proposed Intelligence based VSC control algorithms
  - Novel modified synchronous reference frame-based control algorithm

3.6.1 Conventional Control Algorithms

3.6.1.1 *Synchronous reference frame theory-based conventional control algorithm* [110]-[113],[55]

Figure 3.10 represents the block diagram of reference current estimation using SRF control algorithm under UPF mode of operation. Park's transformation has been used to convert load current components from synchronous rotating reference frame to d-q reference frame.

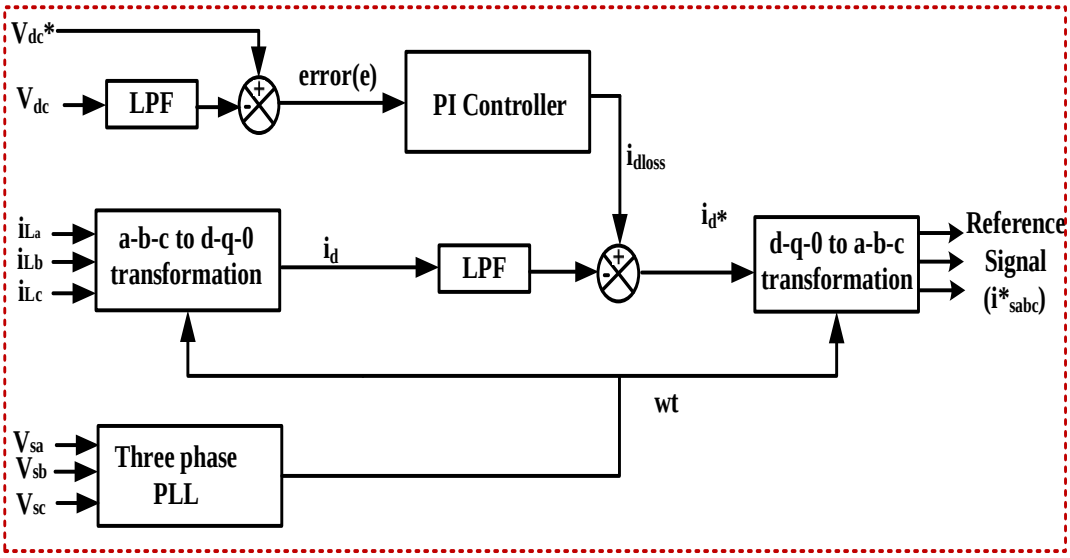

Fig.3.10. Block diagram of SRF control algorithm

Three phase current in the a-b-c frame is transformed into d-q-0 frame by means of Park's conversion as given below:

$$\begin{bmatrix} i_d \\ i_q \\ i_0 \end{bmatrix} = \frac{2}{3}\begin{bmatrix} \cos w\,t & \cos(wt-120) & \cos(wt+120) \\ \sin wt & \sin(wt-120) & \sin(wt+120) \\ 1/2 & 1/2 & 1/2 \end{bmatrix}\begin{bmatrix} i_{La} \\ i_{Lb} \\ i_{Lc} \end{bmatrix} \quad (3.13)$$

PI controller, is used to maintain the voltage across dc link. fundamental active (i_d) and reactive (i_q) component of load current is extracted by means of low pass filter. VSC must supply the reactive power demand of the load to operate the SRF algorithm in unity power factor mode. Reference reactive component (i_q^*) must be zero$(i_q^* = 0)$, to compensate the reactive demand of the load. While (i_d) is added with output of PI controller (i_{dloss}) in order to regulate the dc link voltage.

$$i_d^* = {}_{i_d} + i_{dloss} \quad (3.14)$$

Further converting the reference signal from d-q frame to a-b-c by means of inverse Parks transformation, provides reference current ($i_{sa}^*, i_{sb}^*, i_{sc}^*$).

Generated reference current (i^*_{sabc}) must be in same phase with grid voltage, using reverse Park's conversion as represented below, i^*_{sabc} are obtained:

$$\begin{bmatrix} i_{sa}^* \\ i_{sb}^* \\ i_{sc}^* \end{bmatrix} = \begin{bmatrix} cos\ wt & \sin wt & 1 \\ \cos(wt-120) & \sin(wt-120) & 1 \\ \cos(wt+120) & \sin(wt+120) & 1 \end{bmatrix}\begin{bmatrix} i_d \\ i_q \\ i_0 \end{bmatrix} \quad (3.15)$$

Reference current are compared with sensed grid current $(i_{sa}, i_{sb,} i_{sc})$ in hysteresis control to generate switching signals to operate VSC.

3.6.1.2 *Instantaneous reactive power theory (IRPT) -based conventional control algorithm*

Figure 3.11 depicts the block diagram representation of IRPT control algorithm of reference current. In this control Clark's transformations are used to converts the PCC voltage and load current in to α-β frame respectively as given below:

$$\begin{bmatrix} v_\alpha \\ v_\beta \end{bmatrix} = \sqrt{(2/3)}\begin{bmatrix} 1 & -1/2 & -1/2 \\ 0 & \sqrt{3}/2 & -\sqrt{3}/2 \end{bmatrix}\begin{bmatrix} v_{sa} \\ v_{sb} \\ v_{sc} \end{bmatrix} \quad (3.16)$$

$$\begin{bmatrix} i_{L\alpha} \\ i_{L\beta} \end{bmatrix} = \sqrt{(2/3)}\begin{bmatrix} 1 & -1/2 & -1/2 \\ 0 & \sqrt{3}/2 & -\sqrt{3}/2 \end{bmatrix}\begin{bmatrix} i_{La} \\ i_{Lb} \\ i_{Lc} \end{bmatrix} \quad (3.17)$$

Instantaneous active power (p_L) and Instantaneous reactive power (q_L) are computed using the equations (3.18) and (3.19) as given below:

$$p_L = v_\alpha i_{L\alpha} + v_\beta i_{L\beta} \tag{3.18}$$

$$q_L = v_\alpha i_{L\beta} + v_\beta i_{L\alpha} \tag{3.19}$$

$$\begin{bmatrix} p_L \\ q_L \end{bmatrix} = \begin{bmatrix} \overline{p_L} & +\widetilde{p_L} \\ \overline{q_L} & +\widetilde{p_L} \end{bmatrix} \tag{3.20}$$

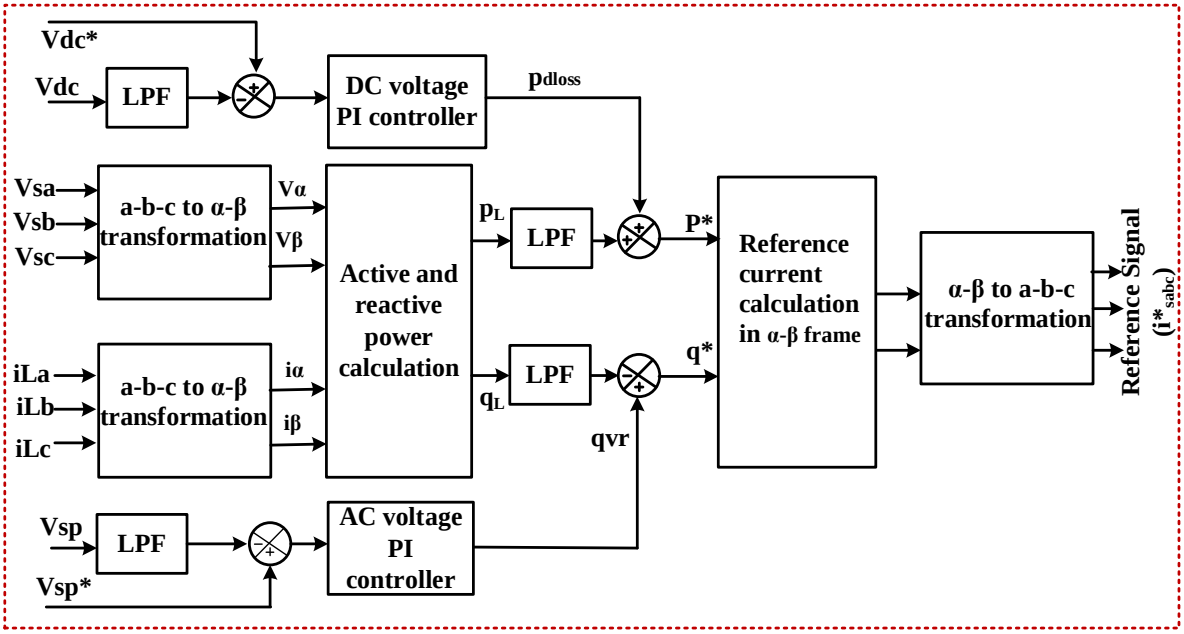

Fig. 3.11. Block diagram of IRPT control algorithm

Computed power contains both dc and ac component. To filter out the fundamental active and reactive power components, low pass filters are used. Reference active and reactive component of power is estimated using equation given below:

$$p^* = \overline{p_L} + p_{loss} \tag{3.21}$$

$$q^* = \overline{q_L} - q_{vr} \tag{3.22}$$

The P_{loss} refers to the instantaneous active power required to adjust the DC capacitor at its reference voltage. Additionally, the PCC voltage must be adjusted to its reference value using q_{vr}, necessary instantaneous reactive power.

Reference current ($i_{sa}^*, i_{sb}^*, i_{sc}^*$) is estimated as given below:

$$\begin{bmatrix} i_{sa}^* \\ i_{sb}^* \\ i_{sc}^* \end{bmatrix} = \sqrt{(2/3)} \begin{bmatrix} 1 & 0 \\ -1/2 & \sqrt{3}/2 \\ -1/2 & -\sqrt{3}/2 \end{bmatrix} \begin{pmatrix} v_\alpha & v_\beta \\ -v_\beta & v_\alpha \end{pmatrix}^{-1} \begin{bmatrix} p^* \\ q^* \end{bmatrix} \quad (3.23)$$

In PFC mode reference reactive power component (q^*) should be zero in the equation (3.23) to maintain the grid at unity power factor. Reference current are compared with sensed grid current ($i_{sa}, i_{sb,} i_{sc}$) in hysteresis control and generate switching signals to operate VSC.

3.6.1.3 *Unit template-based conventional control algorithm* [105],[110]

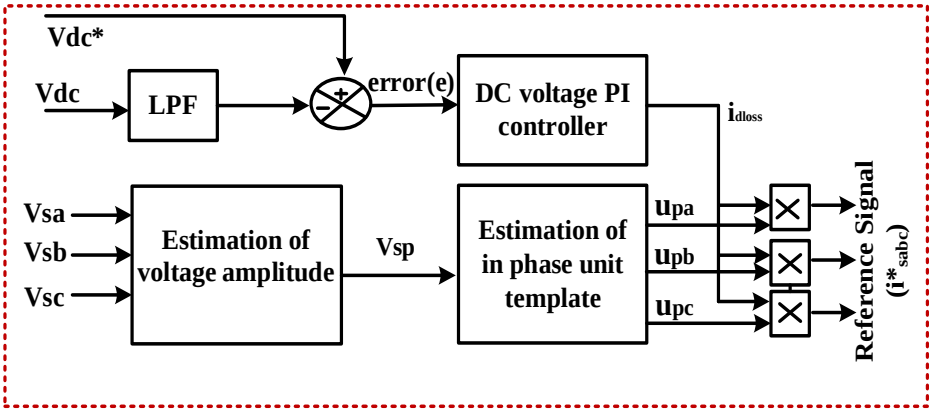

Fig.3.12. Block diagram of unit template control algorithm

Unit template control algorithm of VSC for estimating the reference currents is shown in figure 3.12. The unit template is a simple VSC control technique for estimating the reference current. This control algorithm can be made flexible and it can be modified either for PFC or voltage regulation at PCC. The unit template control algorithm in PFC mode of operation is performed to estimate reference current as shown in the figure 3.12, PCC voltage and DC bus voltage of VSC are used for implementing this control algorithm. A band-pass filter (BPF) can be used to remove distortion in sampled PCC voltages in real time implementation. Assume that after filtering the PCC voltage signal is (v_{sa}, v_{sb}, v_{sc}). Peak amplitude of PCC voltage is calculated as:

$$\mathcal{V}_t = \sqrt{\frac{2}{3}(\mathcal{V}_{sa}^2 + \mathcal{V}_{sb}^2 + \mathcal{V}_{sc}^2)} \quad (3.24)$$

The in-phase unit voltages template ($\mathcal{U}_{pa,} \mathcal{U}_{pb,} \mathcal{U}_{pc}$) can be calculated using phase voltages ($\mathcal{V}_{sa}, \mathcal{V}_{sb}, \mathcal{V}_{sc}$) with peak amplitude ($\mathcal{V}_t$) as follows:

$$\mathcal{U}_{pa} = \frac{\mathcal{V}_{sa}}{\mathcal{V}_t}, \mathcal{U}_{pb} = \frac{\mathcal{V}_{sb}}{\mathcal{V}_t}, \mathcal{U}_{pc} = \frac{\mathcal{V}_{sc}}{\mathcal{V}_t} \quad (3.25)$$

Further, error in DC link voltage is compensated using PI controller. Output of PI controller is considered as amplitude of reference current(i_{dloss}) . Amplitude of reference current(i_{dloss}) are multiplied by in- phase unit template to get reference current ($i_{sa}^*, i_{sb}^*, i_{sc}^*$) as given below:

$$i_{sa}^* = i_{dloss} * \mathcal{U}_{sa}, i_{sb}^* = i_{dloss} * \mathcal{U}_{sb}, i_{sc}^* = i_{dloss} * \mathcal{U}_{sc} \quad (3.26)$$

Reference current($i_{sa}^*, i_{sb}^*, i_{sc}^*$) are compared with sensed grid current ($i_{sa}, i_{sb,} i_{sc}$) in hysteresis control and generate switching signals to operate VSC [112]-[115].

3.6.2 Proposed Intelligence Based Novel Modified Synchronous Reference Frame-Based Control Algorithm

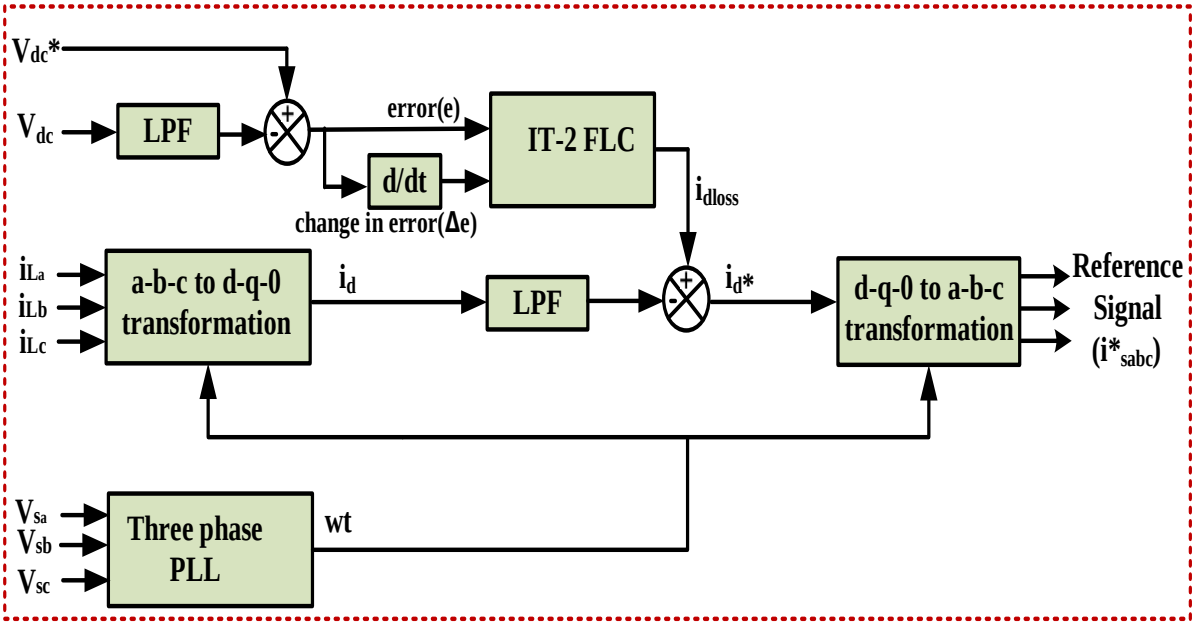

Fig. 3.13. Proposed modified SRF Control algorithm for reference current generation of PV inverter

Novel modified SRF Control algorithm has been presented in figure 3.13. In the present studies, interval type-2 fuzzy logic controller (IT-2 FLC) has been proposed to regulate the DC link voltage of grid integrated SPV system. Proposed IT-2 FLC based control block diagram of DC link voltage of inverter is shown in figure 3.14(a). Controller has two input variables: error ($e(k)$), change in error ($\Delta e(k)$) and one output variable (i_{dloss}).

$$e(k) = V_{dc}^* - V_{dc}(k) \quad (3.27)$$

$$\Delta e(k) = e(k) - e(k-1) \quad (3.28)$$

where V_{dc}^* is reference DC link voltage and $V_{dc}(k)$ is actual sensed DC link voltage at k_{th} iteration, $e(k)$ and $\Delta e(k)$ are error and change in error respectively at k_{th} iteration [71]-[72].

Structure of proposed controller along with, description of each block viz. fuzzification, rule base and defuzzification involving type reduction are presented. Error ($e(k)$) and change in error ($\Delta e(k)$) represents input variables and i_{dloss} as an output variable.

IT-2 FLC has four stages: fuzzification, rule base, inferencing and output processing which are explained below:

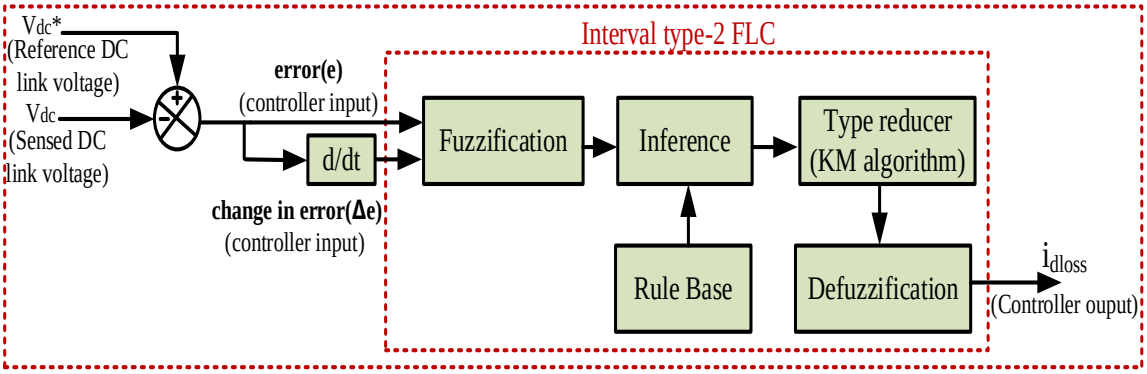

(a) Proposed interval type-2 FLC for DC link voltage control of inverter

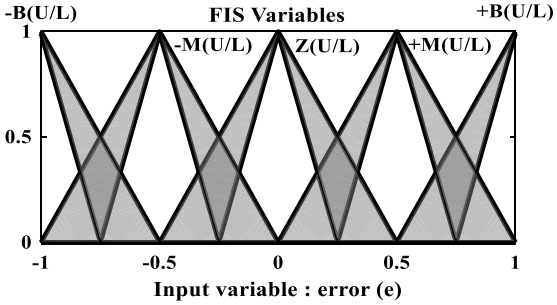

(b)

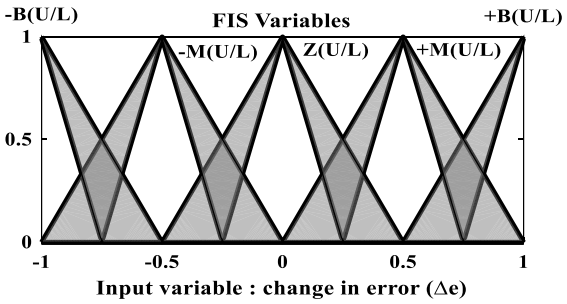

(c)

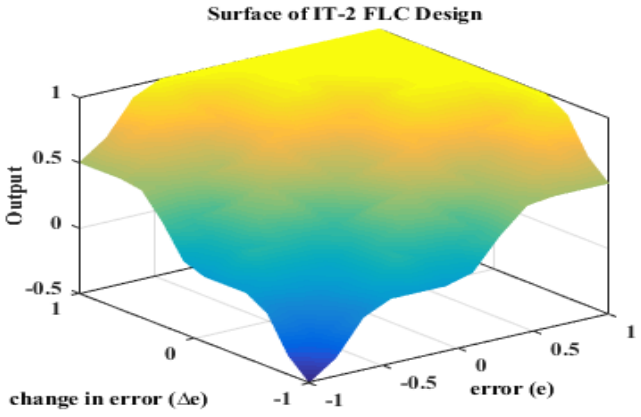

(d)

Fig. 3.14 (a). Block diagram of proposed interval type-2 FLC, (b) and (c) Membership function for input variable 'error' and 'change in error' respectively (d) surface view of IT-2 fuzzy logic design

Interval type-2 fuzzification

Figure 3.15, represents an example for fuzzification of IT-2 FLC. IT-2 FLC membership value in the [0, 1] domain is defined for each input. For each input two membership levels are computed one is called the upper membership function (UMF) and other lower membership function (LMF). Interval type-2 FLC with an extra dimension called footprint of uncertainty (FOU) is capable of handling large amount of uncertainty. In the figure 3.15, when e (k) = α'_1, a vertical line at α'_1 intersects FOU ($\tilde{P}$) everywhere in the interval $\left[\underline{S}_{\tilde{P}}(\alpha'_1), \overline{S}_{\tilde{P}}(\alpha'_1)\right]$ and when Δe(k) = α'_2, vertical line at α'_2 intersects, FOU ($\tilde{Q}$) everywhere in the interval $\left[\underline{S}_{\tilde{Q}}(\alpha'_2), \overline{S}_{\tilde{Q}}(\alpha'_2)\right]$.

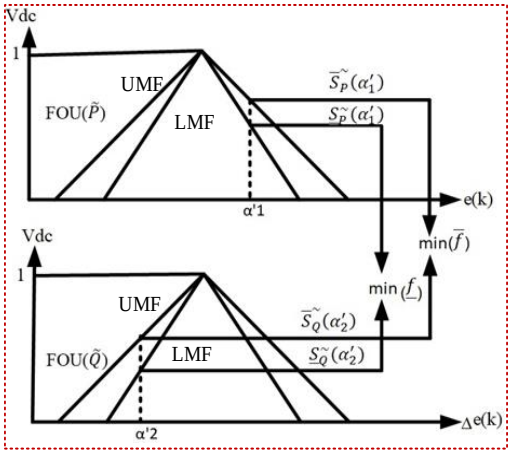

Fig. 3.15. Fuzzification and inference of IT-2 FLC

Rule base and inference system

In the design of rule base of IT-2 FLC for inverter, five sets of triangular membership function are used, as Negative big: ((–B (U/L)), Negative medium (–M (U/L)), zero (Z (U/L)), Positive medium (+M (U/L)), Positive big (+B (U/L)). Interval type-2 fuzzy rule base for proposed controller is written in the equation given below:

IF e(k) is $\tilde{P}$ and Δe(k) is $\tilde{Q}$ THEN output is $\tilde{R}$ (3.29)

where $\tilde{P}$ and $\tilde{Q}$ are IT-2 fuzzy sets and $\tilde{R}$ is output. Therefore, using equation (3.34), 25 rule bases have been developed for computation of i_{dloss} as shown in table 3.2.

Table 3.2. Rule Base for IT-2 FLC

Error(e) \ change in error (Δe)	–B (U/L)	–M (U/L)	Z (U/L)	+M (U/L)	+B (U/L)
–B (U/L)	–M(U/L)	Z(U/L)	Z(U/L)	+M(U/L)	+M(U/L)
–M (U/L)	Z(U/L)	Z(U/L)	+M(U/L)	+M(U/L)	+B(U/L)
Z (U/L)	Z(U/L)	+M(U/L)	+M(U/L)	+B(U/L)	+B(U/L
+M (U/L)	+M(U/L)	+M(U/L)	+B(U/L)	+B(U/L	+B(U/L
+B (U/L)	+M(U/L)	+B(U/L)	+B(U/L	+B(U/L	+B(U/L

Inference process combines rule and gives mapping from input to output. For a single rule inference process is shown in figure 3.15. Two firing levels are then computed, an upper firing level, $\overline{f}$ and a lower firing level $\underline{f}$.

Where, $\overline{f} = min[\overline{S}_P^{\sim}(\alpha_1'), \overline{S}_Q^{\sim}(\alpha_2')]$ and $\underline{f}$ =min $[\underline{S}_P^{\sim}(\alpha_1'), \underline{S}_Q^{\sim}(\alpha_2')]$.

Type reduction and defuzzification

Type 1 fuzzy set is generated by type reduction and the reduced fuzzy set is converted into crisp value in defuzzification stage. In the present work, Karnik Mendel (KM) algorithm has been used for type reduction and defuzzification.

3.7 RESULTS AND DISCUSSIONS

The simulation results for all the VSC control algorithms discussed, have been presented. For conventional algorithm, under nonlinear load along with the THD (%) in grid current has been presented and for the developed novel intelligence based modified SRF control has been analysed in details under various load and environment conditions.

3.7.1 Performance of Various Conventional Control Algorithms Under Nonlinear (Balanced/Unbalanced) Load at STC Input

To analyse the efficacy of various control algorithms under nonlinear load, a bridge rectifier has been considered with RL load (R=100 Ω, L=100 mH). Further, to create the unbalance in the load, one phase is kept open from 0.15 to 0.25 seconds. Proposed system using conventional VSC control algorithm is supposed to be working at standard test condition (1000W/m^2, 25^{0}C) in PFC mode of operation.

Simulation results using various control algorithms viz. SRFT, IRPT and unit template algorithms under nonlinear (balance/unbalance) load are given in the figure 3.16-3.19. To impose the unbalance, one phase is kept open between 0.15 to 0.25 second. It can be seen from figure 3.16-3.18, that all the algorithms are efficient in maintaining the grid current sinusoidal and balanced for the unbalance load current between 0.15 to 0.25 sec. Figure 3.19, shows the THD (%) in load current waveform 29.39%. Furthermore, it can be seen from figure 3.20-3.22, and table 3.3, that grid current THD (%) is well within the IEEE standard-519, while THD (%) in load current is 29.39%.

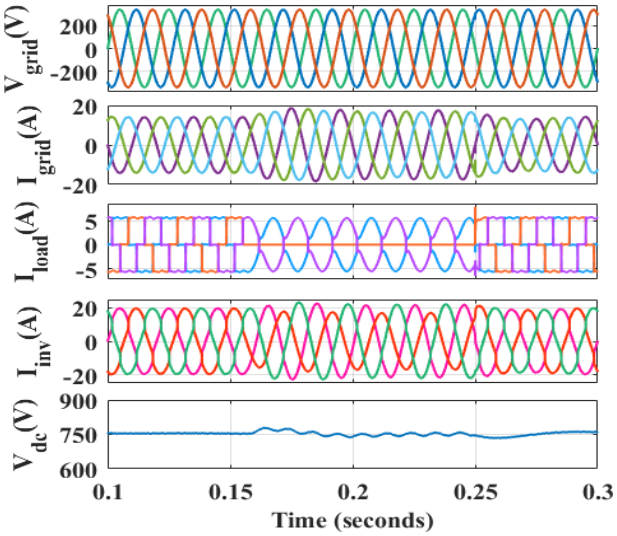

Fig. 3.16. Performance using SRF control

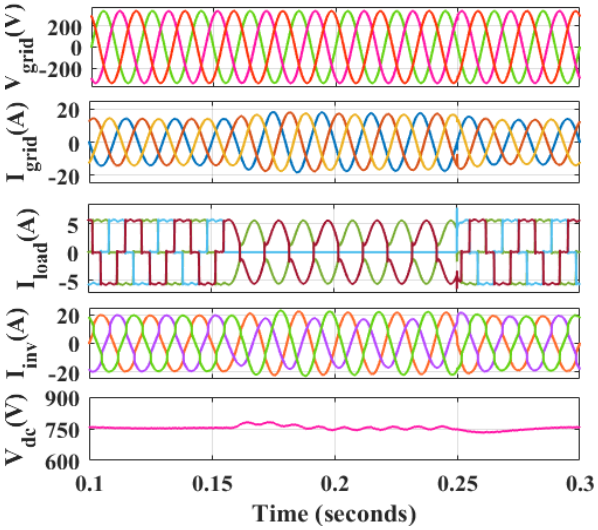

Fig. 3.17. Performance using IRPT control

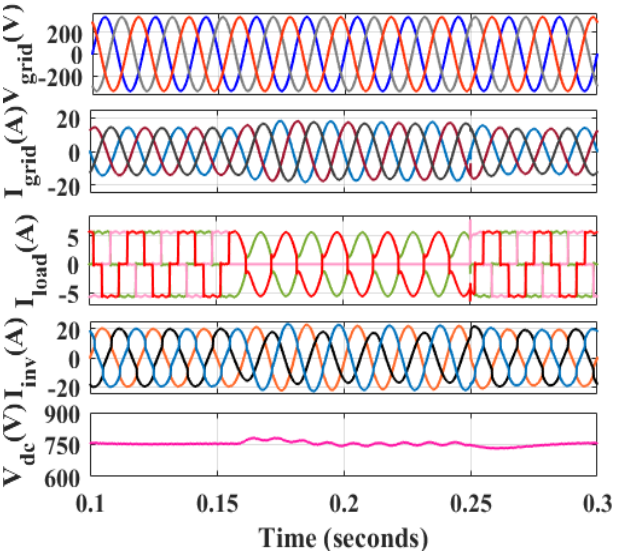

Fig. 3.18. Performance using unit template control

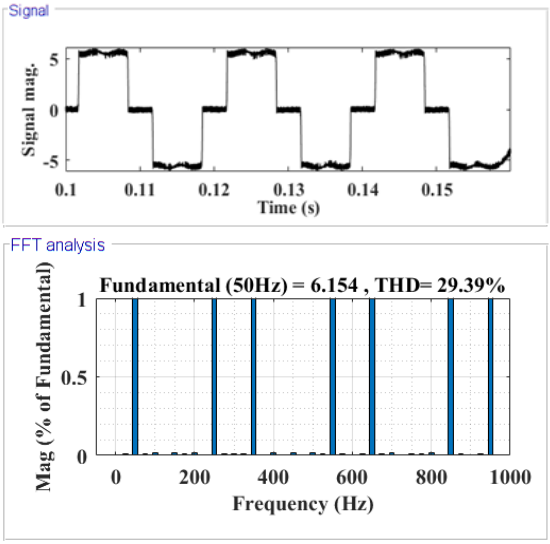

Fig. 3.19. THD (%) in nonlinear load current

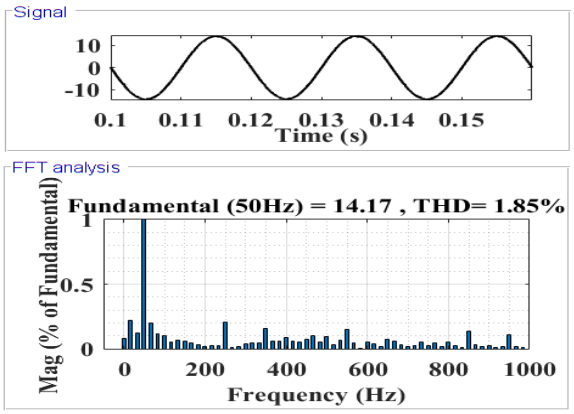

Fig. 3.20. THD (%) in grid current using SRF control

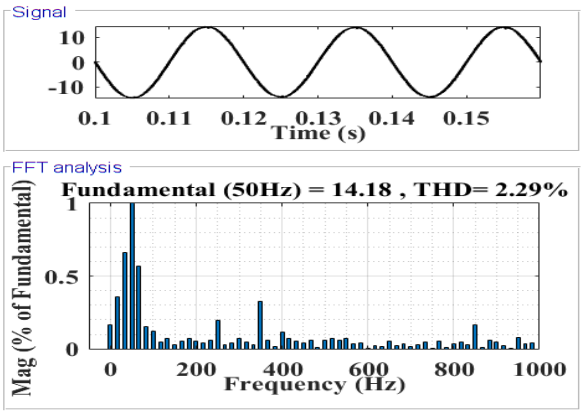

Fig. 3.21. THD (%) in grid current using IRPT control

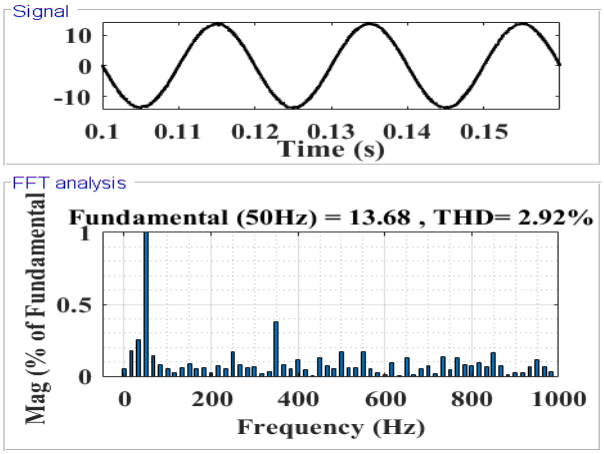

Fig. 3.22. THD (%) in grid current using unit template control

3.7.2 Proposed Novel Intelligence Based Modified SRF Based Control Algorithm

3.7.2.1 *Performance under linear/nonlinear unbalanced load at STC*

The performance of proposed novel intelligent based modified SRF based control algorithm under linear (5kVA, 0.8 pf) and nonlinear load (three phase bridge rectifier with RL load, R=100Ω, L=100mH), depicted in figure 3.23 and figure 3.24 respectively. Various parameter of the system viz. V_{grid}, I_{grid}, I_{load}, I_{inv},V_{dc} and power balance between grid, load and inverter are also analyzed.

It can be seen from figure *3.23* that till 0.15 seconds PV inverter supplies 4kW active and 3.0 kVAR of reactive *power* demand of the load (5kVA, 0.8 pf), Vgrid and Igrid are 180° out of phase (as excess 6.25 kW power is supplied to the grid), Vdc is maintained at 750V. The inverter alone supplies the load active and reactive power demand, which decreases the reactive power drawn from the grid to zero, demonstrating that the proposed control is effective in maintaining the grid at UPF. Further, unbalanced condition occurs at 0.15 seconds. Performance of the proposed control under linear

unbalanced load condition by keeping one phase (phase b) disconnected between 0.15 to 0.35 seconds is studied and various parameters viz. V_{grid}, I_{grid}, I_{load}, I_{inv}, P_{grid}, Q_{grid}, P_{inv}, Q_{inv}, P_{load}, Q_{load}, and V_{dc} are analyzed and depicted in figure 3.23. During unbalance period, inverter current compensates, effect of load unbalance and maintains grid current to be balance. It also supplies the load requirement for reactive power and thus holds the grid at UPF along with the balance grid current. Furthermore, between 0.35 to 0.4 seconds, operating at its initial load (5kVA, 0.8 pf) condition. It has been realised that during single phasing, inverter act as a load balancer by minimizing the unbalanced in grid current while sharing the power between load and grid during single phasing in three phase system, maintains I_{grid} to be sinusoidal and V_{dc} is maintained at 750 V.

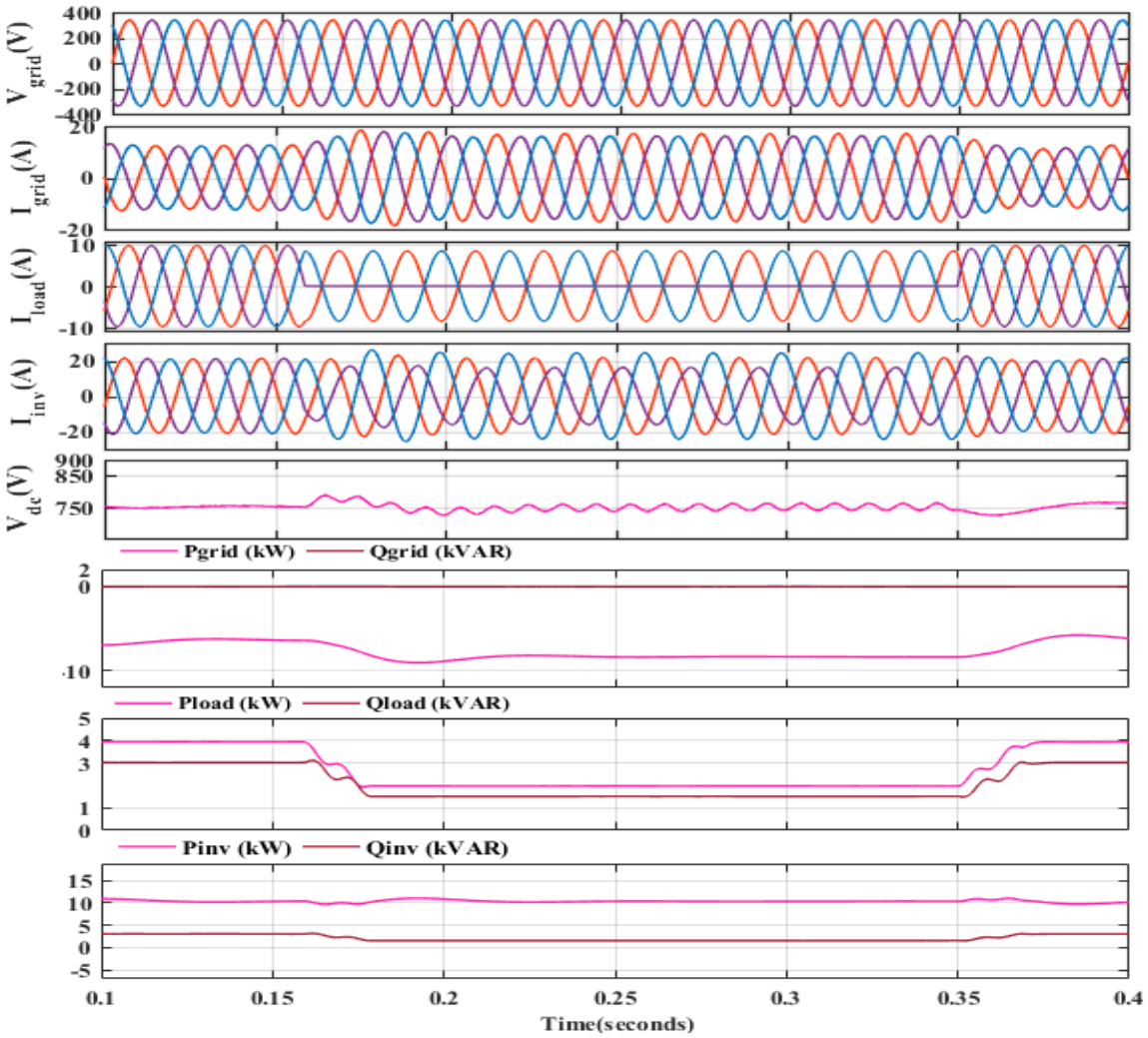

Fig. 3.23. Performance of SPV based microgrid under linear unbalanced load at STC for developed algorithm

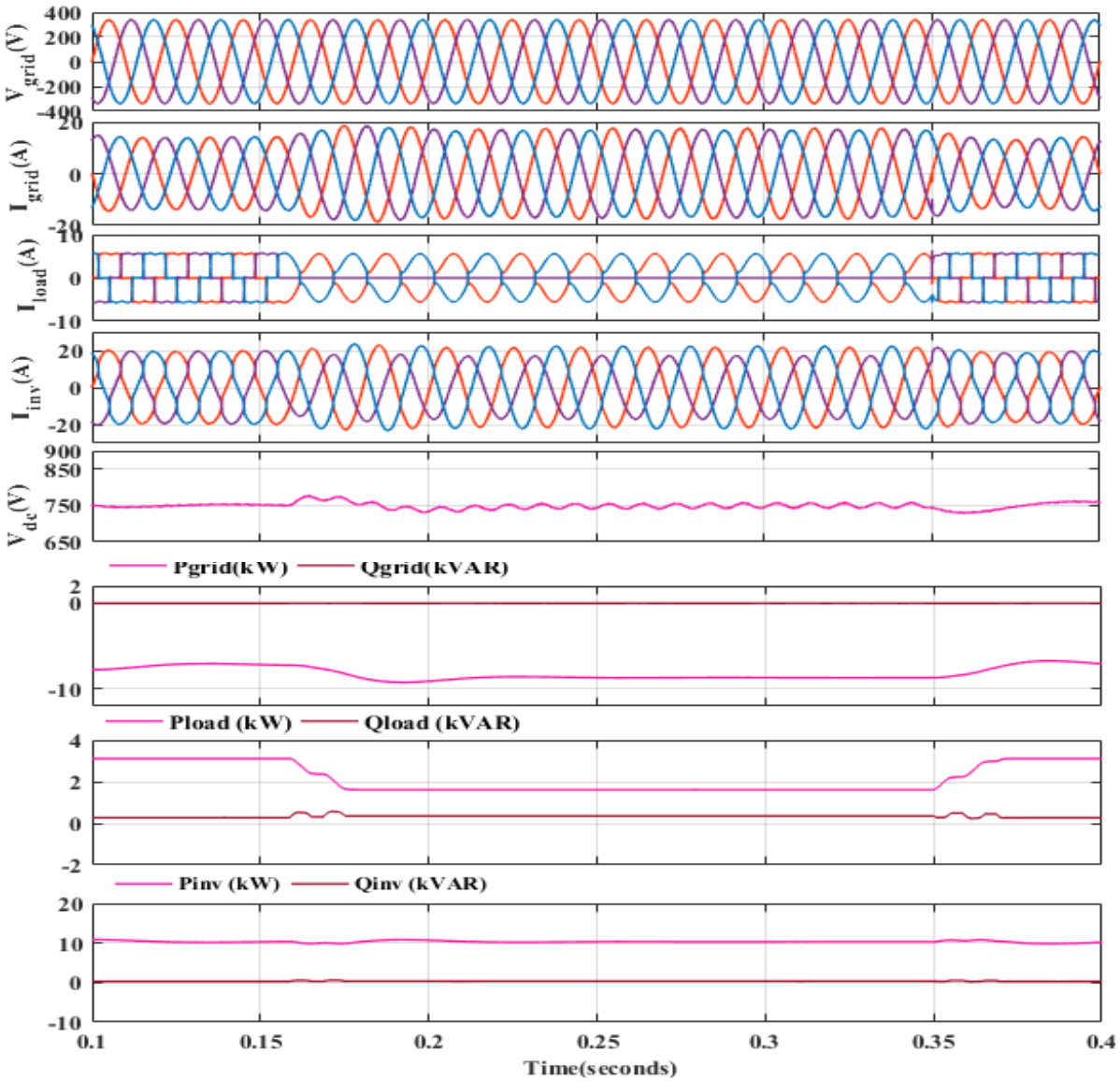

Fig.3.24. Performance of SPV based microgrid under nonlinear unbalanced load at STC for developed algorithm

Further, to test the proposed control under nonlinear load (three phase bridge rectifier with RL load, R=100Ω, L=100mH), has been considered and results are shown in figure 3.24. It is observed that till 0.15 seconds; PV system supplies its nominal power of 10.25kW. It is observed from figure 3.24, that till 0.15 seconds V_{grid} and I_{grid} are 180° out of phase, maintains V_{dc} at 750V, PV inverter supplies 3.1kW active power demand of the load. Further, remaining 7.15 kW power of the PV system is supplied to the grid.

Further, proposed control under nonlinear unbalanced condition is also tested. Under nonlinear unbalanced load condition by one phase 'b' of load disconnected between 0.15 to 0.35 seconds

and various parameters viz. V_{grid}, I_{grid}, I_{load}, I_{inv}, P_{grid}, Q_{grid}, P_{inv}, Q_{inv}, P_{load}, Q_{load}, and V_{dc} are analyzed and presented in figure 3.24, during unbalance period, inverter current compensates, effect of load unbalance and maintains balanced grid current. It also supplies the load requirement for reactive power and thus holds the grid at UPF along with the balance grid current. Furthermore, between 0.35 to 0.4 seconds, operating at its initial nonlinear load (three phase bridge rectifier with RL load, R=100Ω, L=100mH).

It has been realised that during single phasing also grid current is sinusoidal and V_{dc} is maintained at 750 V. THD (%) in I_{grid} is also maintained at 1.71% as depicted in figure 3.25 which is as per IEEE standard 519-2014, are well within the limit, while THD (%) in nonlinear load current is 29.38%, can be seen from figure 3.26.

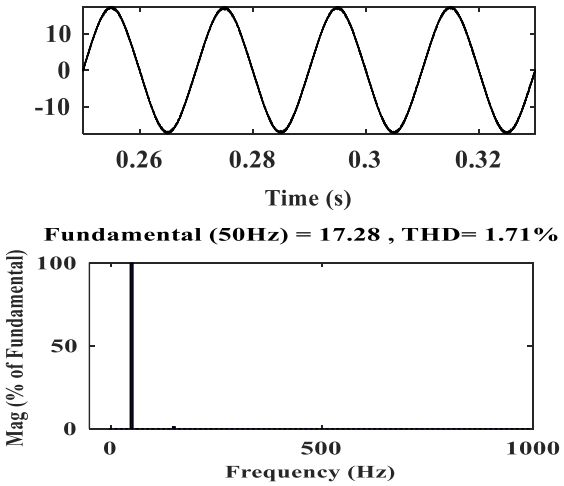

Fig. 3.25. THD (%) in grid current under nonlinear load

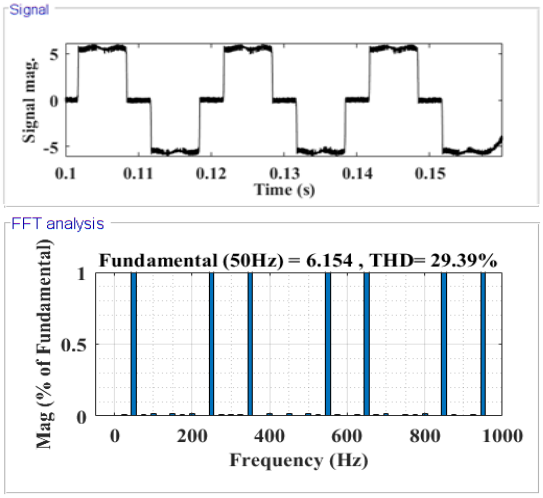

Fig. 3.26. THD (%) in nonlinear load current

3.7.2.2 *Performance under variable load at STC*

Furthermore, to test the robustness of the proposed control under varying load condition has been analysed. A nonlinear load of a three-phase bridge rectifier with RL load (R=100Ω, L=100mH) is connected, and operating at its initial nonlinear load as shown in figure 3.27. For the load varying conditions between 0.15 to 0.35seconds, an extra linear load of 5kVA, 0.8 pf lagging is added at 0.15 seconds in the system of existing nonlinear load. After 0.15 seconds load demand is 7.1kW and 3 kVAR, out of which 7.1kW is supplied by PV inverter, as its generated power is 10.25 kW, after satisfying the load requirement, remaining power 3.15 kW is supplied to grid and reactive demand is met by inverter. It has been realised that during load

variation also grid current is sinusoidal and V_{dc} is maintained at 750 V. The inverter alone supplies the load active and reactive power demand, which decreases the reactive power drawn from the grid to zero, demonstrating that the proposed control is effective in maintaining the grid at UPF. It has been observed that even under non-linear load conditions, the proposed control approach compensates, the effect of reactive power, and non-linearity of the load hence improves the power factor, maintains sinusoidal and balanced grid current.

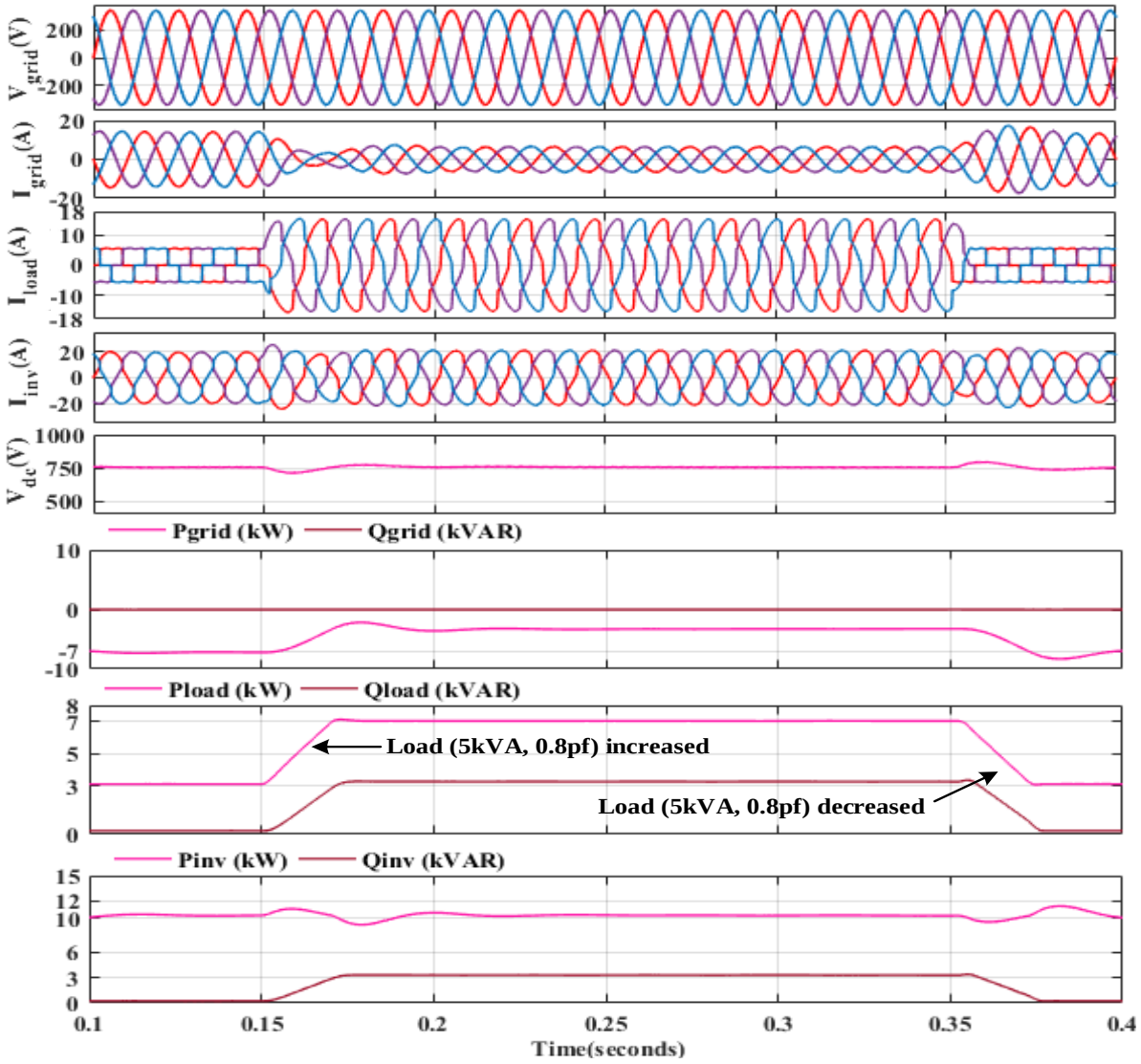

Fig. 3.27. Performance of SPV based microgrid under variable nonlinear load at STC

3.7.2.3. *Performance under linear and nonlinear load condition at Varying insolation*

Further to test robustness of proposed IT-2 FLC, the controller is tested under linear/nonlinear load at varying insolation. Solar insolation is reduced at 0.15 second from 1000W/m^2 to 700W/m^2 till 0.25 second, between 0.25 to 0.35 insolation is minimum i.e.,700W/m^2 and again increased from 0.35 second to 0.45 second upto 1000 W/m^2. Due to decrease in solar insolation, solar PV current decreases that leads to decrease in output power of solar PV and vice versa, between 0.25 to 0.35 insolation is minimum i.e.,700w/m^2, thus power supplied by the inverter is minimum under this period.

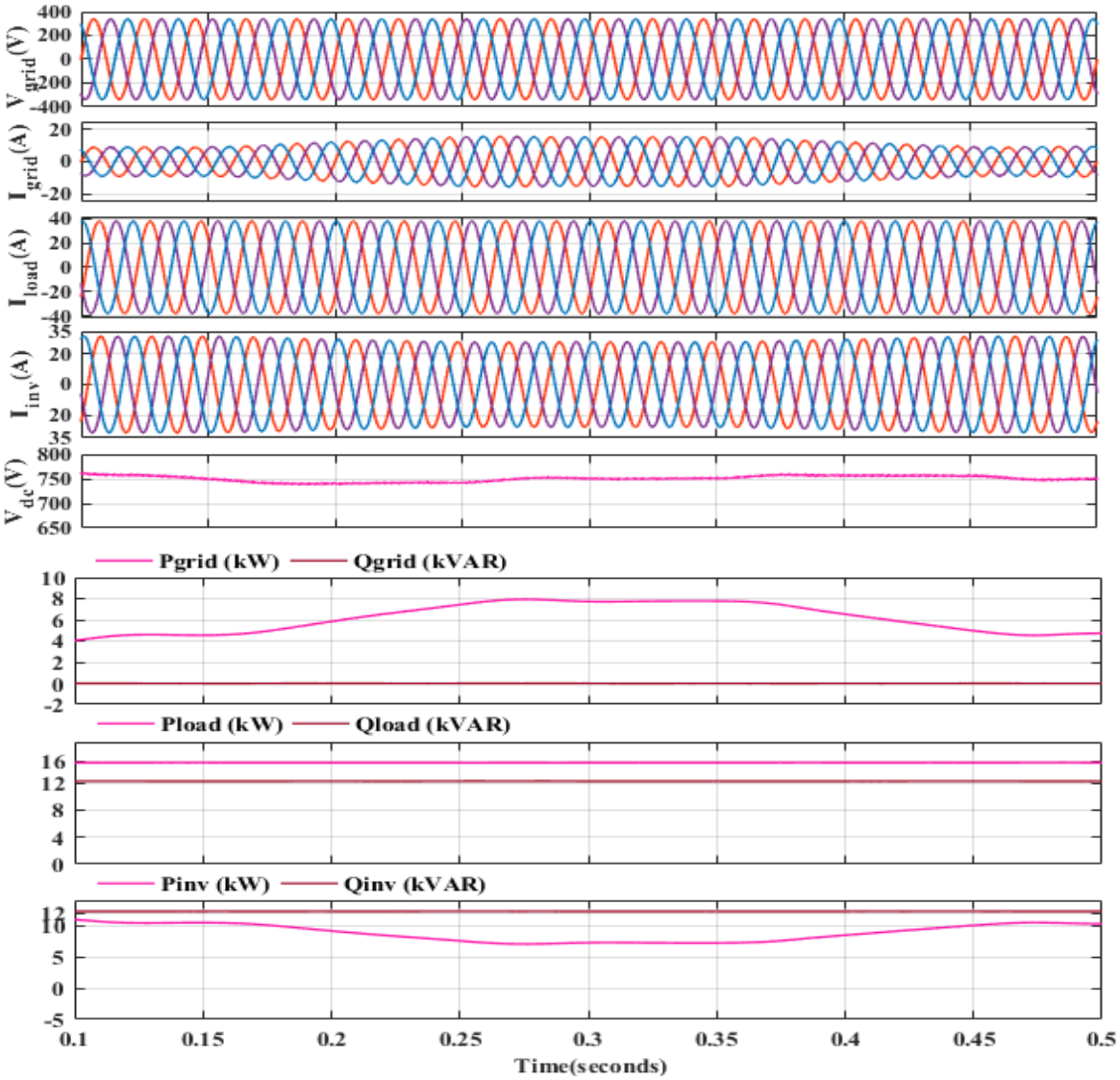

Fig. 3.28. Performance of SPV based microgrid under linear load at varying insolation

A 20kVA, 0.8 pf lag linear load is considered, simulated results and corresponding various parameters viz. V_{grid}, I_{grid}, I_{load}, I_{inv}, P_{grid}, Q_{grid}, P_{inv}, Q_{inv}, P_{load}, Q_{load}, and V_{dc} of the PV inverter are shown in figure 3.28. It is observed from figure 3.28, between 0.1 to 0.15 second, that both V_{grid} and I_{grid} are in phase (as power is supplied from grid to load), V_{dc} is maintained at 750V, PV inverter supplies its generated power 10.25kW which is not enough to fulfil the load demand of 20kVA, 0.8pf lag (16kW and 12kVAR), therefore to meet the load demand, extra power 5.75kW is taken from distribution grid, while 12 kVAR of reactive demand of the load is supplied by PV inverter alone, showing proposed control is efficient in maintaining the grid at UPF. Further the proposed algorithm on linear load (20kVA, 0.8 pf lag) is tested under varying insolation from 0.15 seconds and 0.25second and various parameters are presented in figure 3.28. Due to decrease in solar insolation, P_{inv} is decreased upto 7.75kW till 0.25 seconds causing the grid to share more power by 2.5 kW (total 8.25 kW) to the load(16kW) as depicted in figure 3.28, while, total reactive power demand of load is still supplied by inverter alone hence keeping grid at UPF during the adverse scenario of solar insolation.

After 0.25 second to 0.35 seconds, insolation is constant at 700W/$m^2$and PV power is constant at 7.75kW as can be seen from the figure 3.28.

It has been observed that during solar insolation variation, sharing of active and reactive power between load (P_{load}, Q_{load}), grid (P_{grid}, Q_{grid}) and inverter (P_{inv}, Q_{inv}) is maintained, grid current is sinusoidal and V_{dc} is maintained at 750 V.

After 0.35 second till 0.45 second insolation and hence PV power both has been increased and system regains the initial (0.1 to 0.15 second), steady state condition.

It has been observed that during solar insolation variation, sharing of active and reactive power between load (P_{load}, Q_{load}), grid (P_{grid}, Q_{grid}) and inverter (P_{inv}, Q_{inv}) is maintained, grid current is sinusoidal and maintains V_{dc} at 750 V.

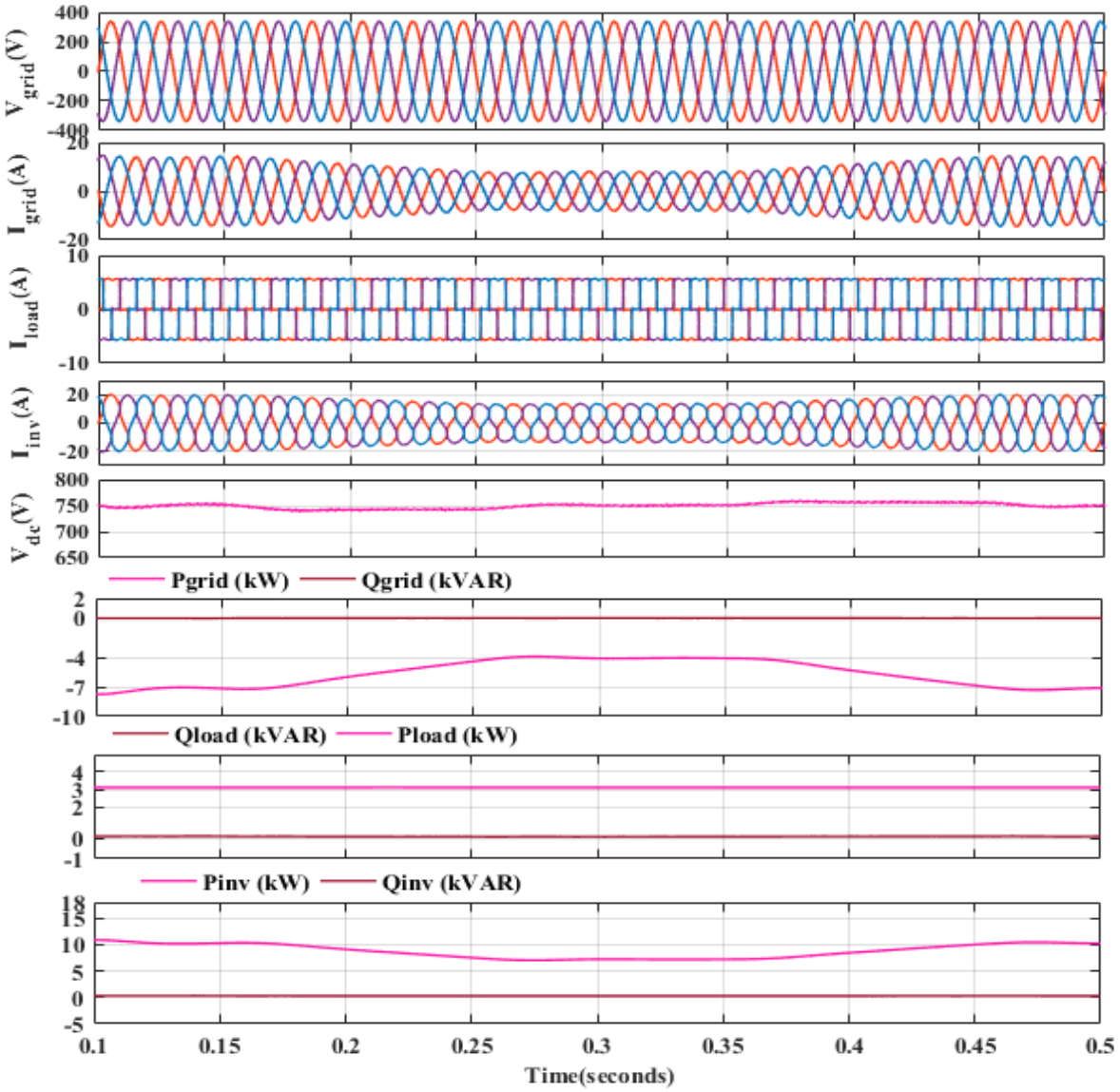

Fig.3.29. Performance of SPV based microgrid under nonlinear load at varying insolation

Further for a nonlinear load (three phase bridge rectifier with RL load, R=100Ω, L=100mH) at varying irradiance, simulated results and corresponding various parameters viz. V_{grid}, I_{grid}, I_{load}, I_{inv}, P_{grid}, Q_{grid}, P_{inv}, Q_{inv}, P_{load}, Q_{load}, and V_{dc} of the PV inverter are shown in figure 3.29. It is observed from figure between 0.1 to 0.15 second, V_{grid} and I_{grid} are out of phase by 180^0 (as power is supplied to grid), V_{dc} is maintained at 750V, PV inverter supplies its generated power 10.25kW. After satisfying the load demand of 3.1 kW, rest power 7.15kW is fed back to grid, while PV inverter alone supplying reactive power demand of the load, showing proposed control is efficient in maintaining grid at UPF.

After decrease in solar insolation at 0.15 seconds till 0.25 seconds, PV inverter power is decreased from 10.25kW to 7.75kW, leading to decrease in the power fed to the grid by 2.5kW as shown in figure 3.29. While reactive power demand of load is supplied by PV inverter (VSC) alone hence keeping grid at UPF during the adverse scenario of solar insolation.

After 0.25 second, to 0.35 seconds, insolation is constant at 700W/$m^2$and PV power is constant at 7.75kW as can be seen from the figure 3.29. After 0.35 second, insolation and PV power both has been increased and system regains the initial (0.1 to 0.15 second), steady state condition.

It has been observed that during solar insolation variation, active and reactive power is balanced between inverter (P_{inv}, Q_{inv}) load (P_{load}, Q_{load}) and grid (P_{grid}, Q_{grid}) is maintained, I_{grid} is sinusoidal and V_{dc} is maintained at 750 V. Also, it is observed from figure 3.30 and that using proposed control during the varying insolation, THD (%) in I_{grid} is 1.45% which is well within IEEE limits, whereas THD (%) in load current is 29.39% can be seen from figure 3.31.

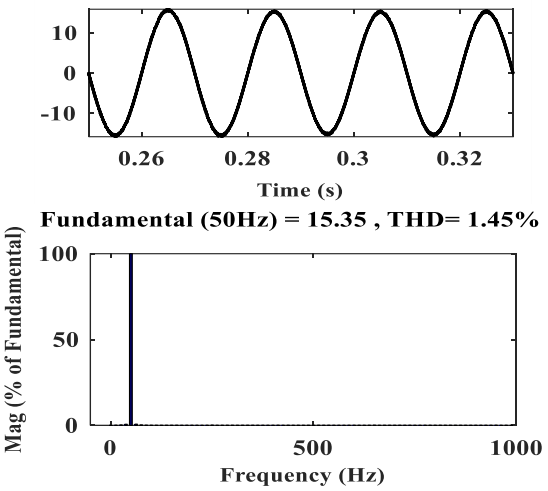

Fig. 3.30. THD (%) in grid current at varying insolation under nonlinear load

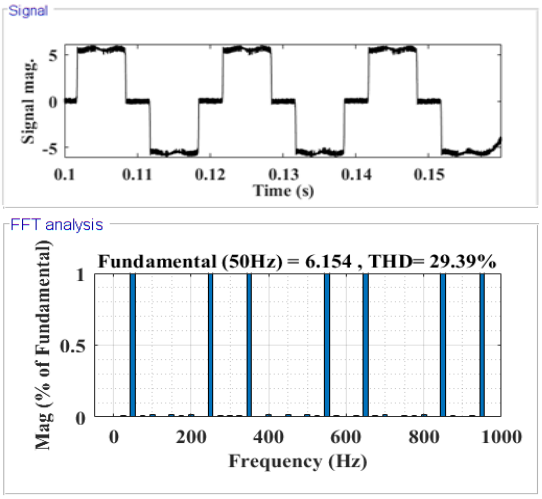

Fig. 3.31. THD (%) in nonlinear load current

3.8 COMPARATIVE ANALYSIS OF VARIOUS CONTROL ALGORITHMS

In this section, the proposed control algorithms viz. novel modified SRF have been analysed and compared with other conventional VSC control viz. SRF, IRPT, and unit template in terms of THD (%) in the grid current under the non-linear load. The obtained THD (%) using novel intelligent based modified SRF control algorithms and other conventional control schemes are presented below in table 3.3. The THD (%) in load current is 29.53% while the THD (%) in grid current in the case of all the VSC algorithms is well within the IEEE standards.

Table 3.3 THD *(%)* in grid current using various control algorithms

S.N.	THD in grid current	
	Control algorithms	***THD* (%)**
1	SRF	1.85
2	IRPT	2.29
3	Unit template	2.92
5	Novel intelligent based Modified SRF	1.71

3.9 CONCLUDING REMARKS

In this chapter, design and development of two-stage, three phase grid connected SPV based microgrid has been carried out. The VSC control algorithms viz. conventional and a novel intelligence-based control is modelled and simulated for the SPV system.

Numerous simulation results from various operating scenarios have been shown to demonstrate the viability of the developed control techniques. Under all test environments, the proposed algorithms' performance was found to be efficient. It has been observed that the developed control algorithm ensures power balance and compensates for the load's reactive power and nonlinearity. The THD (%) in grid current is observed to be less than 5% which is within IEEE-519 standard.

CHAPTER-IV
ADAPTIVE THEORY BASED VSC CONTROL ALGORITHMS FOR GRID INTEGRATION OF SPV BASED MICROGRID

4.1 INTRODUCTION

In previous chapter, design and development of grid connected SPV based microgrid has been discussed. The VSC control algorithms viz. conventional and a novel intelligence-based control is modelled and simulated for the two-stage, three-phase grid interfaced SPV system and detailed simulation results have been studied.

This chapter contributes toward the design, modelling, and simulation of adaptive theory-based VSC control algorithms.

In adaptive theory-based control algorithms, the calculation of fundamental active and reactive power components of load currents is based on adaptive parameters of input signals, which can be constant or variable. The benefit of adopting fixed parameters is lower complexity, which reduces the burden of computation on the DSP processor. In the case of fixed parameters, there is a trade-off between convergence rate and steady-state error. The benefits of employing variable parameters include faster convergence and lower steady-state error, but this increases the computational burden on the DSP processor. For control of SPV-based microgrids, the novel control methods on adaptive approach are developed. The following are the control algorithms used in the current work to estimate reference currents.

- Adaptive Control Algorithms
  - Least Mean Square (LMS) based Adaptive Control Algorithm
- Proposed Adaptive Theory-Based Control Algorithms
  - Variable Step Size LMS
  - Robust Least Mean Logarithmic Square (RLMLS)

4.2 LEAST MEAN SQUARE (LMS) BASED ADAPTIVE CONTROL ALGORITHM

The least mean square (LMS) adaptive control algorithm, consists of an adaptive process, which requires automatically adjusting of system parameters based on the estimation error. The conventional least mean square techniques, is used to estimate the fundamental active and reactive power weight components of load currents. The calculated weights are employed to generate reference currents and, eventually, switching pulses. The mathematical formulation of

an LMS-based control method is covered in this section. LMS control technique computes the reference currents to generate pulses for VSC operation as demonstrated in figure 4.1 [116]-[118]. Control algorithms based on Least Mean Squares (LMS) are developed for generating switching pulses as below:

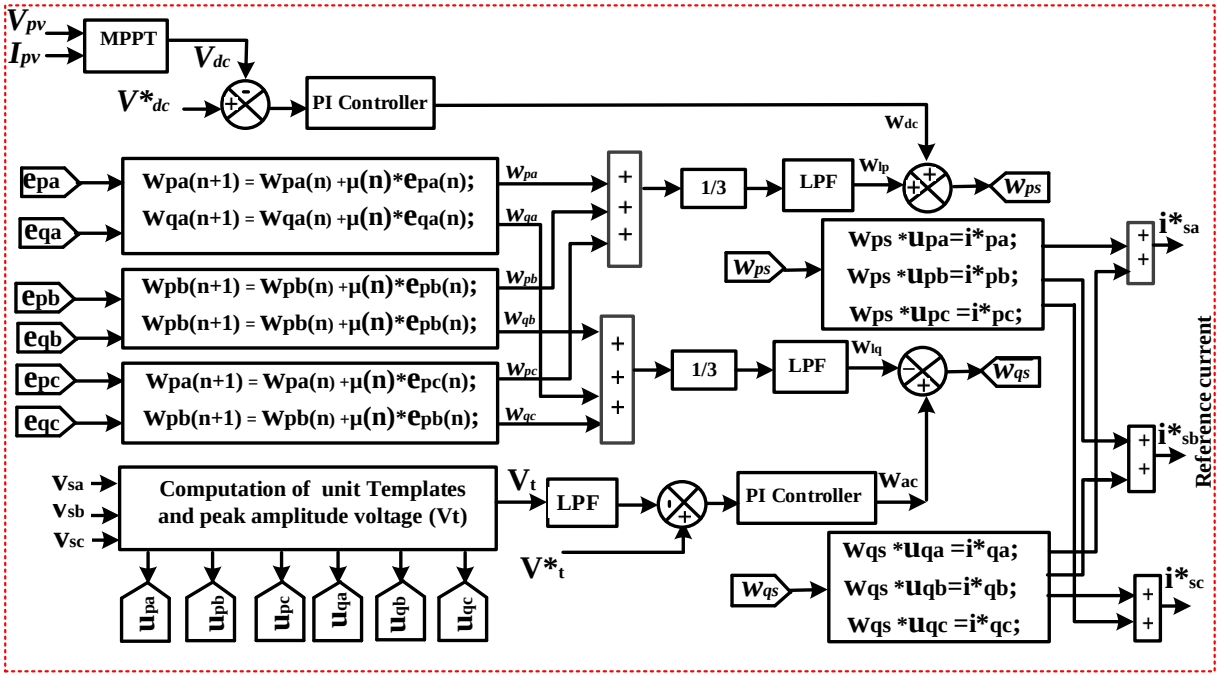

Fig. 4.1. Adaptive LMS Control algorithm

Estimation of in phase and unit templates of voltages

The peak amplitude of voltage ($\mathcal{V}_t$) of grid voltage, can be calculated by:

$$\mathcal{V}_t = \sqrt{\frac{2}{3}(\mathcal{V}_{sa}^2 + \mathcal{V}_{sb}^2 + \mathcal{V}_{sc}^2)} \tag{4.1}$$

The in-phase unit voltages template ($\mathcal{U}_{pa}, \mathcal{U}_{pb}, \mathcal{U}_{pc}$) can be calculated by the relation of phase voltages ($\mathcal{V}_{sa}, \mathcal{V}_{sb}, \mathcal{V}_{sc}$) with peak amplitude ($\mathcal{V}_t$) voltage as follows:

$$\mathcal{U}_{pa} = \frac{\mathcal{V}_{sa}}{\mathcal{V}_t}, \mathcal{U}_{pb} = \frac{\mathcal{V}_{sb}}{\mathcal{V}_t}, \mathcal{U}_{pc} = \frac{\mathcal{V}_{sc}}{\mathcal{V}_t} \tag{4.2}$$

Estimation of fundamental active and reactive components

Error in active component of load current in each phase ($e_{pa};\ e_{pb};\ e_{pc}$) at nth instant is estimated by using in-phase unit template ($\mathcal{U}_{pa}; \mathcal{U}_{pb};\ \mathcal{U}_{pc}$) and fundamental active component ($w_{pa}; w_{pc}; w_{pc}$) of load current ($i_{La}; i_{Lb}; i_{Lc}$) as follows:

$$e_{pa}(n) = i_{La}(n) - u_{pa} * w_{pa}(n) \tag{4.3}$$

$$e_{pb}(n) = i_{Lb}(n) - u_{pb} * w_{pb}(n) \tag{4.4}$$

$$e_{pc}(n) = i_{Lc}(n) - u_{pc} * w_{pc}(n) \quad (4.5)$$

The fundamental active weights w_{pa}, w_{pb}, w_{pc} at (n+1) instant be computed as:

$$w_{pa}(n+1) = w_{pa}(n) + \mu(n) * e_{pa}(n) \quad (4.6)$$

$$w_{pb}(n+1) = w_{pb}(n) + \mu(n) * e_{pb}(n) \quad (4.7)$$

$$w_{pc}(n+1) = w_{pc}(n) + \mu(n) * e_{pc}(n) \quad (4.8)$$

where, step size (μ) value must be small and positive taken as 0.1.

The average fundamental active weight components can be computed as:

$$w_{lp} = \frac{(w_{pa}+w_{pb}+w_{pc})}{3} \quad (4.9)$$

Similarly, estimation error in reactive component (e_q) of different phases (e_{qa}, e_{qb}, e_{qc}) is estimated using quadrature unit templates ($\mathcal{U}_{qa}, \mathcal{U}_{qb}, \mathcal{U}_{qc}$) and load current ($i_L$) of the phases "a", "b", and "c" at nth instant as follows:

$$e_{qa}(n) = i_{La}(n) - u_{qa}(n) * w_{qa}(n) \quad (4.10)$$

$$e_{qb}(n) = i_{Lb}(n) - u_{qb}(n) * w_{qb}(n) \quad (4.11)$$

$$e_{qc}(n) = i_{Lc}(n) - u_{qc}(n) * w_{qc}(n) \quad (4.12)$$

Fundamental reactive weights (w_{qa}, w_{qb}, w_{qc}) at (n+1)th instant for the phases "a", "b", and "c" can be computed as:

Updated reactive weight vector for different phases given below:

$$w_{qa}(n+1) = w_{pa}(n) + \mu(n) * e_{pa}(n) \quad (4.13)$$

$$w_{qb}(n+1) = w_{pb}(n) + \mu(n) * e_{pb}(n) \quad (4.14)$$

$$w_{qc}(n+1) = w_{pc}(n) + \mu(n) * e_{pc}(n) \quad (4.15)$$

The total fundamental reactive weight component of load (w_{lq}) is estimated by taking average of updated weight vector.

$$w_{lq} = \frac{(w_{qa}+w_{qb}+w_{qc})}{3} \quad (4.16)$$

The sensed voltage of dc-link (V_{dc}) is compared with reference dc bus voltage (V_{dc}^*) to estimate error in DC link voltage and compensated using proportional integral (PI) controller. The output of the controller is dc loss weight (w_{dc}).

The total active weight (w_{ps}) component of the supply reference current is given by:

$$w_{ps} = w_{lp} + w_{dc} \quad (4.17)$$

The active in-phase reference current can be evaluated as:

$$i_{sa}^* = w_{ps}\mathcal{U}_{pa}, i_{sb}^* = w_{ps}\mathcal{U}_{pb}, i_{sc}^* = w_{ps}\mathcal{U}_{pc} \quad (4.18)$$

The sensed peak magnitude of supply voltage is compared with set reference peak magnitude and generated error is compensated by PI controller. Output of the controller is ac loss weight (w_{ac}) is given as:

$$w_{ac}(n+1) = w_{ac}(n) + K_{pa}\{v_{te}(n+1) - v_{te}(n)\} + K_{ia}v_{te}(n+1) \quad (4.19)$$

Where K_{pa}, K_{ia} are gains of ac voltage PI controller and $v_{te}(n+1)$ is the error of the sensed ac voltage and reference ac bus voltage at (n+1) th sampling time.

Total reactive weight component (w_{qs}) of the reference current as shown below:

$$w_{qs} = w_{ac} - w_{lq} \quad (4.20)$$

Reactive reference current components can be evaluated as:

$$i_{qa}^{*} = w_{qs} * \mathcal{U}_{qa};\ i_{qb}^{*} = w_{qs} * \mathcal{U}_{qb}; i_{qc}^{*} = w_{qs} * \mathcal{U}_{qc} \quad (4.21)$$

Estimation of reference current and switching signal for VSC

The active and reactive reference current ($i_{pa}^{*}, i_{pb}^{*}, i_{pc}^{*}$), ($i_{qa}^{*}, i_{qb}^{*}, i_{qc}^{*}$) respectively are added to get reference current ($i_{sa}^{*}, i_{sb}^{*}, i_{sc}^{*}$) which is given by:

$$i_{sa}^{*} = i_{pa}^{*} + i_{qa}^{*}, i_{sb}^{*} = i_{pb}^{*} + i_{qb}^{*}, i_{sc}^{*} = i_{pc}^{*} + i_{qc}^{*} \quad (4.22)$$

Furthermore, reference current ($i_{sa}^{*}, i_{sb}^{*}, i_{sc}^{*}$) are compared with sensed grid current ($i_{sa}, i_{sb,} i_{sc}$) in hysteresis control and generate switching signals to operate VSC.

4.3 PROPOSED ADAPTIVE THEORY BASED CONTROL ALGORITHMS

Because of its simplicity, conventional LMS adaptive control has been widely implemented, but the performance is frequently unsatisfactory due to poor dynamic performance caused by a trade-off between tracking capability and accuracy in fixed step size.

4.3.1 Variable Step Size LMS Adaptive Theory-Based Control Algorithm

The proposed control generates reference current by extracting the fundamental active and reactive component from load current. The control, offers better initial transients, dynamic performance and better convergence than conventional LMS and SRF based control. The proposed VSSLMS control of VSC has been discussed in details in the present section.

The proposed control algorithm is depicted in figure 4.2, proposed control algorithm extracts the fundamental components from load current to estimate reference current. It improves the PQ of the grid by compensating harmonics, reactive power, and unbalancing of the load. It is more efficient, than conventional LMS and SRF control due to faster tracking abilities during dynamic loading condition, and is efficient under adverse grid scenario viz. unbalance and distorted grid

voltage. Grid integrated PV system is modelled in MATLAB/Simulink2016(a) and various system parameters are given in the appendix: A.

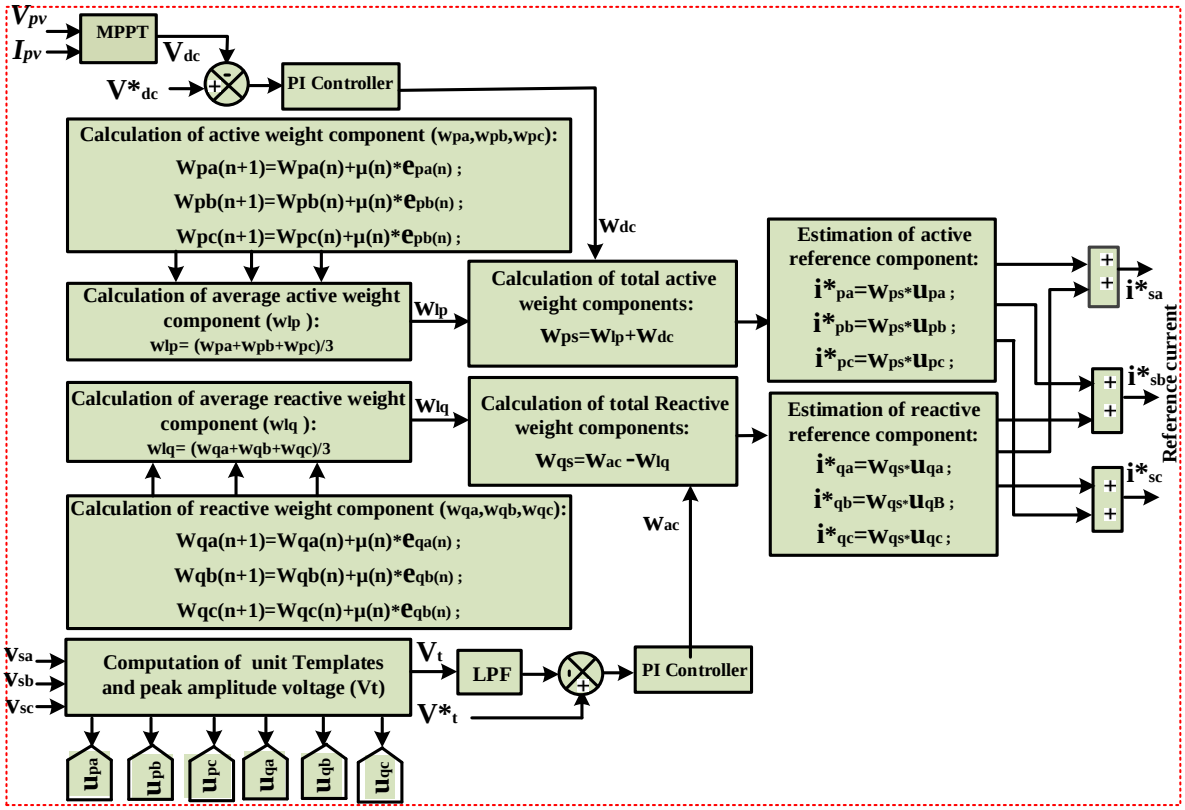

Fig.4.2 VSSLMS adaptive control for reference current generation

Estimation of in phase and orthogonal unit templates of voltages

The peak amplitude of voltage ($\mathcal{V}_t$)of grid voltage, can be calculated by:

$$\mathcal{V}_t = \sqrt{\frac{2}{3}(\mathcal{V}_{sa}^2 + \mathcal{V}_{sb}^2 + \mathcal{V}_{sc}^2)} \tag{4.23}$$

The in-phase unit template voltages ($\mathcal{U}_{pa}, \mathcal{U}_{pb}, \mathcal{U}_{pc}$) can be calculated from phase voltages ($\mathcal{V}_{sa}, \mathcal{V}_{sb}, \mathcal{V}_{sc}$) and peak amplitude of voltages ($\mathcal{V}_t$) [68] as follows:

$$\mathcal{U}_{pa} = \frac{\mathcal{V}_{sa}}{\mathcal{V}_t}, \mathcal{U}_{pb} = \frac{\mathcal{V}_{sb}}{\mathcal{V}_t}, \mathcal{U}_{pc} = \frac{\mathcal{V}_{sc}}{\mathcal{V}_t} \tag{4.24}$$

The reactive/orthogonal/quadrature unit templates ($\mathcal{U}_{qa}, \mathcal{U}_{qb}, \mathcal{U}_{qc}$) can be obtained from in phase unit template voltages as follows:

$$u_{qa} = -\frac{u_{pb}}{\sqrt{3}} + \frac{u_{pc}}{\sqrt{3}}\ ;\ u_{qb} = \frac{\sqrt{3}\,u_{pa}}{2} + \frac{(u_{pb}-u_{pc})}{2\sqrt{3}};\ u_{qc} = -\frac{\sqrt{3}\,u_{pa}}{2} + \frac{(u_{pb}-u_{pc})}{2\sqrt{3}} \tag{4.25}$$

Estimation of active and reactive weight components

Instantaneous estimation error (e_p) of active component in each phase at n[th] instant is estimated from in phase unit template (u_p) and load current (i_L) for phases "a", "b" and "c" can be computed using the equation (4.26) -(4.28):

Estimation error (e_p) of different phases (e_{pa}, e_{pb}, e_{pc}) is estimated using in phase unit template (u_p) and load current (i_L) at n[th] instant as follows:

$$e_{pa}(n) = i_{La}(n) - u_{pa}(n) * w_{pa}(n) \quad (4.26)$$

$$e_{pb}(n) = i_{Lb}(n) - u_{pb}(n) * w_{pb}(n) \quad (4.27)$$

$$e_{pc}(n) = i_{Lc}(n) - u_{pc}(n) * w_{pc}(n) \quad (4.28)$$

New variable step size (μ) for proposed control algorithm can be realized by mathematical equations as given below [116],[120]:

$$\mu(n) = \frac{\beta}{\{[1 + \exp(-\alpha|e(n)e(n-1)|)] - 0.5\}} \quad (4.29)$$

where e (n) represents the estimation error at n[th] instant, and scaling factor $(\alpha)\ and\ (\beta)$ are positive scalar constant, taken as 20 and 0.01 respectively for minimum error.

Fundamental active weights w_{pa}, w_{pb}, w_{pc} at (n+1) instant for the phases "a", "b" and "c" can be computed using equation (4.30) -(4.32).

Where, $e_{pm}(n)$ is the priori estimation error and $\mu(n)$ is step size for minimum error. Updated active weight vector $w_{pm}\ (n+1)$ is calculated from weight $w_{pm}(n)$ for overall error minimization. Updated active weight vector for different phases given below:

$$w_{pa}(n+1) = w_{pa}(n) + \mu(n) * e_{pa}(n) \quad (4.30)$$

$$w_{pb}(n+1) = w_{pb}(n) + \mu(n) * e_{pb}(n) \quad (4.31)$$

$$w_{pc}(n+1) = w_{pc}(n) + \mu(n) * e_{pc}(n) \quad (4.32)$$

The total fundamental active weight component of load (w_{lp}) is estimated by taking average of updated weight vector.

$$w_{lp} = \frac{(w_{pa}+w_{pb}+w_{pc})}{3} \quad (4.33)$$

The purpose of proposed control technique is to minimize the error. Similarly, estimation error (e_q) of different phases (e_{qa}, e_{qb}, e_{qc}) is estimated using quadrature unit templates ($\mathcal{U}_{qa}$,$\mathcal{U}_{qb}, \mathcal{U}_{qc}$) and load current ($i_L$) of the phases "a", "b", and "c" at n[th] instant as follows:

$$e_{qa}(n) = i_{La}(n) - u_{qa}(n) * w_{qa}(n) \quad (4.34)$$

$$e_{qb}(n) = i_{Lb}(n) - u_{qb}(n) * w_{qb}(n) \quad (4.35)$$

$$e_{qc}(n) = i_{Lc}(n) - u_{qc}(n) * w_{qc}(n) \quad (4.36)$$

Fundamental reactive weights (w_{qa}, w_{qb}, w_{qc}) at (n+1)th instant for the phases "a", "b", and "c" can be computed as:

Updated reactive weight vector for different phases given below:

$$w_{qa}(n+1) = w_{pa}(n) + \mu(n) * e_{pa}(n) \quad (4.37)$$

$$w_{qb}(n+1) = w_{pb}(n) + \mu(n) * e_{pb}(n) \quad (4.38)$$

$$w_{qc}(n+1) = w_{pc}(n) + \mu(n) * e_{pc}(n) \quad (4.39)$$

The total fundamental reactive weight component of load (w_{lq}) is estimated by taking average of updated weight vector.

$$w_{lq} = \frac{(w_{qa}+w_{qb}+w_{qc})}{3} \quad (4.40)$$

The error in sensed actual dc-link voltage (V_{dc}) as compared to (V_{dc}^*) reference voltage is compensated using PI controller. Output is dc loss weight (w_{dc}) of PI controller is given as:

$$w_{dc}(n+1) = w_{dc}(n) + K_{pd}\{v_{dc(e)}(n+1) - v_{dc(e)}(n)\} + K_{id}v_{dc(e)}(n+1) \quad (4.41)$$

Where K_{pd}, K_{id} are gains of dc bus PI controller. $v_{dc(e)}(n+1)$ is the error of the sensed V_{dc} and V_{dc}^* dc bus voltage at (n+1)th sampling time.

Total active weight (w_{ps}) component in reference current can be calculated as:

$$w_{ps} = w_{lp} + w_{dc} \quad (4.42)$$

The active in-phase reference current components can be evaluated as:

$$i_{pa}^* = w_{ps} * \mathcal{U}_{pa};\ i_{pb}^* = w_{ps} * \mathcal{U}_{pb};\ i_{pc}^* = w_{ps} * \mathcal{U}_{pc} \quad (4.43)$$

The sensed peak magnitude of supply voltage is compared with set reference peak magnitude and generated error is compensated by PI controller. Output of the controller is ac loss weight (w_{ac}) is given as:

$$w_{ac}(n+1) = w_{ac}(n) + K_{pa}\{v_{te}(n+1) - v_{te}(n)\} + K_{ia}v_{te}(n+1) \quad (4.44)$$

Where K_{pa}, K_{ia} are gains of ac voltage PI controller and $v_{te}(n+1)$ is the error of the sensed ac voltage and reference ac bus voltage at (n+1) th sampling time.

Total reactive weight component (w_{qs}) of the reference current as shown below:

$$w_{qs} = w_{ac} - w_{lq} \quad (4.45)$$

Reactive reference current components can be evaluated as: $i_{qa}^* = w_{qs} * \mathcal{U}_{qa};\ i_{qb}^* = w_{qs} * \mathcal{U}_{qb}; i_{qc}^* = w_{qs} * \mathcal{U}_{qc}$ (4.46)

Estimation of reference current and switching signal for VSC

The active and reactive reference current $(i_{pa}^*, i_{pb}^*, i_{pc}^*)$, $(i_{qa}^*, i_{qb}^*, i_{qc}^*)$ respectively are added to get reference current $(i_{sa}^*, i_{sb}^*, i_{sc}^*)$ which is given by:

$$i_{sa}^* = i_{pa}^* + i_{qa}^*, i_{sb}^* = i_{pb}^* + i_{qb}^*, i_{sc}^* = i_{pc}^* + i_{qc}^* \quad (4.47)$$

Furthermore, reference current $(i_{sa}^*, i_{sb}^*, i_{sc}^*)$ are compared with sensed grid current $(i_{sa}, i_{sb,} i_{sa})$ in hysteresis control and generate switching signals to operate VSC.

4.3.2 Robust Least Mean Logarithmic Square Based Control Algorithm

To overcome the limitations of LMS VSC control algorithm, a novel VSC control technique based on a robust least mean logarithmic square (RLMLS) adaptive filter is proposed. It provides, better performance in terms of transient, steady-state, dynamic response and faster convergence speed.

It compensates unbalance and nonlinearity of the loads, even under ideal and weak grid scenarios. The control scheme is efficient in the event of an unbalanced or distorted grid voltage.

It also significantly improves accuracy of the algorithm during the dynamic load condition and offer less oscillations in the estimation of active component. The proposed control scheme does not require a complicated block for synchronization, such as a phase lock loop (PLL). Hence, proposed control eliminates the additional computational burden, with the added benefit of reduced complexity, ease of implementation, and adaptability.

Figure 4.3, depicts the proposed RLMLS control, various input signal such as load current, grid voltages at PCC along-with DC link voltages are sensed. In- phase, quadrature unit templates of voltage, and fundamental active and reactive weights component are estimated. Furthermore, total active and reactive weights are estimated by adding compensated current from DC and AC side PI controller respectively. In the next stage, active and reactive components of reference current are estimated by multiplying in-phase and quadrature unit template respectively. In the final stage, active and reactive reference components of respective phases are added to get reference current. Furthermore, hysteresis current control is used for generation of controlled switching pulses of VSC. Proposed RLMLS control of VSC has been discussed in details in this section.

Estimation of in phase and orthogonal unit templates of voltages

The peak amplitude of voltage $(\mathcal{V}_t)$of grid voltage, can be calculated by:

$$\mathcal{V}_t = \sqrt{\frac{2}{3}(\mathcal{V}_{sa}^2 + \mathcal{V}_{sb}^2 + \mathcal{V}_{sc}^2)} \quad (4.48)$$

The in-phase unit template ($\mathcal{U}_{pa}, \mathcal{U}_{pb}, \mathcal{U}_{pc}$):

$$\mathcal{U}_{pa} = \frac{\mathcal{V}_{sa}}{\mathcal{V}_t}, \mathcal{U}_{pb} = \frac{\mathcal{V}_{sb}}{\mathcal{V}_t}, \mathcal{U}_{pc} = \frac{\mathcal{V}_{sc}}{\mathcal{V}_t}; \quad \text{where } (\mathcal{V}_{sa}, \mathcal{V}_{sb}, \mathcal{V}_{sc}) \text{ are phase voltages.} \quad (4.49)$$

Quadrature unit templates ($\mathcal{U}_{qa}, \mathcal{U}_{qb}, \mathcal{U}_{qc}$):

$$u_{qa} = -\frac{u_{pb}}{\sqrt{3}} + \frac{u_{pc}}{\sqrt{3}}, u_{qb} = \frac{\sqrt{3}\,u_{pa}}{2} + \frac{(u_{pb}-u_{pc})}{2\sqrt{3}}, u_{qc} = -\frac{\sqrt{3}\,u_{pa}}{2} + \frac{(u_{pb}-u_{pc})}{2\sqrt{3}} \quad (4.50)$$

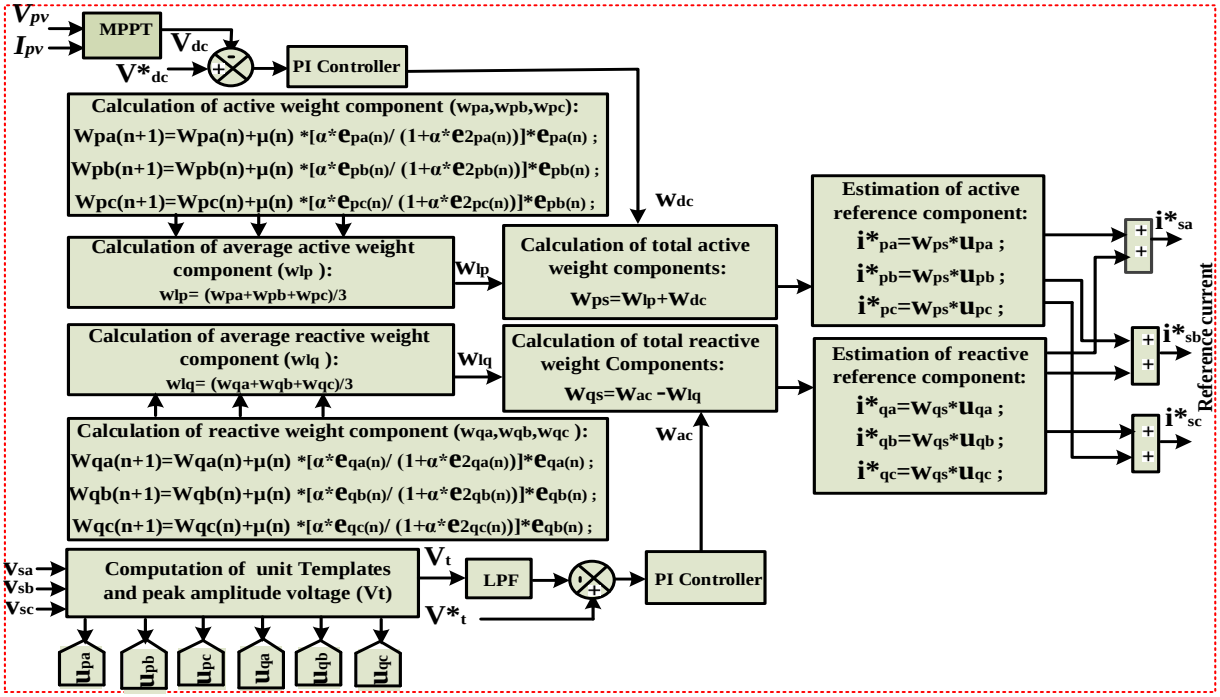

Fig.4.3. RLMLS adaptive control for reference current generation

Weight Extraction by Proposed Control

Using the load current (i_L) and in-phase unit template ($\mathcal{U}_{pa}, \mathcal{U}_{pb}, \mathcal{U}_{pc}$) at the n_{th} instant, the estimation error (e_p) of distinct phases e_{pa}, e_{pb}, e_{pc} is calculated as follows:

$$e_{pa}(n) = i_{La}(n) - u_{pa}(n) * w_{pa}(n) \quad (4.51)$$

$$e_{pb}(n) = i_{Lb}(n) - u_{pb}(n) * w_{pb}(n) \quad (4.52)$$

$$e_{pc}(n) = i_{Lc}(n) - u_{pc}(n) * w_{pc}(n) \quad (4.53)$$

Fundamental active weights w_{pa}, w_{pb}, w_{pc} at $(n+1)^{th}$ instant for different phases are computed by equation (4.54)-(4.56). Where, $e_{pa}(n)$, $e_{pb}(n)$, $e_{pc}(n)$ are the priori estimation error. step size (μ) and scaling factor (α) are positive scalar constant and taken as 0.1 and 0.0035 respectively for minimum error.

For overall error reduction, updated weight $w_{pm}\,(n+1)$ is computed from weight $w_{pm}(n)$. The following is an updated weight vector for various phases:

$$w_{pa}(n+1) = w_{pa}(n) + \mu(n)\frac{\alpha * e_{pa}(n)}{1+\alpha * {e_{pa}}^2(n)} * e_{pa}(n) \quad (4.54)$$

$$w_{pb}(n+1) = w_{pb}(n) + \mu(n)\frac{\alpha * e_{pb}(n)}{1+\alpha * {e_{pb}}^2(n)} * e_{pb}(n) \quad (4.55)$$

$$w_{pc}(n+1) = w_{pc}(n) + \mu(n)\frac{\alpha * e_{pc}(n)}{1+\alpha * {e_{pc}}^2(n)} * e_{pc}(n) \quad (4.56)$$

By averaging the active component of load (w_{lp}), is calculated.

$$w_{lp} = \frac{(w_{pa}+w_{pb}+w_{pc})}{3} \quad (4.57)$$

Using the load current (i_L) and quadrature unit template ($\mathcal{U}_{qa}, \mathcal{U}_{qb}, \mathcal{U}_{qc}$) at the nth instant, the estimation error (e_q) of distinct phases e_{qa}, e_{qb}, e_{qc} is calculated as follows:

$$e_{qa}(n) = i_{La}(n) - u_{qa}(n) * w_{qa}(n) \quad (4.58)$$

$$e_{qb}(n) = i_{Lb}(n) - u_{qb}(n) * w_{qb}(n) \quad (4.59)$$

$$e_{qc}(n) = i_{Lc}(n) - u_{qc}(n) * w_{qc}(n) \quad (4.60)$$

For overall error reduction, updated weight $w_{qm}\,(n+1)$ is computed from weight $w_{qm}(n)$. The following is an updated weight vector for various phases:

$$w_{qa}(n+1) = w_{qa}(n) + \mu(n)\frac{\alpha * e_{qa}(n)}{1+\alpha * {e_{pa}}^2(n)} * e_{qa}(n) \quad (4.61)$$

$$w_{qb}(n+1) = w_{qb}(n) + \mu(n)\frac{\alpha * e_{qa}(n)}{1+\alpha * {e_{pa}}^2(n)} * e_{qb}(n) \quad (4.62)$$

$$w_{qc}(n+1) = w_{qc}(n) + \mu(n)\frac{\alpha * e_{qa}(n)}{1+\alpha * {e_{qa}}^2(n)} * e_{qc}(n) \quad (4.63)$$

The proposed control technique's aim is to reduce error. The average fundamental reactive components of load (w_{lq}) can be calculated in the same way:

$$w_{lq} = \frac{(w_{qa}+w_{qb}+w_{qc})}{3} \quad (4.64)$$

The error $v_{dc(e)}(n)$, in sensed actual dc-link voltage (V_{dc}) with respect to reference voltage (V_{dc}^*) is given as at n$_{th}$ sampling,

$$v_{dc(e)}(n) = V_{dc}^*(n) - V_{dc}(n) \quad (4.65)$$

PI controller output is dc loss weight (w_{dc}), which regulates the dc-link voltage. DC loss weight (w_{dc}) is estimated by $v_{dc(e)}$ and gains of PI controller gains (K_{pd}, K_{id}) given as:

$$w_{dc}(n+1) = w_{dc}(n) + K_{pd}\{v_{dc(e)}(n+1) - v_{dc(e)}(n)\} + K_{id}v_{dc(e)}(n+1) \quad (4.66)$$

Where K_{pd}, K_{id} are gains of PI controller of DC link. Error in the DC link voltage at (n+1)th sampling time with respect to V_{dc}^* is represented by $v_{dc(e)}(n+1)$.

The $v_{dc(e)}(n+1)$ represents the error in the DC link voltage at (n+1)th sampling time with respect to V_{dc}^{*} , where K_{pd}, K_{id} are the gain of dc side PI controller.

Total active weight (w_{ps}) component:

$$w_{ps} = w_{lp} + w_{dc} \tag{4.67}$$

Active reference current can be evaluated below:

$$i_{pa}^{*} = w_{ps} * \mathcal{U}_{pa} \; ; \; i_{pb}^{*} = w_{ps} * \mathcal{U}_{pb} \; ; i_{pc}^{*} = w_{ps} * \mathcal{U}_{pc} \tag{4.68}$$

Error in the supply voltage with respect to set reference voltage compensated by PI controller. ac loss weight (w_{ac}) output of PI controller is given as:

$$w_{ac}(n+1) = w_{ac}(n) + K_{pa}\{v_{te}(n+1) - v_{te}(n)\} + K_{ia} v_{te}(n+1) \tag{4.69}$$

Error at (n+1) th sampling time with respect to set reference ac voltage is presented by $v_{te}(n+1)$, where K_{pa}, K_{ia} are gain of ac side PI controller.

The reference current's total reactive weight component (w_{qs}) is illustrated below:

$$w_{qs} = w_{ac} - w_{lq} \tag{4.70}$$

Reactive reference components can be estimated as:

$$i_{qa}^{*} = w_{qs} * \mathcal{U}_{qa}, i_{qb}^{*} = w_{qs} * \mathcal{U}_{qb}, i_{qc}^{*} = w_{qs} * \mathcal{U}_{qc} \tag{4.71}$$

Switching Pulse Generation

The addition of $(i_{pa}^{*}, i_{pb}^{*}, i_{pc}^{*})$ and $(i_{qa}^{*}, i_{qb}^{*}, i_{qc}^{*})$ are utilized to estimate reference current $(i_{sa}^{*}, i_{sb}^{*}, i_{sc}^{*})$ which is given by:

$$i_{sa}^{*} = i_{pa}^{*} + \; i_{qa}^{*}, i_{sb}^{*} = i_{pb}^{*} + i_{qb}^{*}, i_{sc}^{*} = i_{pc}^{*} + i_{qc}^{*} \tag{4.72}$$

Furthermore, reference current ($i_{sa}^{*}, i_{sb}^{*}, i_{sc}^{*}$) are compared with sensed grid current $(i_{sa}, i_{sb,} i_{sc})$ in hysteresis control and generate switching signals to operate VSC.

4.4 RESULTS AND DISCUSSIONS

4.4.1 Least Mean Square (LMS) Control Algorithm

The simulation results of LMS are presented and analysed under nonlinear balanced and unbalanced load at STC. To analyze the efficacy of conventional LMS control algorithms under nonlinear load, a bridge rectifier has been considered with RL load (R=100 Ω, L=100 mH). Further, to create the unbalance in the load, one phase is kept open from 0.15 to 0.25 seconds. System is supposed to be working at standard test condition (1000w/m^2, 25^{0}C).

Simulation results using LMS control algorithms under nonlinear(balance/unbalance) load are given in the figure 4.4. To impose the unbalance between 0.15 to 0.25 second one phase is kept

open. It can be seen from figure, that LMS is efficient in maintaining the grid current sinusoidal and balanced under the unbalance load current between 0.15 to 0.25 sec. Figure 4.5 shows the grid current waveform and THD (%). It can be seen from figure 4.9 and figure 4.5, that load current THD is 29.28% while grid current THD 1.92% respectively, which is well within the IEEE standard-519.

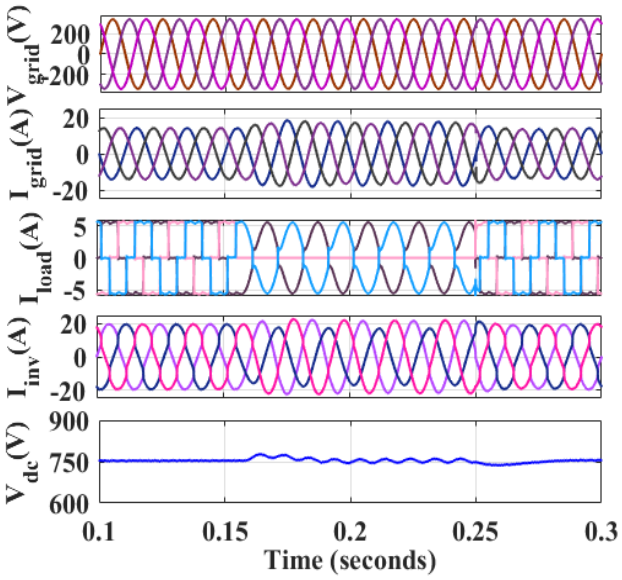

Fig. 4.4. Performance using adaptive LMS control

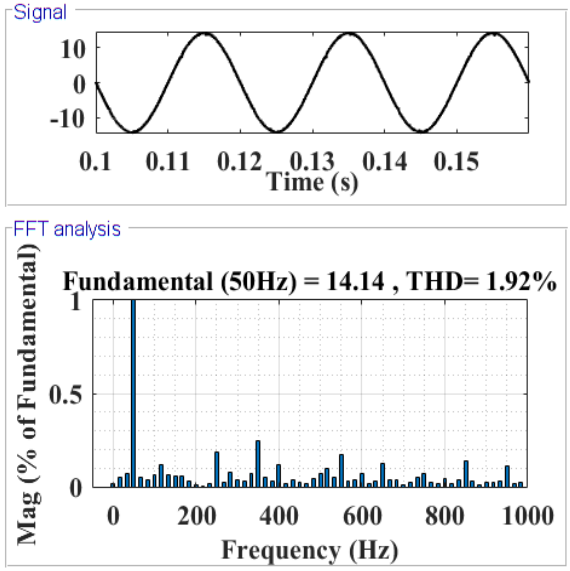

Fig.4.5. Grid current waveform and THD (%): after compensation using LMS control

4.4.2 Variable Step Size Least Mean Square Control Algorithm

4.4.2.1 *Performance under linear/nonlinear (unbalanced) and variable load at STC*

The performance of proposed new VSSLMS adaptive control under linear (5kVA, 0.8 pf) and nonlinear load (three phase bridge rectifier with RL load, R=100Ω, L=100mH), depicted in figure 4.6 and figure 4.7 respectively. Various parameter of the system viz. V_{grid}, I_{grid}, I_{load}, I_{inv}, V_{dc} and power balance between grid, load and inverter are also analyzed.

It can be seen from figure 4.6 that till 0.15 seconds PV inverter supplies 4kW active power and 3.0 kVAR of reactive demand of the load (5kVA, 0.8 pf), Vgrid and Igrid are 180° out of phase (as excess 6.25 kW power is supplied to the grid), Vdc is maintained at 750V. The inverter alone supplies the load active and reactive power demand, which decreases the reactive power drawn from the grid to zero, demonstrating that the proposed control is effective in maintaining the grid at UPF.

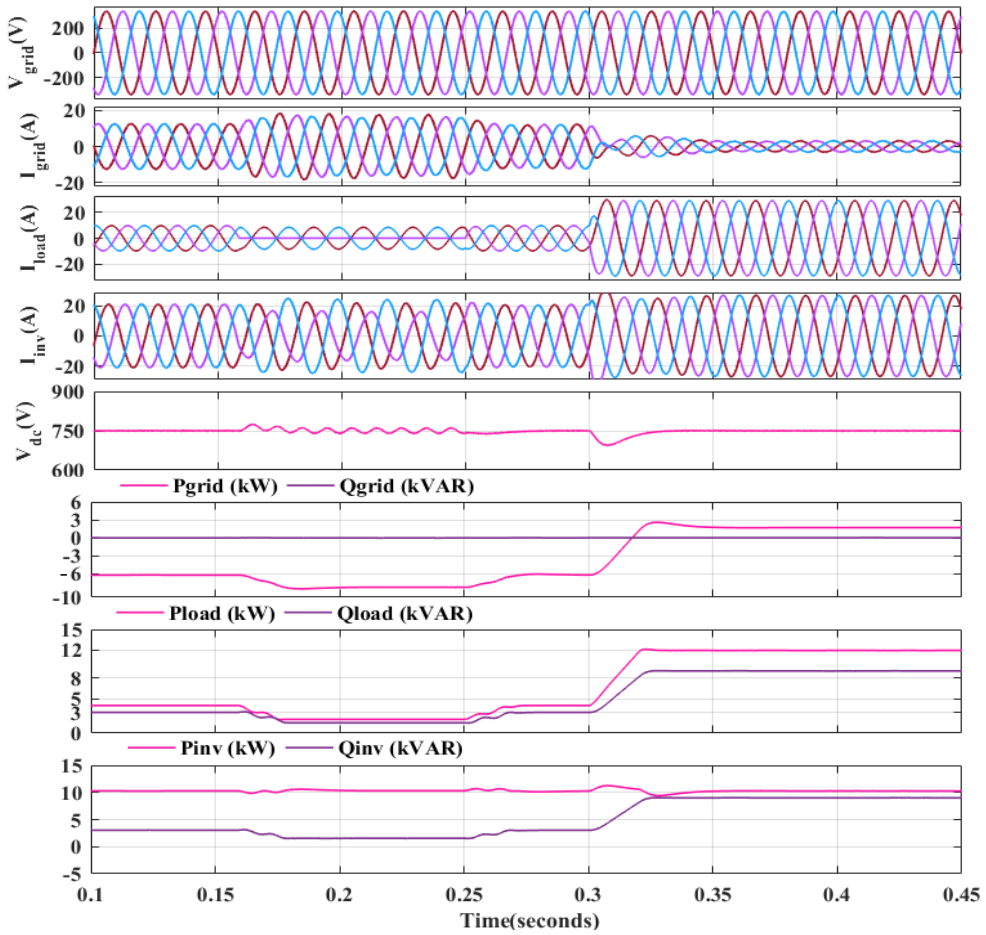

Fig. 4.6. Performance at STC input under linear (balance/unbalance) and load variable

Further, unbalanced and load varying condition occurs at 0.15 seconds and 0.30 second respectively. Performance of the proposed control under linear unbalanced load condition by keeping one phase (phase b) disconnected between 0.15 to 0.25 seconds is studied and various parameters viz. V_{grid}, I_{grid}, I_{load}, I_{inv}, P_{grid}, Q_{grid}, P_{inv}, Q_{inv}, P_{load}, Q_{load}, and V_{dc} are analyzed and depicted in figure 4.6. During unbalance period, inverter current compensates, effect of load unbalance and maintains grid current to be balance. It also supplies the load requirement for reactive power and thus holds the grid at UPF along with the balance grid current. Furthermore, between 0.25 to 0.3 seconds, operating at its initial load (5kVA, 0.8 pf) condition. For the load varying condition between 0.3 to 0.45 seconds, an extra linear load of 10kVA, 0.8 pf lagging is added at 0.3 seconds in the system. After 0.3 seconds load demand is 15kVA, 0.8 pf lagging (12kW and 9 kVAR). Power supplied by PV inverter is 10.25kW which is not enough to fulfill the load requirement therefore to meet the load demand extra required power 1.75 kW is taken from distribution grid and the reactive power demand of the load is met by inverter, and the grid is at UPF. It has been realised that during load variation and single phasing also that I_{grid} is sinusoidal and V_{dc} is maintained at 750 V.

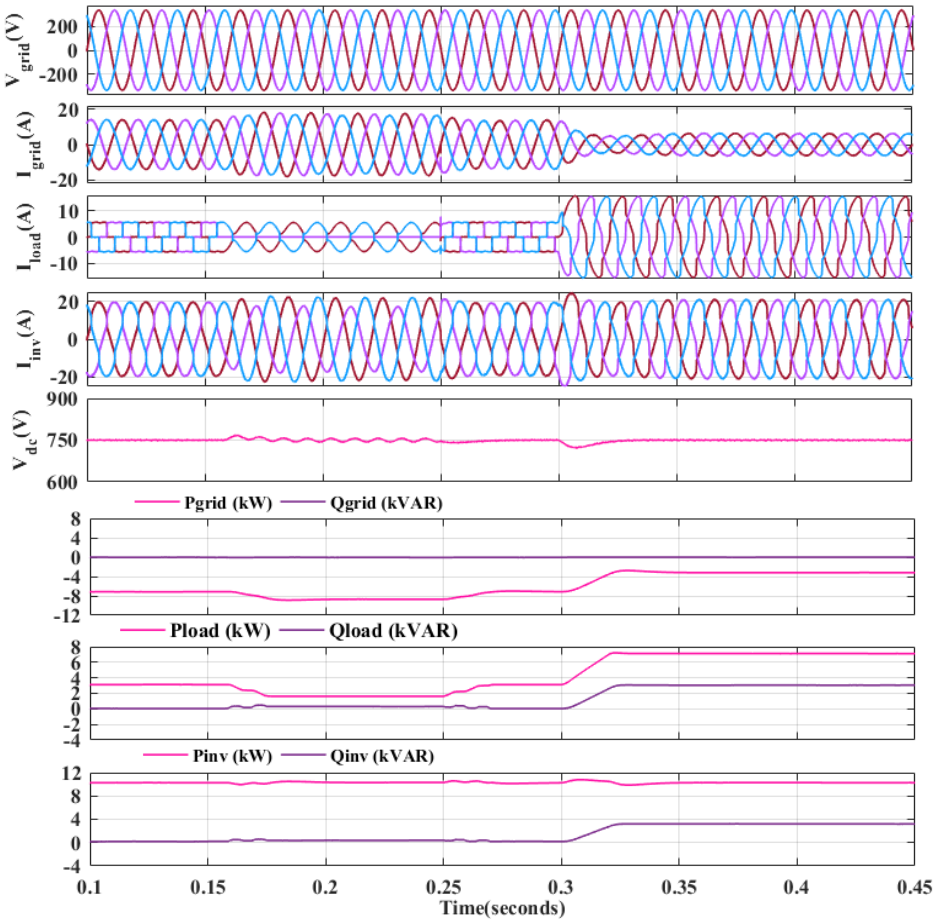

Fig. 4.7. Performance at STC input under nonlinear (balance/unbalance) and load varying

Further, to test the proposed control under nonlinear load (three phase bridge rectifier with RL load, R=100Ω, L=100mH), has been considered and results are shown in figure 4.7 It is observed that till 0.15 seconds; PV system supplies its nominal power of 10.25kW. It is observed from figure 4.7 that till 0.15 seconds V_{grid} and I_{grid} are 180° out of phase, maintains V_{dc} at 750V, PV inverter supplies 3.1kW active power demand of the load. Further, remaining 7.15 kW power of the PV system is supplied to the grid.

Further, proposed control under nonlinear unbalanced and load varying condition are also tested. Under nonlinear unbalanced load condition by one phase 'b' of load disconnected between 0.15 to 0.25 seconds and various parameters viz. V_{grid}, I_{grid}, I_{load}, I_{inv}, P_{grid}, Q_{grid}, P_{inv}, Q_{inv}, P_{load}, Q_{load}, and V_{dc} are analyzed and presented in figure 4.7, During unbalance period, inverter current compensates, effect of load unbalance and maintains balanced grid current. It also supplies the load requirement for reactive power and thus holds the grid at UPF along with the balance grid current. Furthermore, between 0.25 to 0.3 seconds, operating at its initial nonlinear load (three phase bridge rectifier with RL load, R=100Ω, L=100mH).

For the load varying conditions between 0.3 to 0.45 seconds, an extra linear varying load of 5kVA, 0.8 pf lagging is added at 0.3 seconds in the system of existing nonlinear load. After 0.3 seconds load demand is 7.1kW and 3 kVAR, out of which 7.1kW is supplied by PV inverter, as its generated power is 10.25 kW, after satisfying the load requirement, remaining power 3.15 kW is supplied to grid and reactive demand is met by inverter. It has been realised that during load variation and single phasing also grid current is sinusoidal and V_{dc} is maintained at 750 V. THD (%) in I_{grid} is also maintained at 1.38% as depicted in figure 4.8 which is as per IEEE standard 519-2014, are well within the limit, while THD (%) in nonlinear load current is 29.38%.

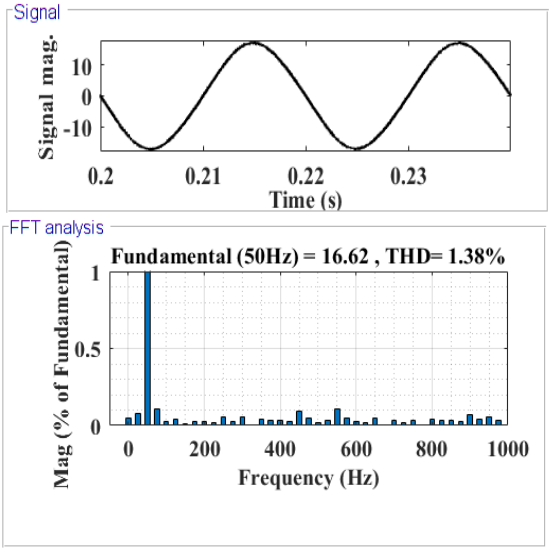

Fig. 4.8. THD (%) in grid current under nonlinear load

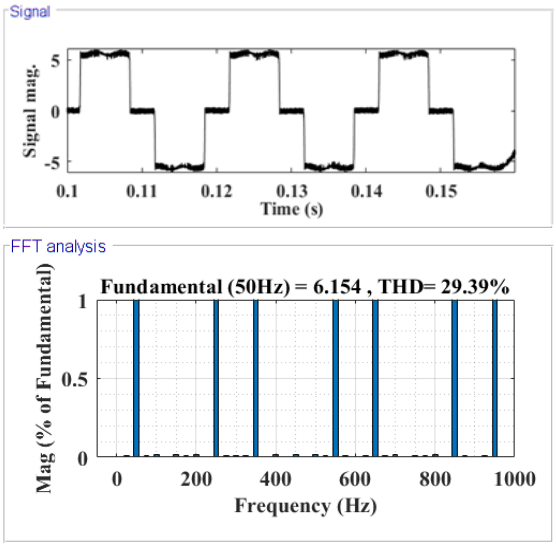

Fig. 4.9. THD (%) in nonlinear load current

4.4.2.2 *Performance under linear and nonlinear load at varying insolation*

Further, the proposed new VSSLMS control is also tested at varying insolation under linear and nonlinear load. Solar irradiance is decreased at 0.15 second from 1000W/m^2 to 700W/m^2 and again increased to 1000W/m^2 at 0.25 second; thus, solar PV current decreased; thus, PV output power is reduced and vice versa.

A 20kVA, 0.8 pf lag linear load is considered, simulated results and corresponding various parameters viz. V_{grid}, I_{grid}, I_{load}, I_{inv}, P_{grid}, Q_{grid}, P_{inv}, Q_{inv}, P_{load}, Q_{load}, and V_{dc} of the PV inverter are shown in figure 4.10. It is observed from figure 4.10, between 0.1 to 0.15 second, that both V_{grid} and I_{grid} are in phase (as power is supplied from grid to load), V_{dc} is maintained at 750V, PV inverter supplies its generated power 10.25kW which is not enough to fulfil the load demand of 20kVA, 0.8pf lag (16kW and 12kVAR), therefore to meet the load demand, extra power 5.75kW is taken from distribution grid, while 12 kVAR of reactive demand of the load is

supplied by PV inverter alone, showing proposed control is efficient in maintaining the grid at UPF. Further the proposed algorithm on linear load (20kVA, 0.8 pf lag) is tested under varying insolation from 0.15 seconds and 0.25second. The performance of system using proposed algorithm under linear load condition under varying insolation between 0.15 to 0.25 seconds is analysed and various parameter viz. V_{grid}, I_{grid}, I_{load}, I_{inv}, P_{grid}, Q_{grid}, P_{inv}, Q_{inv}, P_{load}, Q_{load}, and V_{dc} are presented in figure 4.10. Due to decrease in solar insolation, P_{inv} is decreased to 7.75kW at 0.15 seconds causing the grid to supply more power by 2.5 kW (total 8.25 kW) to the load as depicted in figure 4.10, while, total reactive power demand of load is still supplied by inverter alone hence keeping grid at UPF during the adverse scenario of solar insolation. After 0.25 second, insolation and PV power both has been increased and system regains the initial (0.1 to 0.15 second), steady state condition.

It has been observed that during solar insolation variation, sharing of active and reactive power between load (P_{load}, Q_{load}), grid (P_{grid}, Q_{grid}) and inverter (P_{inv}, Q_{inv}) is maintained, grid current is sinusoidal and maintains V_{dc} at 750 V.

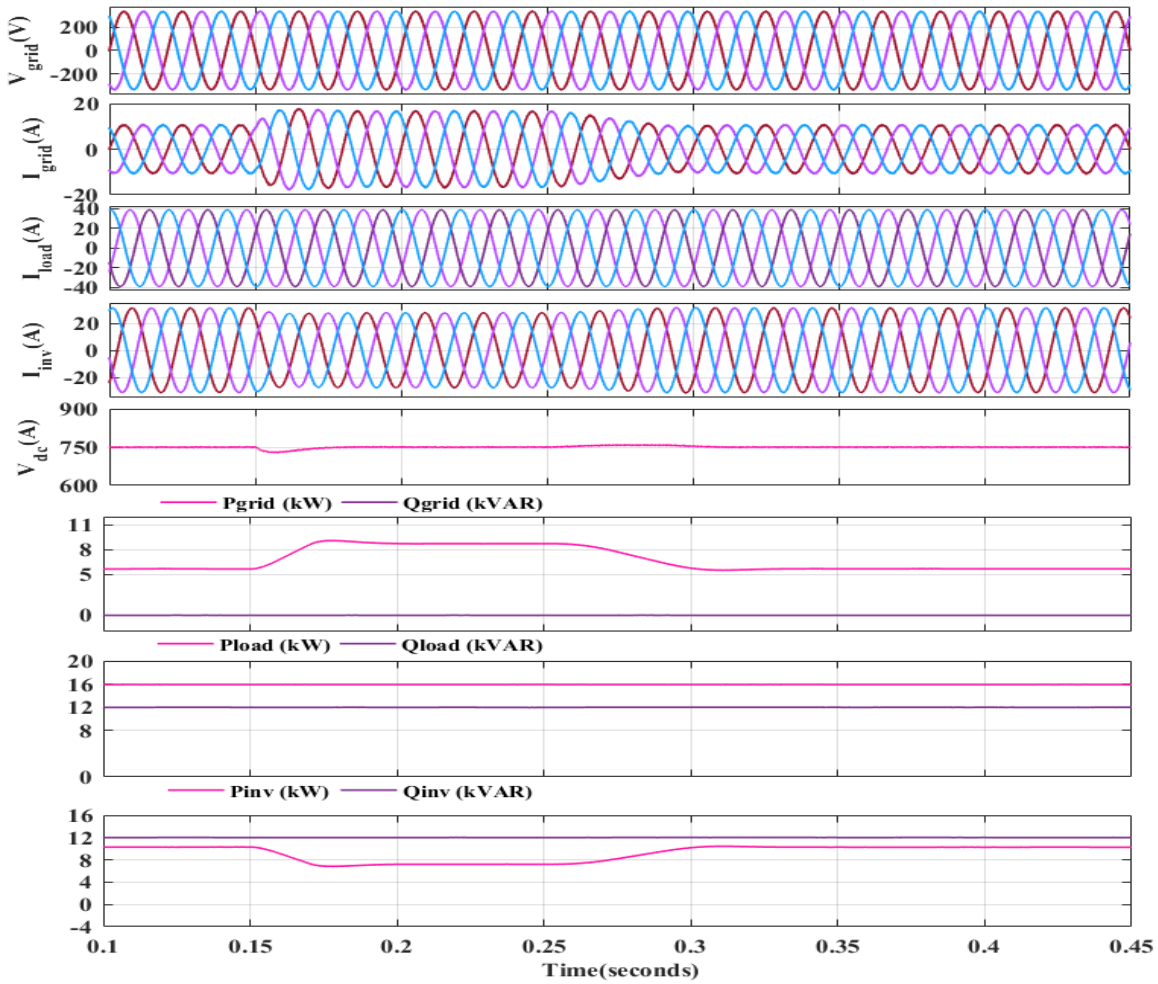

Fig. 4.10. Performance of system under linear load at varying insolation

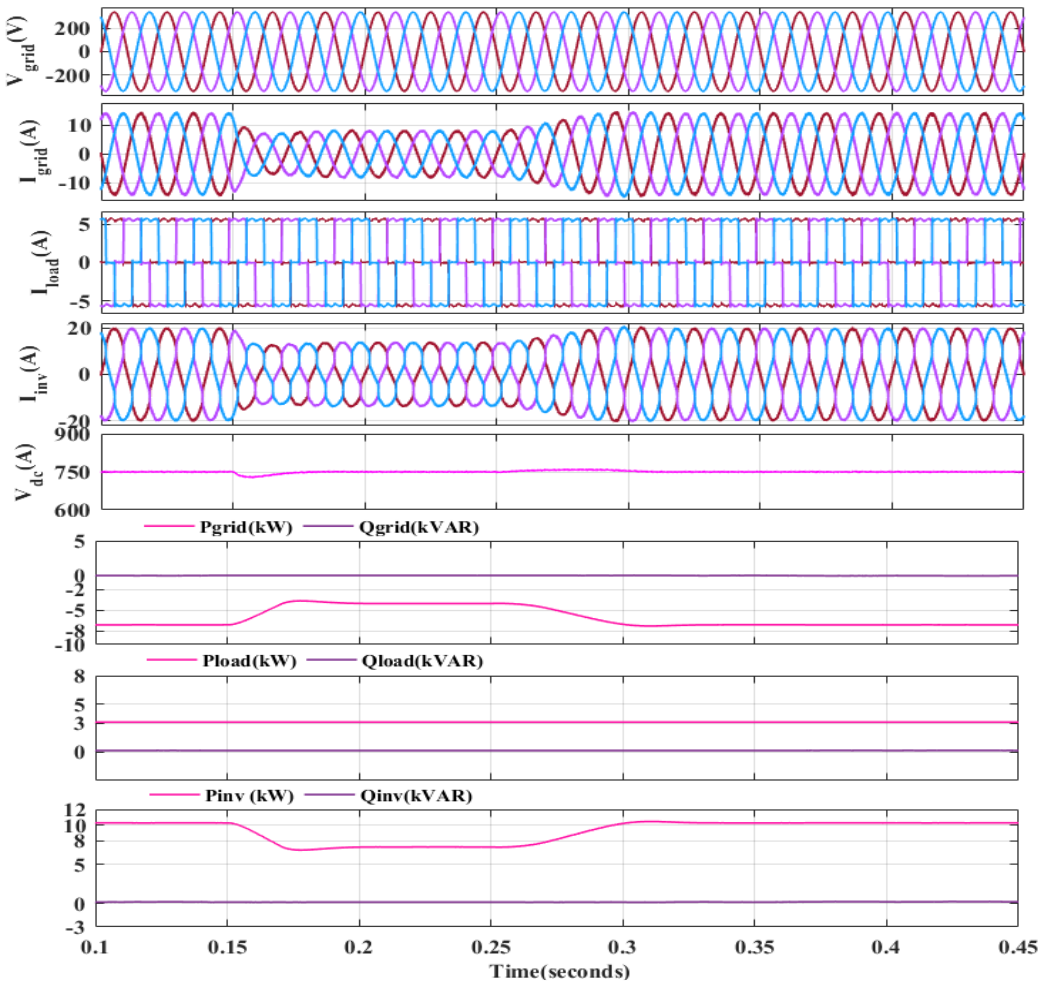

Fig. 4.11. Performance of system under nonlinear load at varying insolation

Further for a nonlinear load (three phase bridge rectifier with RL load, R=100Ω, L=100mH) at varying irradiance, simulated results and corresponding various parameters viz. V_{grid}, I_{grid}, I_{load}, I_{inv}, P_{grid}, Q_{grid}, P_{inv}, Q_{inv}, P_{load}, Q_{load}, and V_{dc} of the PV inverter are shown in figure 4.11. It is observed from figure between 0.1 to 0.15 second, V_{grid} and I_{grid} are out of phase by 180^0 (as power is supplied to grid), V_{dc} is maintained at 750V, PV inverter supplies its generated power 10.25kW after satisfying the load demand of 3.1 kW, rest power 7.15kW is fed back to grid, while PV inverter alone supplying reactive power demand of the load, showing proposed control is efficient in maintaining grid at UPF.

After decrease in solar insolation at 0.15 seconds, PV inverter power is decreased from 10.25kW to 7.75kW, leading to decrease in the power fed to the grid by 2.5kW as shown in figure 4.11. While reactive power demand of load is supplied by PV inverter (VSC) alone hence keeping grid at UPF during the adverse scenario of solar insolation. After 0.25 second, insolation and PV power both has been increased and system regains the initial (0.1 to 0.15 second), steady state condition.

It has been observed that during solar insolation variation, active and reactive power is balanced between inverter (P_{inv}, Q_{inv}) load (P_{load}, Q_{load}) and grid (P_{grid}, Q_{grid}) is maintained, I_{grid} is sinusoidal and V_{dc} is maintained at 750 V.

4.4.2.3 *Comparison of active weight convergence of proposed VSSLMS algorithm and conventional SRF and LMS control algorithms*

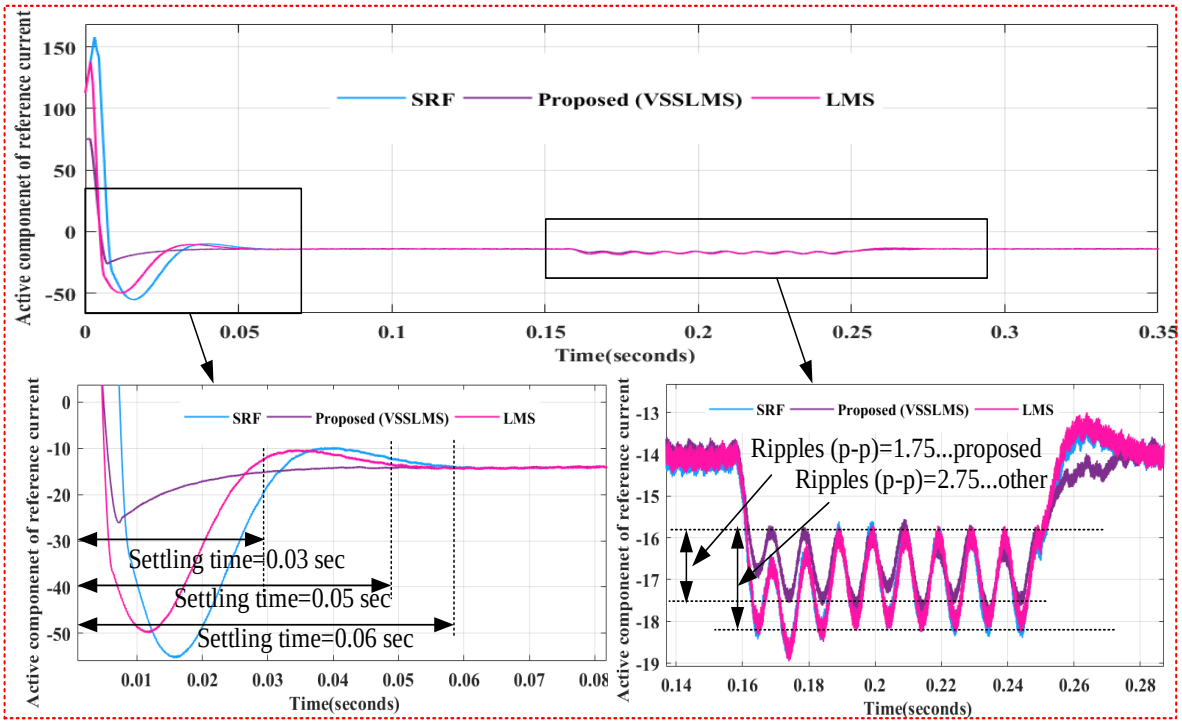

Fig. 4.12 Comparative performance of proposed VSSLMS with SRF and LMS control

Table 4.1. Comparison of VSSLMS control algorithm with SRF and LMS

Control algorithm	Settling time (sec)	Overshoot in active component (W_{ps})	Undershoot in active component (W_{ps})
SRF	0.06	160	-58
LMS	0.05	140	-50
VSSLMS	0.03	75	-25

Figure 4.12, shows comparison of proposed VSSLMS control with conventional SRF and LMS adaptive control. Nonlinear load viz. three phase bridge rectifiers with RL load (R=100Ω,100mH) is considered and further to investigate the transient response during load perturbation one phase of load is kept removed from 0.15 to 0.25 second.

It can be seen from figure 4.7, that till 0.30 seconds; PV system supplies its rated active power. It is observed that till 0.30 seconds V_{grid} and I_{grid} are 180° out of phase (as power is fed to the

grid) therefore, active component of reference current is negative as it can be seen from figure 4.12.

Figure 4.12, shows the comparison of transient and dynamic performance under considered load. It can be seen from the figure., that during grid integration, proposed control gives better initial transient response in terms of settling time, overshoot and undershoot as given in table 4.1 and has less oscillations. Further during load perturbation, it can be seen that proposed control has lower ripples as compared to that of the conventional SRF and LMS control, settling time using proposed VSSLMS control is 30msec whereas it's 50msec and 60msec respectively in case of conventional SRF and LMS. Hence the proposed control, is more efficient than that of other conventional SRF and LMS adaptive control.

4.4.3 Robust Least Mean Logarithmic Square Control Algorithm

4.4.3.1 *Performance under linear/nonlinear (unbalanced) and load varying at STC*

Figure 4.13 and 4.14 show the performance of control under linear (5kVA, 0.8 pf) and nonlinear load (three phase bridge rectifier with RL load, R=100Ω, L=100mH), respectively. V_{grid}, I_{grid}, I_{load}, I_{inv}, V_{dc}, and power sharing between VSC, grid and load are among the system's parameters that are examined.

VSC supplies 4kW and 3.0 kVAR demand of the load until 0.15 seconds, I_{grid} and V_{grid} are 180° out of phase (as grid is receiving reserve 6.25 kW power), and V_{dc} is maintained at its reference (V^*_{dc}). VSC alone meets reactive power requirement of load, resulting in a 0% reactive power delivered from the grid, proving that control scheme is efficient under UPF mode.

Furthermore, performance under linear unbalanced conditions is evaluated by disconnecting one phase 'b' for 0.15 to 0.25 seconds and investigating several system parameters such as V_{grid}, I_{grid}, I_{load}, I_{inv}, P_{grid}, Q_{grid}, P_{inv}, Q_{inv}, P_{load}, Q_{load}, and V_{dc} as shown in figure 4.13.

During the unbalance moment, the VSC compensates for the effect of the load unbalance and keeps the I_{grid} balanced. It also meets the reactive demand, keeping the grid at UPF while balancing the I_{grid}. Furthermore, between 0.25 to 0.3 seconds, operating at its initial load (5kVA, 0.8 pf) condition. A 10kVA linear load with 0.8 pf lagging connected to PCC at 0.3 to 0.4 seconds to examine the load variation performance. At 0.3 second's, demand is 15kVA, 0.8 pf lagging (12kW and 9 kVAR). VSC is insufficient to meet the load requirement, an additional 1.75 kW is drawn from the grid to meet the load requirement.

It has been observed that I_{grid} is sinusoidal and V_{dc} is maintained at V^*_{dc} during single phasing and load variation. It has been observed the proposed control approach compensates, the effect

of reactive power and unbalance of the load hence improves the power factor and maintains sinusoidal grid current under different loading conditions under STC.

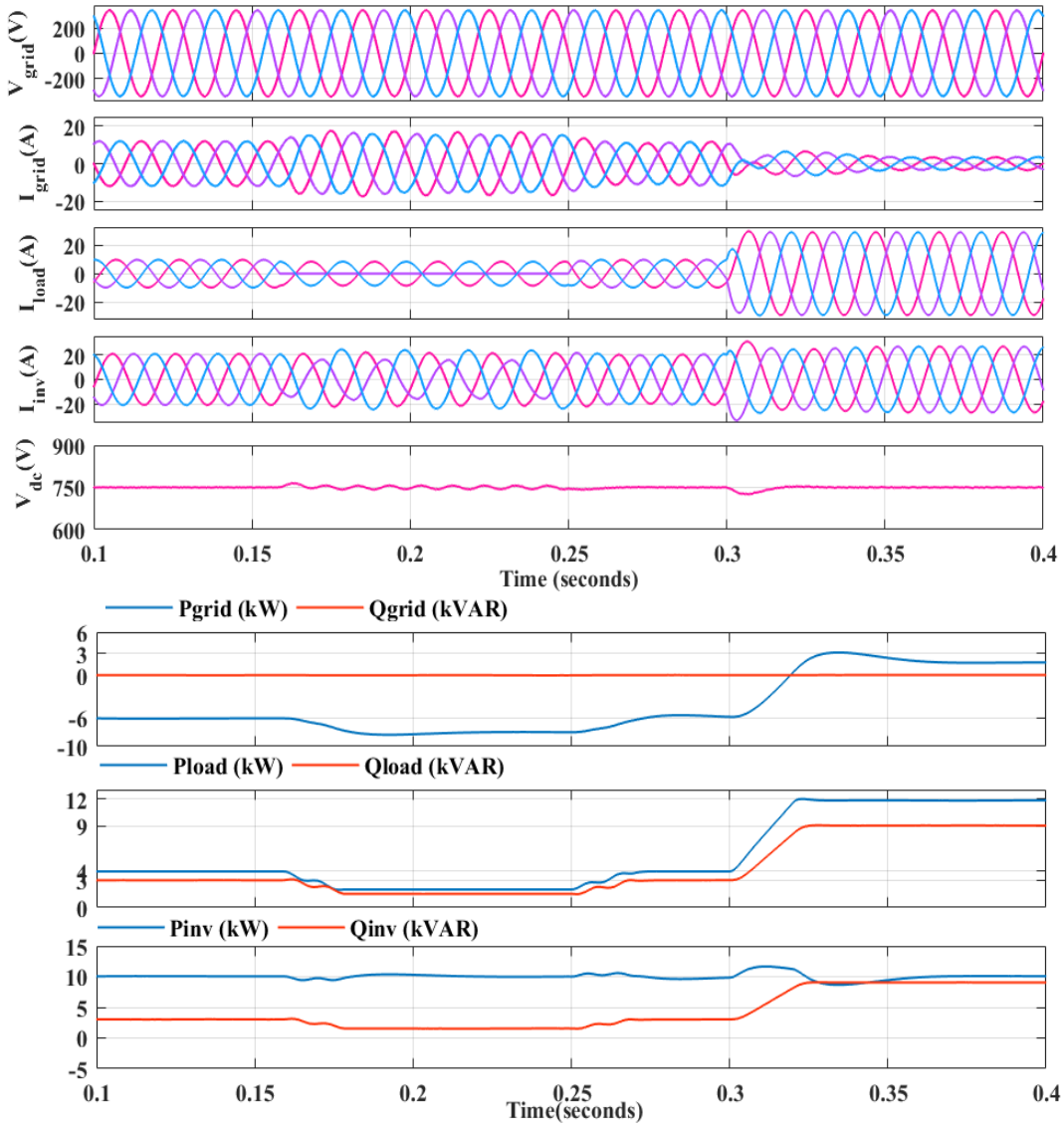

Fig. 4.13. Performance at STC input under linear (balance/unbalance) and variable load

Further, under non-linear load (three phase bridge rectifier with RL load, R=100Ω, L=100mH), proposed control has been validated, and the results are given in figure 4.14.

The VSC supplies 3.1 kW, until 0.15 seconds, I_{grid}, V_{grid} are 180° out of phase (as grid is receiving reserve 6.25 kW power), and V_{dc} is maintained at its reference (V^*_{dc}). VSC alone meets the load requirement, resulting in a 0% reactive power delivered from the grid, proving that suggested control is effective under UPF mode by keeping the grid at UPF.

Furthermore, the performance under nonlinear unbalanced load conditions is evaluated by disconnecting one phase 'b' for 0.15 to 0.25 seconds and investigating various system parameters such as V_{grid}, I_{grid}, I_{load}, I_{inv}, V_{dc}, P_{grid}, Q_{grid}, P_{inv}, Q_{inv}, P_{load}, Q_{load}, and V_{dc} as shown

in figure 4.14. During the unbalance moment, the VSC compensates for the effect of the load unbalance and keeps the I_{grid} balanced. It also meets the for reactive load demand, keeping the grid at UPF while balancing the I_{grid}. A 5 kVA, 0.8 pf lag, is connected at PCC from 0.3 to 0.4 seconds to examine the load variation performance. At 0.3 second's Load requirement is (7.1kW and 3 kVAR), because the power produced by the PV inverter is sufficient to meet the load requirement, remaining 3.15 kW is delivered to the grid.

It can be seen that VSC compensates the harmonics and maintains I_{grid} sinusoidal, Vdc is maintained at V*dc, during single phasing and load variation. THD (%) in Igrid is 2.49 percent, as depicted in figure 4.15, it lies inside the bounds of IEEE standard 519-2014, whereas THD (%) in I_{load} is 29.39% given in the figure 3.16.

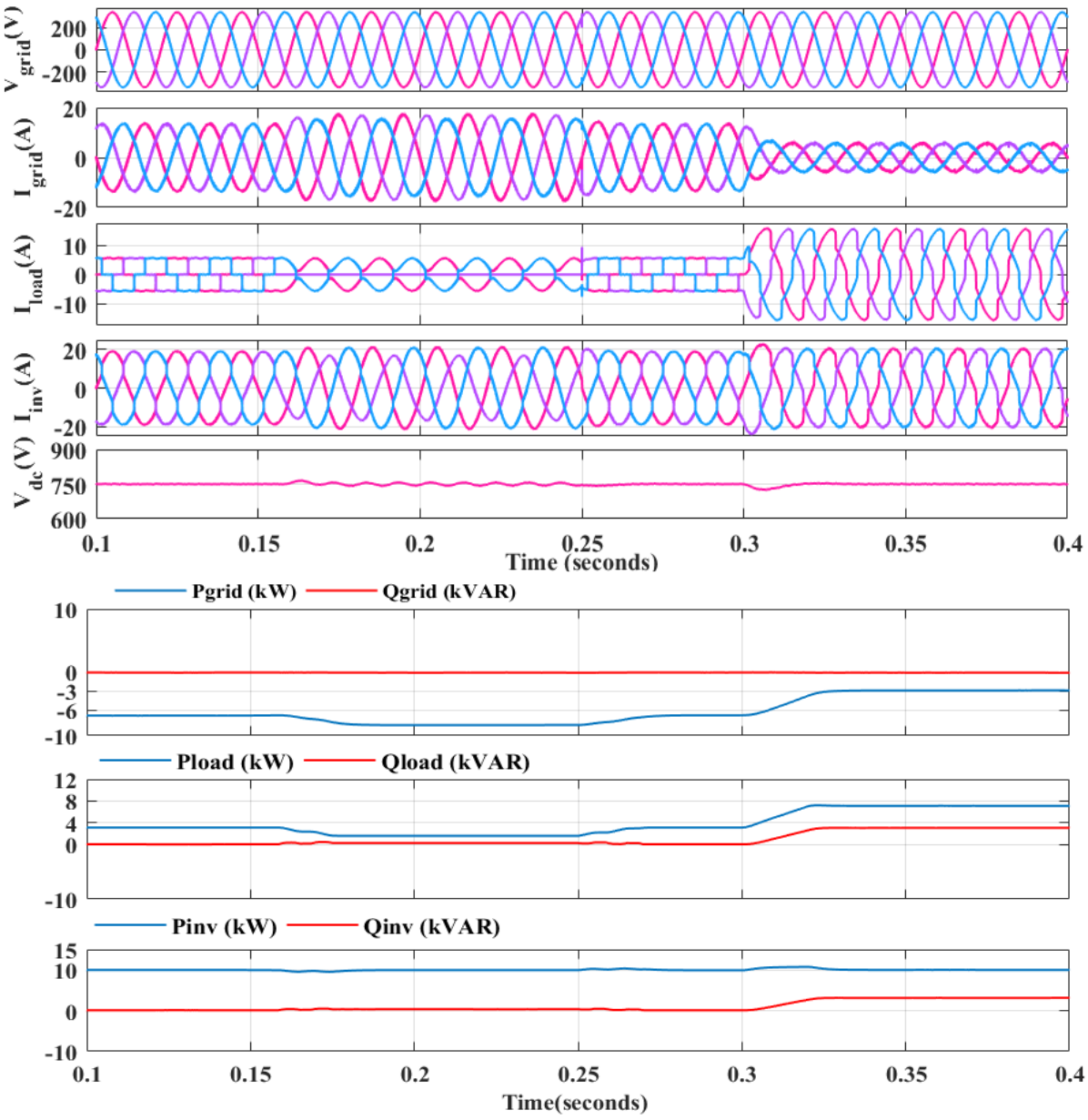

Fig. 4.14. Performance at STC input under nonlinear (balance/unbalance) and load varying

It has been observed that even under non-linear load conditions, the proposed control approach compensates, the effect of reactive power, unbalance and non-linearity of the load hence improves the power factor, maintains sinusoidal and balanced grid current. Further, harmonics in the I_{grid} is 2.49% which satisfies the IEEE standards.

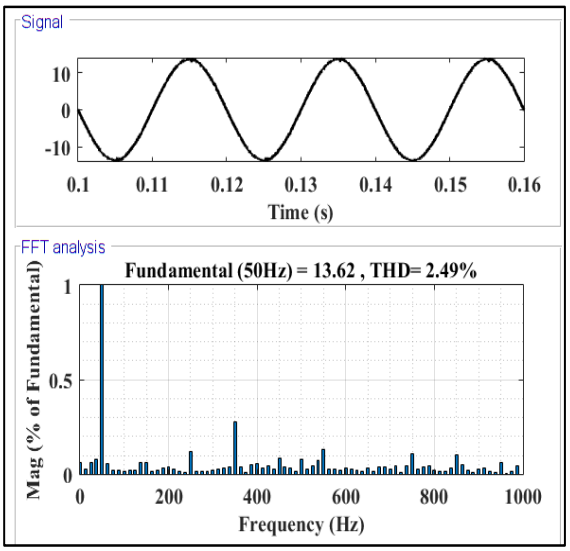

Fig. 4.15. THD (%) in grid current waveform

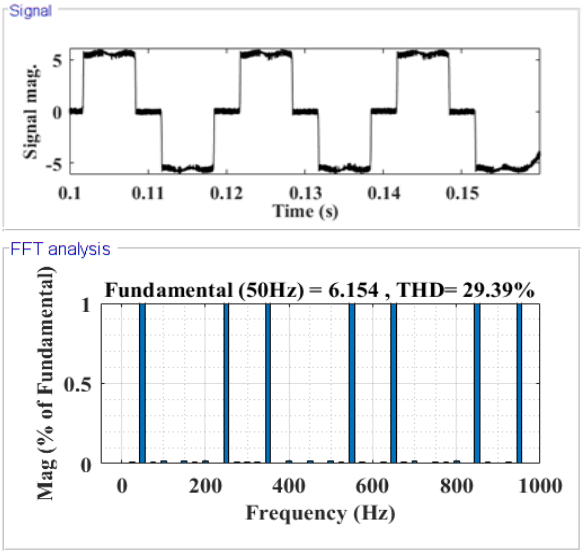

Fig. 4.16 THD (%) in nonlinear load current waveform

4.4.3.2 *Performance under linear and nonlinear load at varying insolation*

Furthermore, control is validated under variable insolation. Solar irradiance is lowered from 1000W/m^2 to 700W/m^2 at 0.25 seconds, resulting in a fall in solar PV current as a result, a reduction in PV output power and results has been discussed for linear and nonlinear load respectively in the figure 17 and 18.

The simulated results under 20 kVA, 0.8 pf lag linear load and associated different parameters such as V_{grid}, I_{grid}, I_{load}, I_{inv}, V_{dc}, P_{grid}, Q_{grid}, P_{inv}, Q_{inv}, P_{load}, Q_{load}, and $V_{dc,}$ are presented in figure 4.17. It can be shown in figure 4.16, until 0.25 seconds that both I_{grid} and V_{grid} are in phase, V_{dc} is maintained at V^*_{dc}, VSC delivers its developed 10.25 kW, which is insufficient to meet the load requirement of 20 kVA, 0.8pf lag (16 kW and 12 kVAR), so balanced power of 5.75 kW is drawn from the grid to meet the load demand, while 12 kVAR of reactive demand is fed by VSC alone, proving that the control is effective under UPF mode. The proposed technique has also been evaluated on a linear load with insolation ranging from 0.25 seconds to 0.4 seconds. After 0.25 seconds, due to reduction in solar irradiance, P_{inv} is reduced to 7 kW at 0.25 seconds, causing additional 3.25 kW has been supplied by grid to the load as shown in figure 4.17.

Whereas the complete reactive power is still met by the VSC alone, the grid remains at UPF during periods of low solar irradiance.

The sharing of power between load (P_{load}, Q_{load}), VSC (P_{inv}, Q_{inv}) and grid (P_{grid}, Q_{grid}) is maintained throughout solar insolation variation, I_{grid} is sinusoidal, V_{dc} is sustained at reference dc link voltage (V*dc).

It has been observed the proposed control approach compensates, the effect of reactive power, hence improves the power factor, under varying insolation.

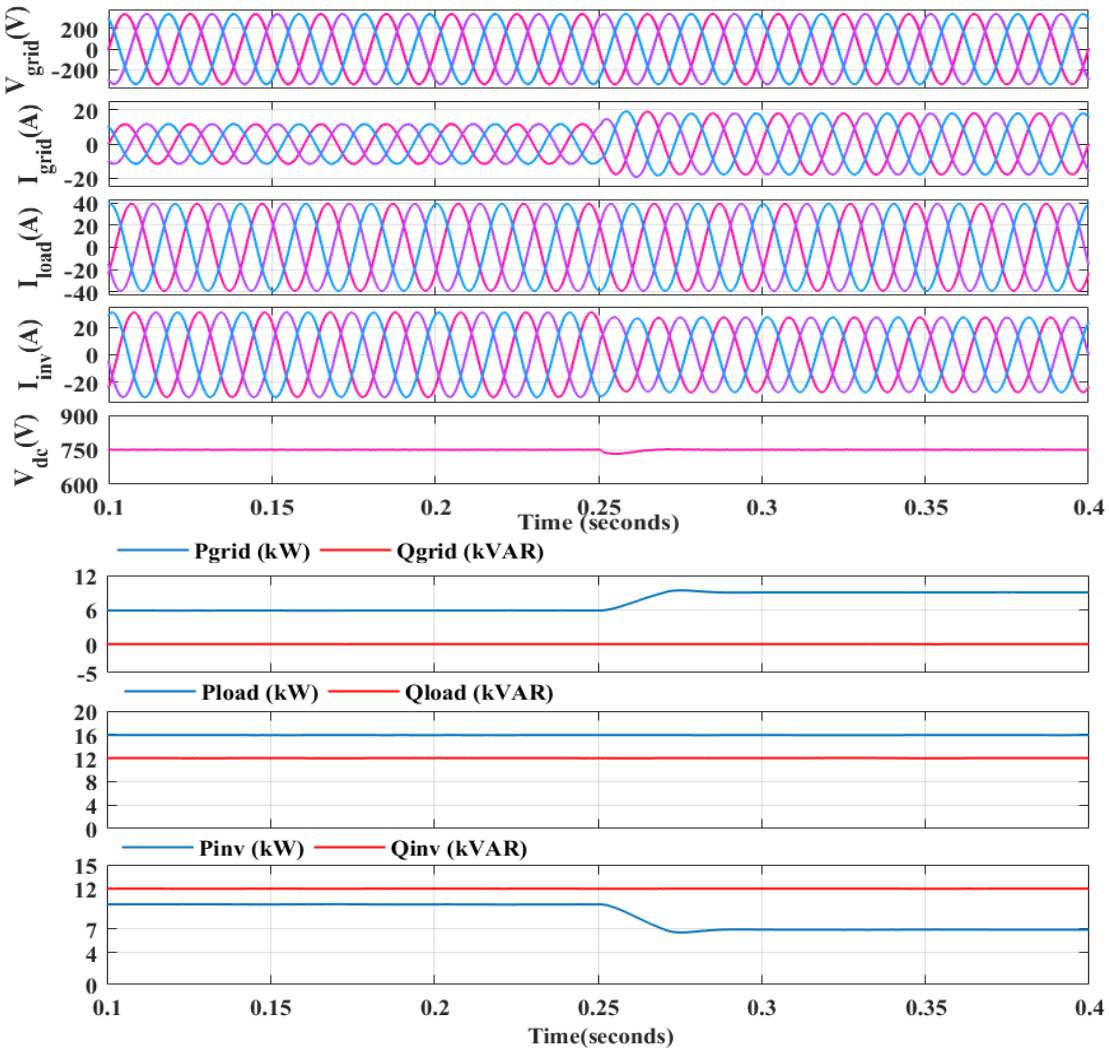

Fig. 4.17. Performance at varying irradiance under linear load

Further, under nonlinear load (three phase bridge rectifier with RL load, R=100Ω, L=100mH), and varying irradiance, has been validated and corresponding different parameters such as V_{grid}, I_{grid}, I_{load}, I_{inv}, P_{grid}, Q_{grid}, P_{inv}, Q_{inv}, P_{load}, Q_{load}, and V_{dc} of the VSC are depicted in figure 4.18. Until 0.25 seconds, I_{grid} and V_{grid} are out of phase by 180^0 (as grid is receiving power), V_{dc} is maintained at V^*_{dc}, VSC supplies 10.25 kW. After meeting the 3.1 kW load demand, the excess 7.15 kW is supplied to the grid, the VSC delivers the load's reactive demand, showing that the

control is effective under UPF mode. After 0.25 seconds, due to reduction in solar irradiance, P_{inv} is reduced to 7 kW at 0.25 seconds, causing decrease the power fed to the grid and load as depicted in figure. 4.18. The sharing of active and reactive power between load (P_{load}, Q_{load}), grid (P_{grid}, Q_{grid}) and inverter (P_{inv}, Q_{inv}) is maintained throughout solar insolation variation, I_{grid} is sinusoidal, V_{dc} is maintained at V^*_{dc}. THD in I_{grid} is 1.95% under varying insolation, as depicted in figure 4.19.

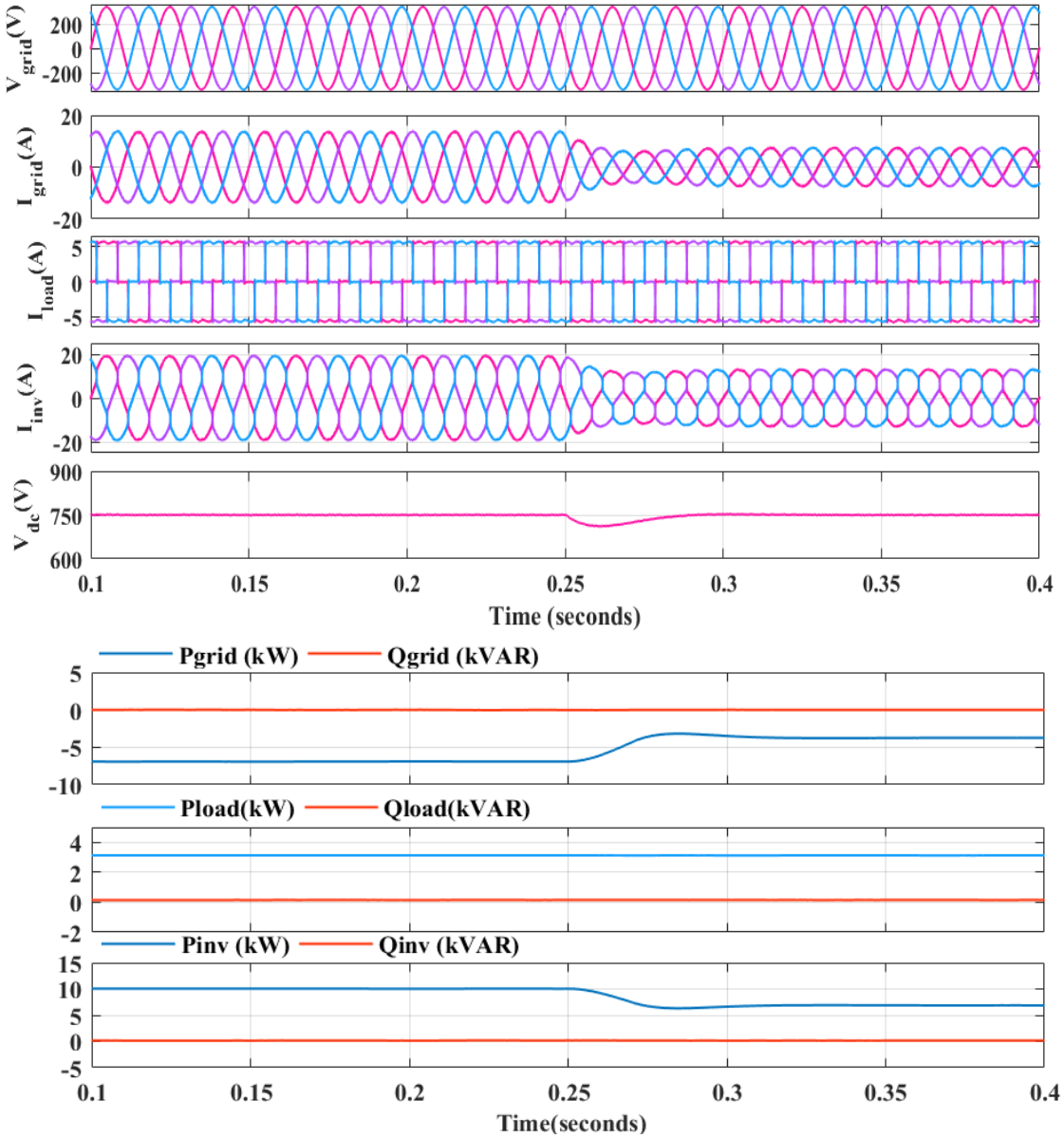

Fig. 4.18. Performance at varying insolation under nonlinear load

it lies inside the bounds, of IEEE standard 519-2014, while THD in I_{load} is 29.39% as depicted in figure 4.20. It has been observed the proposed control approach compensates, the effect of harmonics in load current, hence improves the I_{grid}, under varying insolation.

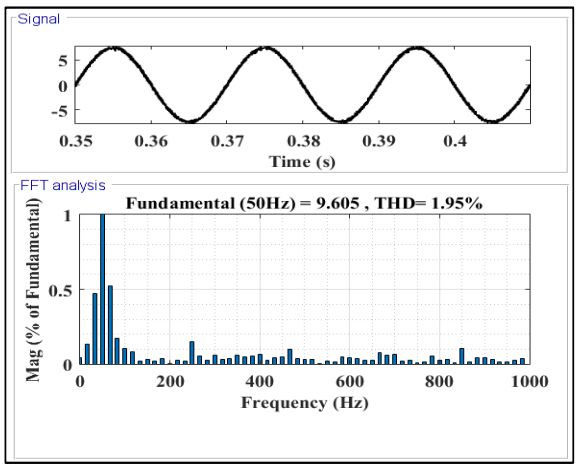

Fig. 4.19. THD (%) in grid current waveform

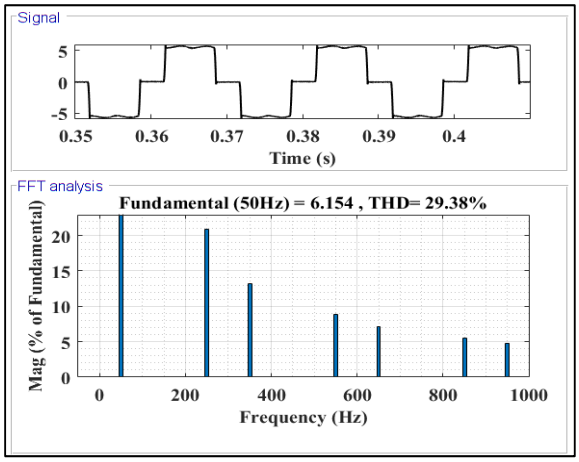

Fig. 4.20. THD (%) in nonlinear load current waveform

4.4.3.3 *Comparison of active weight convergence of proposed RLMLS algorithm with SRF and LMS control algorithms*

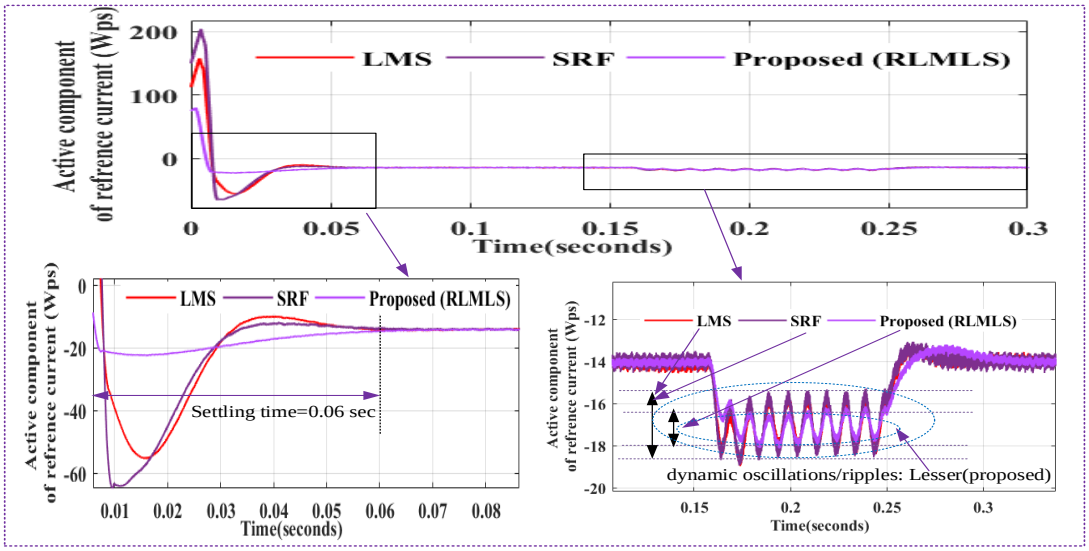

Fig. 4.21 Comparative performance of proposed RLMLS, and conventional SRF and LMS control

Table 4.2. Comparison of RLMLS control algorithm with SRF and LMS

Control algorithm	Settling time (sec)	Overshoot in active component (W_{ps})	Undershoot in active component (W_{ps})
SRF	0.06	205	-65
LMS	0.06	158	-55
RLMLS	0.06	80	-22

Figure 4.21, depicts performance comparison of proposed RLMLS, SRF and LMS algorithm under transient and dynamic performance. Nonlinear load is considered to study both transient and dynamic response. Further, from 0.15 to 0.25 second, one phase of load is eliminated for dynamic response. As can be observed from the figure 4.13, and table 4.2, the proposed control provides the better initial transient response in terms of overshoot and undershoot. Further during load perturbation, from 0.15 to 0.25 seconds, it can be seen, that proposed control scheme has lower ripples than LMS and SRF control, in the active component estimation, during single phasing that refers faster convergence. Furthermore, the control scheme does not require a complicated block for synchronization, such as a phase lock loop (PLL), which eliminates the additional computational burden, with the added benefit of reduced complexity, ease of implementation, and adaptability.

4.5 COMPARATIVE ANALYSIS OF VARIOUS CONTROL ALGORITHMS

THD (%) in grid current using the proposed control algorithms viz. VSSLMS, RLMLS and conventional LMS, SRF control are presented in table 4.3, under non-linear load. THD (%) in grid current using proposed control algorithms are 1.38%, 1.95% and THD (%) in grid current using conventional SRF and LMS control are 1.85% and 1.92% respectively while THD (%) in load current is 29.53%. THD (%) in grid current under nonlinear load is observed to be less than 5% which is within the limit of IEEE-519 standard. Furthermore, the proposed control scheme does not require a complicated block for synchronization, such as a phase lock loop (PLL), which eliminates the additional computational burden, with the added benefit of reduced complexity, ease of implementation, and adaptability along with the better response of transient and dynamic load condition.

Table 4.3. Comparison of THD (%) in grid current using various adaptive control algorithms

S.N.	**THD in grid current**	
	Control algorithms	***THD***
1	SRF	*1.85*
2	LMS	1.92
3	VSSLMS	1.38
4	RLMLS	1.95

4.6 CONCLUDING REMARKS

In this chapter, adaptive theory based VSC control algorithms viz. conventional LMS, and proposed novel VSSLMS, and RLMLS, for two-stage, three-phase grid interfaced SPV system have been presented. The efficiency of the proposed control algorithms has been tested under different input/output condition such as insolation variation, load variation, load unbalancing, nonlinear load, reactive load, grid voltage unbalancing, and distorted grid voltage etc. Furthermore, the performance of the proposed algorithms is compared with conventional SRF and LMS control in terms of THD (%) in grid current and weight convergence. The performance of the proposed control algorithms is verified on MATLAB/ Simulink. It has been observed that developed control algorithms maintain power balance, compensates reactive power, and harmonics. THD (%) in grid current under nonlinear load is observed to be less than 5% which is within the limit of IEEE-519 standard. Furthermore, both VSSLMS, RLMLS have better weight convergence capability and better initial transient response in terms of overshoot and undershoot and lesser oscillations in the response during dynamic scenario. Performance of the proposed VSC control algorithms has been found to be satisfactory under all test conditions.

CHAPTER-V

DEVELOPMENT OF PROTOTYPE HARDWARE FOR THE GRID CONNECTED PV SYSTEM

5.1 INTRODUCTION

In the earlier chapter two novel adaptive control algorithms viz. variable step size LMS(VSSLMS) and robust least mean logarithmic square control algorithm (RLMLS) has been developed and simulated in the MATLAB/Simulink. In this chapter, the performance of these algorithm is tested in the real- time on a prototype model of a grid connected PV system.

In this chapter, the development of prototype hardware for the grid connected PV system and its various components has been presented. Furthermore, due to limitations (non-availability) of solar PV array/PV simulator in the laboratory, developed VSC control algorithms are tested on the DSTATCOM in the laboratory and real- time hardware results have been presented. The layout of three phase DSTATCOM connected to grid is shown in the figure 5.1.

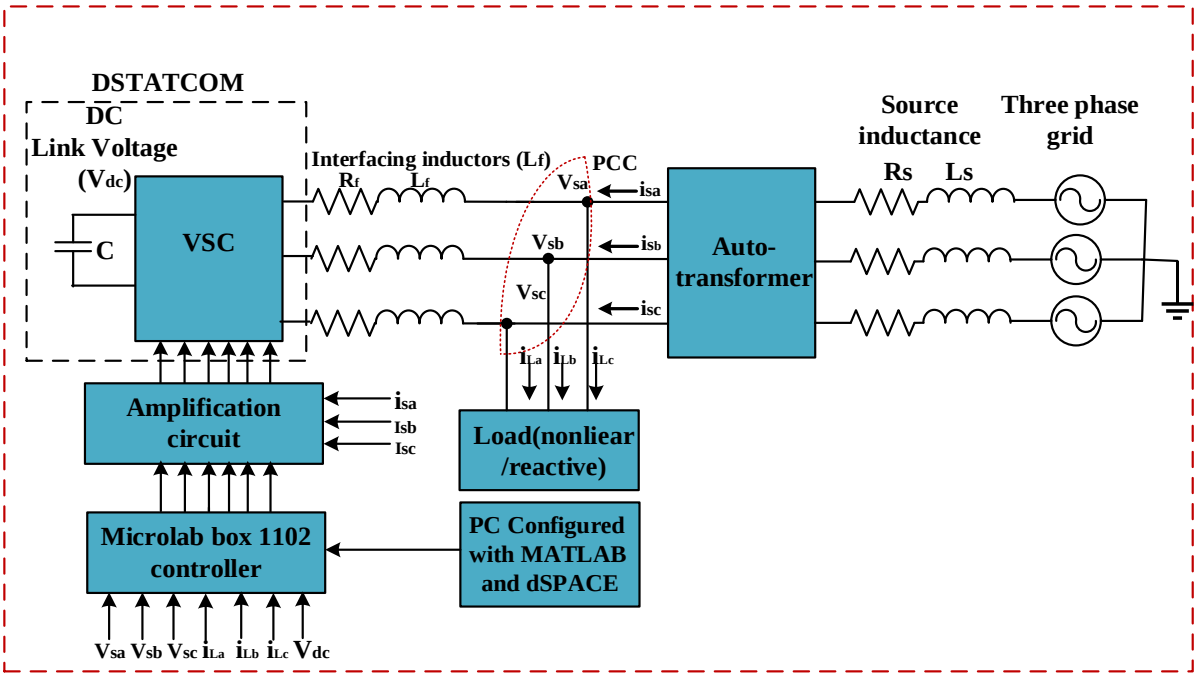

Fig. 5.1. Layout of three phase DSTATCOM connected to grid

5.2 HARDWARE CONFIGURATION AND DEVELOPMENT OF PROTOTYPE OF THREE PHASE DSTATCOM

The prototype hardware set -up of grid connected PV system requires primarily the design, and development of VSC, DC-DC converter, and solar PV array. Furthermore, the design and

selection of various components viz. interfacing inductors, DC link capacitor, voltage sensing circuits, current sensing circuits, linear, reactive and nonlinear loads to be compensated, are also required for the prototype hardware set -up in the laboratory.

A three-phase nonlinear load is fed by three-phase AC mains with grid impedance, as depicted using a series R_S-L_S combination. IGBTs along with anti-parallel diodes are used in the three-leg of VSC, and a DC link capacitor (C_{dc}) on the DC side. On the AC side of the VSC, interfacing inductors (L_f) are employed to connect the VSC to the grid. The uncontrolled bridge rectifier with RL load (R=0-100Ω, L=20mH) is used for the nonlinear load. The DSP receives sensing signal of the three-phase voltage from the PCC i.e. (V_{sa},V_{sb} and V_{sc}), grid current (i_{sa}, i_{sb} and i_{sc}), DC link voltage (V_{dc}) and load current (i_{La}, i_{Lb} and i_{Lc}). DSP processes these signals to provide the proper switching pulses for the three phase VSC.

The prototype of three-phase DSTATCOM is implemented in the laboratory. The system is developed at lower voltage rating of 110V, 50Hz due to unavailability of equipment rating constrains in the laboratory. Single line diagram of the three-phase DSTATCOM's is depicted in figure 5.1, shows the AC mains (three-phase, 415V, 50Hz) is the input to the auto transformer, and its output voltage is 110V,50Hz. Three phase VSC is designed using three leg IGBTs (six IGBTs, anti-parallel diodes), and a large capacitor are used on the DC side [121].

The DSP (Microlab box/dSPACE 1102) embeded in the personal computer is used to perform the real- time control operation of the VSC. The VSC control algorithm for the estimation of reference current is modelled in the MATLAB/ Simulink and have been implemented using MicroLabbox (dSPACE1102).

Hall effect voltage and current sensors are used to measure the PCC i.e. (V_{sa} V_{sb} and V_{sc}), grid current (i_{sa}, i_{sb} and i_{sc}), DC link voltage (V_{dc}) and load current (i_{La}, i_{Lb} and i_{Lc}).

The outputs of the voltage and current sensors are sent into the DSP's ADC channels. The ADC channel signals are scaled up to obtain the real values of PCC voltages, grid,and load currents, and DC link voltage. These input signals are sent into the control algorithm, which generates reference currents. The switching pulses for VSC are obtained via the DSP-dSPACE's PWM port through the gate driver circuit. Interfacing inductors connect the VSC's alternating current side to the PCC.

5.3 DESIGN OF COMPONENTS AND TESTING FOR PROTOTYPE HARDWARE

For designing a prototype hardware, design of its each component is required.

5.3.1 Design of Voltage Source Converter (VSC) [121]

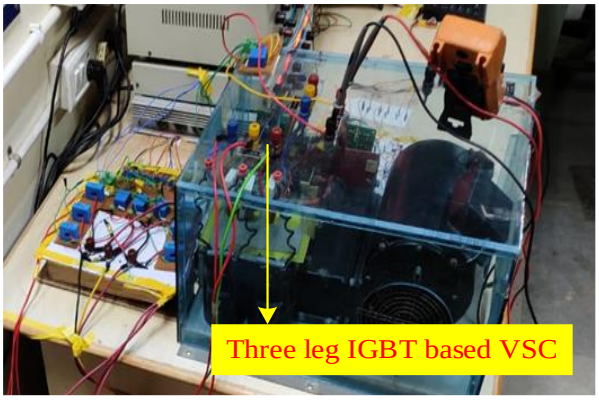

Fig. 5.2. IGBT based VSC

VSC is an IGBT based three leg converters used to feed power to the load and utility grid. VSC supplies, power to the load/grid and operate at UPF mode thus maintain grid power factor at unity.

The VSC (Semikron make) used as DSTATCOM in the laboratory is depicted in figure 5.2. Insulated gate bipolar transistors (IGBTs) and antiparallel diodes make up this device. The DC bus capacitor has a rating of 1650 μF, 1200 V. For real- time control of VSC, the switching pulses are provided through microlab box (dSPACE1102). Switching pulses are produced from the MicrolabBox's PWM port and supplied to the gate driver circuit, which produces 15V output pulses for the IGBTs' functioning. The proposed system's simulation model is developed in MATLAB/Simulink.

5.3.1.1 *Design and selection of rating for inverter switches*

The voltage rating of IGBTs of VSC under dynamic load condition is presented below: [121],

$$Vsm = Vdc + \Delta Vdc = 200 + 20 = 220\text{V} \quad (5.1)$$

where ΔVdc is the 10% overshoot in the DC link voltage under dynamic load condition. If a reference value of DC bus voltage is selected as 200V, then voltage rating of switches is calculated to be 220V. The IGBTs voltage rating is selected 750/1200V, after considering appropriate safety factor.

Current rating of IGBTs of VSC under dynamic load condition is presented below:

$$ism = 1.25(Isw + Icr) = 1.25(14.41 + 2.8) = 21.5A \quad (5.2)$$

where Isw and Icr are the peak values of compensator current (for nonlinear load specified in Appendix-B: maximum available load in the lab is up to 10A) and the allowed ripple currents considering 20%. The current rating is calculated 21.5A. The IGBT module, SKM150GB12V (Semikron make) is selected. The available voltage and current rating for IGBT module in the laboratory are 1200V and 120 A respectively.

5.3.1.2 *Design and selection of DC link voltage* [121]-[122], [55].

Minimum required voltage across dc link capacitor must be more than two times of the voltage per phase of the system.

$$V_{dc} = 2\sqrt{2} * V_{LL}/(\sqrt{3}) \quad (5.3)$$

V_{dc}= (2√2) *110 / (√3) =180V

Voltage across dc link obtained from equation (5.3) is 180V for V_{LL} of 110 V and is chosen as 200V.

5.3.1.3 *Design and selection of DC link capacitance* [122]-[123], [55]

The DC capacitor's design is determined by how the DC bus voltage changes when a load is applied and how it changes when a load is removed. The equation governing C_{dc} depends on the principle of energy conservation as given below:

$$\frac{1}{2} C_{dc}(V^2{}_{dc} - V^2{}_{dc1}) = \ k_1\, 3VhIt \quad (5.4)$$

Where C_{dc} is dc link capacitor, V_{dc} and V_{dc1} are reference dc link voltage and minimum dc link voltage level respectively. Overloading factor (h=1.2), V is phase voltage ($110 = \sqrt{3}$), t is time to be recovered by dc link voltage. Variation of energy under dynamics =10% ($k_1 = 0.1$), I=10.5A, considering $1kVA$, reactive power compensation by VSC with safety factor of 0.1 in a 110V, 50Hz distribution system.

C_{dc}= 1040 μF

The estimated value of C_{dc} using equation (5.4) is 1040 μF, selected value of C_{dc} is 1650 μF due to availability of capacitor in the laboratory.

5.3.2 Design of Interfacing Inductors [122]-[124], [55]

Interfacing inductor rating of VSC depends on switching frequency (f_{sw}), current ripple (Δi) and dc link voltage (V_{dc}). Interfacing inductor (L_f) is given as follows:

$$L_f = \sqrt{3} * m * V_{dc}/(12 * h * f_{sw} * \Delta i) \quad (5.5)$$

$L_f = 2.29\ mH$

Where h is overloading factor, m is modulation index and Δi is current ripple. Assuming, $m = 1,\ V_{dc} = 200\ V, h = 1.2, f_{sw} = 10\ kHz\ and\ \Delta i = 10\%$ of VSC current (10.5A). The calculated value of L_f is 2.29 mH. In the prototype hardware, interfacing inductor (L_f) of roughly 3mH has been considered.

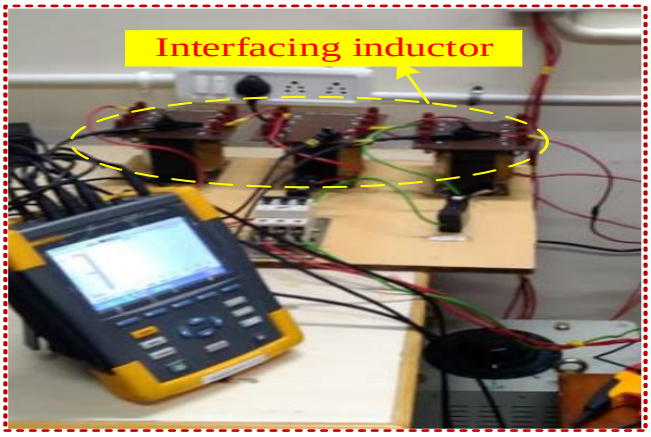

Fig. 5.3. Interfacing inductor

Figure 5.3 shows the interfacing inductors. The value of the interface inductors depends on the VSC's DC link voltage, allowed percentage of ripple current and switching frequency. The interface inductor used in this setup is rated at 3mH and 10A current.

5.3.3 Design and testing of Sensor Circuit

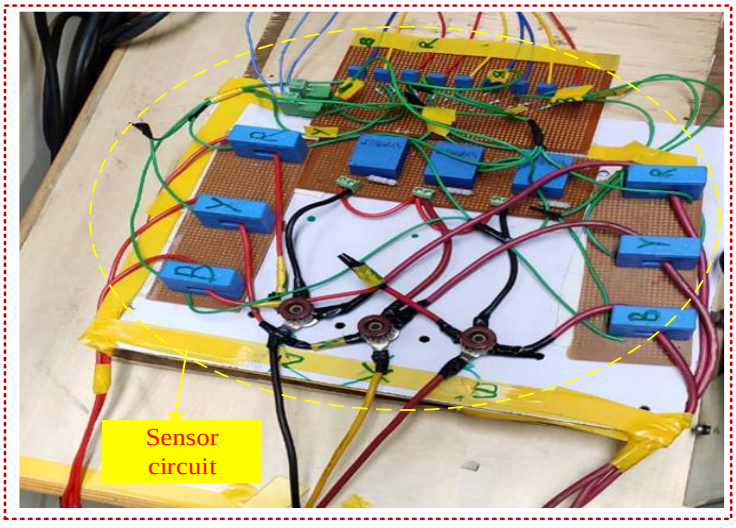

Fig. 5.4. PCC voltage sensors, load current and grid current sensors

For the designing of three phase balanced AC mains PCC voltage, and currents, Hall-effect-based sensors, voltage (LV 25-P) and current (LA 55-P) are used [123]. These sensors

operate at ±15V DC supply as shown in figure 5.4. The output signal of sensor circuit is given as input to the developed control algorithm through analog to digital (ADC) channel of DSP-dSPACE. Figure shows different sensors for the test set up. The output signal of this sensor is given to the ADC channel of DSP-dSPACE.

5.3.3.1 *Testing Results of Voltage Sensors*

The PCC voltage sensors' test results are shown in figure 5.5. The three phase voltages of a three-phase system are sensed with three phase PCC voltage sensors. Actual PCC voltages and sensed PCC voltages corresponding to phases “a”, “b”, and “c” are depicted in figure 5.5(a) and (b), respectively. The sensed PCC voltage magnitude is 100mV (peak), whereas the actual PCC voltage magnitude is 90V (peak). In order for the output signals of PCC voltage sensors to achieve actual magnitudes, the value of gains is selected at approximately 900. The waveforms of the sensed three phase voltages at PCC are shown in figure 5.5(a). Actual PCC voltage waveforms are shown in figure 5.5(b).

The output of the DC bus voltage sensor is 150mV when the DC bus voltage is initially at its peak amplitude of line voltage, which is roughly 150V. As a result, the gain value selected for the DC bus voltage sensor is near to 1000, which is used to determine the true value of the DC bus voltage.

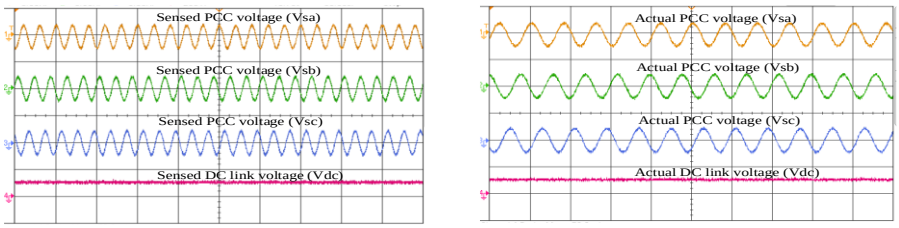

(a) Ch. 1-2-3: 200mV/div, ch.4:300mV/div, (b)Ch. 1-2-3: 200V/div, ch.4:300V/div

Fig. 5.5. Sensed and actual PCC voltages and DC bus voltage

5.3.3.2 *Testing Results of Grid Current Sensors*

Figure 5.6 depicts the testing results of grid current sensor. Three current sensors were used to sense the grid currents of three phases. Figures 5.6 (a) and (b) depicts the waveforms for sensed and actual grid currents respectively for the phases ‘a’, ‘b’, and ‘c’, Actual grid current are observed by using current probe (power quality analyser: FLUKE).

The sensed, grid current magnitude is 100mA (peak), the actual grid current magnitude is 2A (peak). The value of gains was chosen at around 20, in order to achieve actual magnitudes from the output signals of grid current sensors. The waveforms of the grid current sensed, are shown in figure 5.6(a). Actual grid current waveforms are shown in figure 5.6(b).

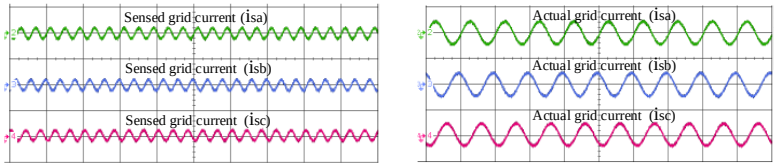

(a) Ch. 2-3-4: 500mA/div, (b) Ch. 2-3-4: 5A/div

Fig. 5.6. Sensed and actual grid current

5.3.3.3 *Testing results of load current sensors*

The test results of load current sensors are shown in figure 5.7. Three current sensors were used to sense the load currents of three phases. Figures 5.7(a) and (b) depicts waveforms of sensed and actual load currents respectively for phases ‘a’, ‘b’, and ‘c’.

Actual load currents are observed by using current probe (power quality analyser: FLUKE). Whereas the sensed, load current magnitude is 300mA (peak), the actual load current magnitude is 3A (peak). The value of gains was chosen at around 10, in order to achieve actual magnitudes from the output signals of load current sensors. Figure 5.7 depicts the signal of sensed and actual, three phases of load current.

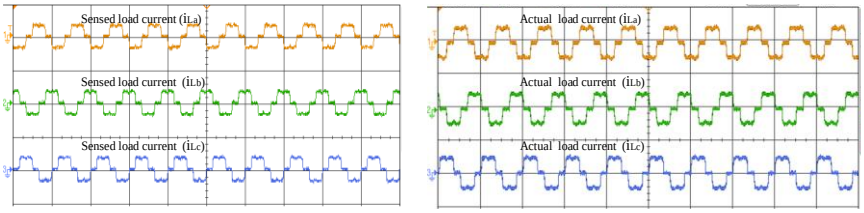

(a)Ch. 1-2-3: 500mA/div, (b)Ch. 1-2-3: 5A/div

Fig. 5.7. Sensed and actual nonlinear load current

5.3.4 *Testing Results of PWM Port of Micro-Lab box(dSPACE-1202)*

It is observed from these results that the amplitude of pulses output from DAC channels are 5V. Figure 5.8. depicts the gating pulse generated from PWM current controller of DSP and their inverted pulses corresponding to phase ‘a’, phase ‘b’ and phase ‘c’. Furthermore, pulses generated from PWM port of DSP-dSPACE get amplified up to 15V using developed gating circuit, which is sufficient to derive IGBTs of VSC. The developed DSTSTCOM has been depicted in the figure 5.9.

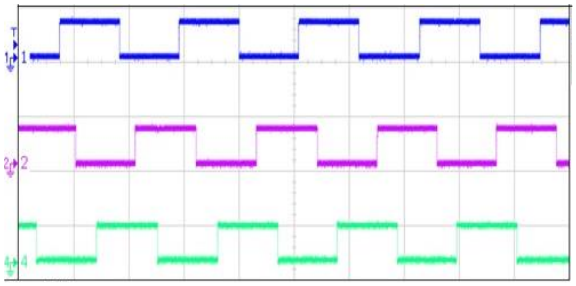

Fig. 5.8. Output pulse of PWM port of DSP-Dspace

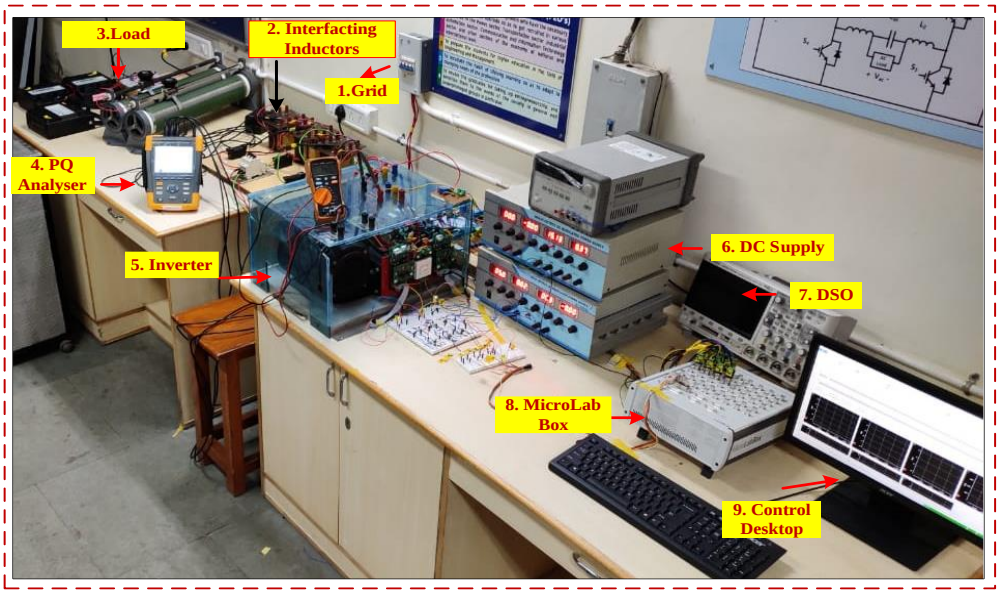

Fig.5.9. Prototype Hardware set-up

5.4 RESULTS AND DISCUSSIONS OF PROPOSED CONTROL ALGORITHMS

5.4.1 Variable Step Size Least Mean Square Control Algorithm

The proposed VSSLMS control, has been tested in real- time on prototype hardware. Performance of algorithm under various loads viz. linear, nonlinear, unbalanced load and under unbalance voltage of the grid has been analysed and various experimental results are presented in this section.

5.4.1.1 *Performance under balanced linear load*

Performance of proposed control, under linear load of 0.46 kVA, 0.93 pf lagging has been considered. V_{grid}, I_{grid}, I_{load}, current supplied by inverter (I_{inv}) of one phase "a", before and after compensation are shown in figure 5.10 (a). Power factor of the load is 0.93 pf lagging, before compensation, it can be seen from figure 5.10(b), while after compensation reactive power supplied by grid is approximately zero, showing UPF operation of proposed control as shown in figure 5.10(c). After compensation load reactive demand is fulfilled by the VSC

alone. Figure (b) and (c) shows the power factor of the grid before and after compensation respectively. Power factor of grid is maintained UPF after compensation as it can be seen from figure 5.10(c) as reactive power fed by grid zero.

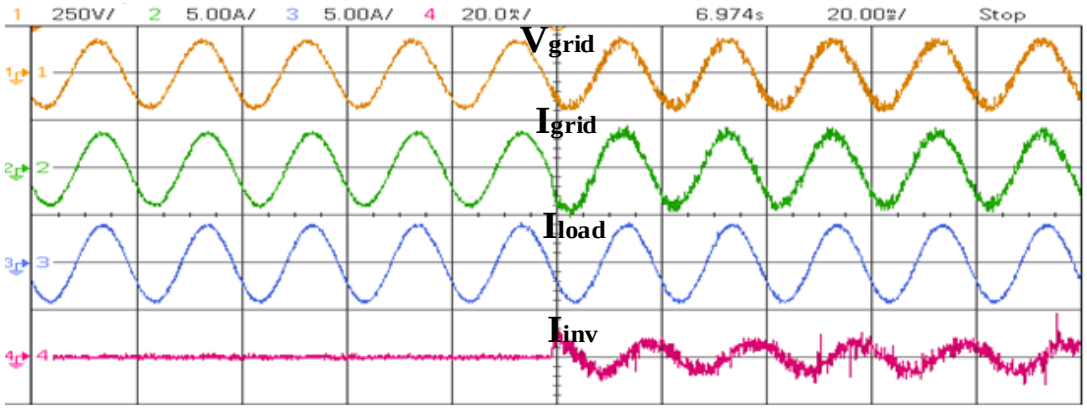

(a)

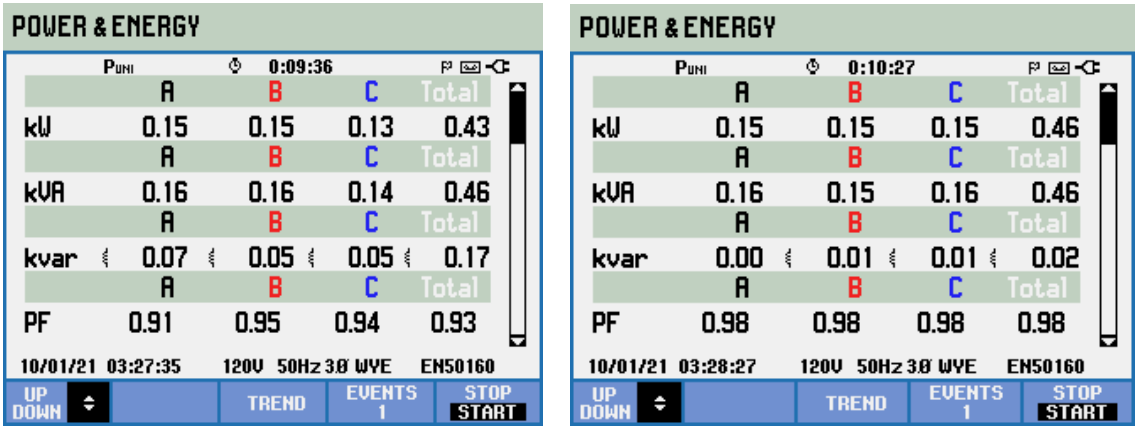

(b) (c)

Fig.5.10. Experimental result using proposed control: (a) waveform; (b) power factor, before compensation; (c) power factor, after compensation

5.4.1.2 *Performance under balanced nonlinear and variable load*

Performance of proposed control is tested on hardware prototype under nonlinear load by connecting a diode bridge rectifier with RL load (R= 50Ω, L=20mH). Figure 5.11 (a) depicts the V_{grid}, I_{grid}, I_{load}, and current supplied by inverter (I_{inv}) respectively of one phase ('a') and figure 5.11(b) shows the load resistance (R) changed from 50Ω to 40Ω. Inverter act as a harmonic compensator by compensating the harmonics of local loads. THD (%) in Igrid is 2.4% while THD (%) in Iload is 27.7% as depicted in figure 5.11(c) and (d) respectively, which is well within IEEE standard 519-2014. It is analyzed that using proposed control, grid current is improved significantly in terms of distortion by removing the harmonics.

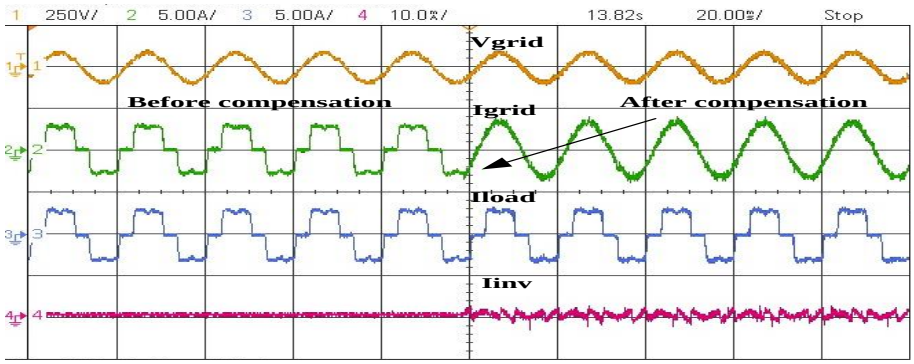

(a)

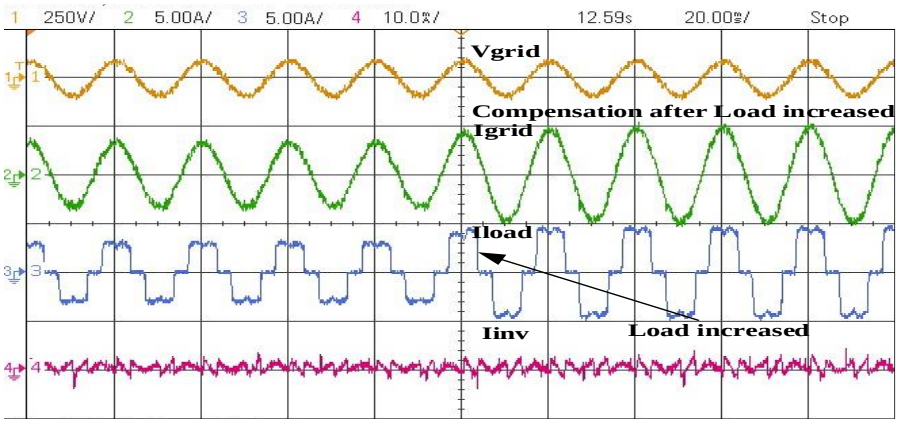

(b)

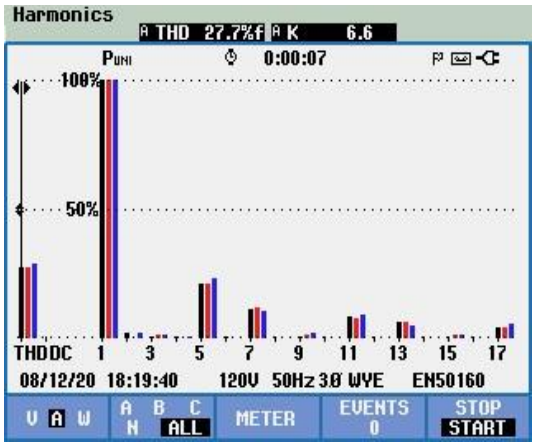

(c)

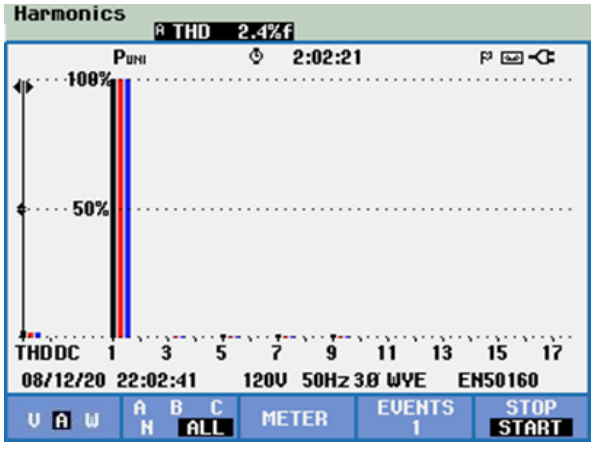

(d)

Fig.5.11. Parameter:(a) performance under nonlinear load; (b) performance under nonlinear load during load variation(increased); (c) THD in grid current before compensation under nonlinear load (d) THD in grid current after compensation under nonlinear load

5.4.1.3 *Performance under nonlinear unbalance load*

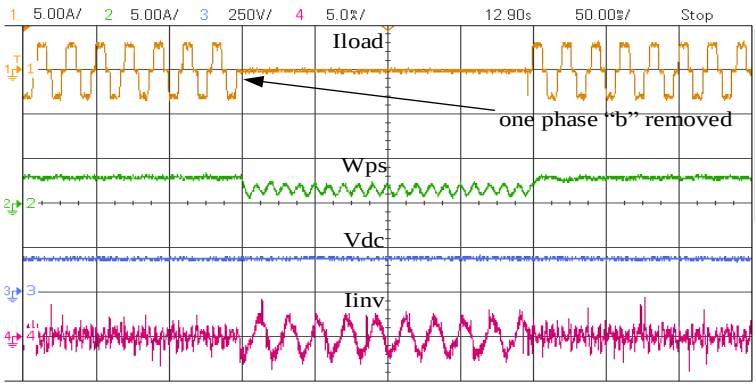

Fig .5.12. Experimental result under nonlinear unbalance load

To study the performance of proposed control under nonlinear unbalanced load existing diode bridge rectifier with RL load (R=50Ω, L=20mH) is taken. Unbalancing is formed by removing one phase for few cycles and again connected back. The system's many experimental parameters, including Iload, Wps, Vdc, and Iinv, can be seen in figure 5.12. Performance is effective, according to the experiment's results.

5.4.1.4 *Performance under unbalanced voltage of grid*

Performance of proposed control is also tested under unbalance grid voltage at nonlinear and unbalanced load both. From figure 5.13(a), it can be seen that, during the unbalance of voltage of the grid which is decreased by 17%(approx.) in phase 'a', proposed control is efficient in maintaining the grid current to be balance and free from harmonics. Furthermore, during the unbalance of the load by means of removing one phase of load, different phases of load current are depicted in figure 5.13(b). It has been found that performance using proposed control is efficient under unbalance scenario of the grid voltage also.

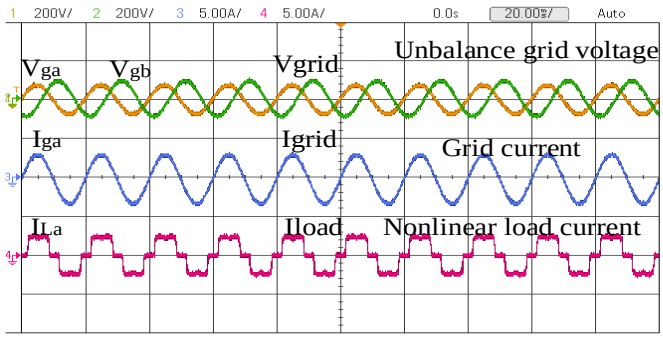

(a)

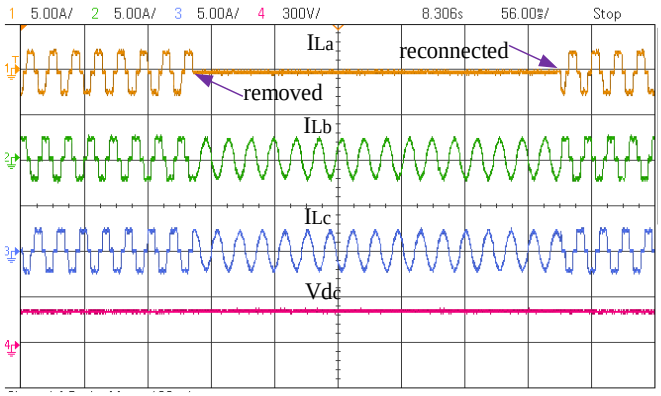

(b)

Fig 5.13. Performance of the system under unbalance voltage of grid:(a) under nonlinear load; (b) unbalance load

5.4.2 Robust Least Mean Logarithmic Square Control Algorithm

The proposed RLMLS control, has been tested in real- time on prototype hardware of the DSTATCOM. Performance of algorithm under various load viz. linear, nonlinear, unbalanced and unbalance voltage of the grid also has analysed and presented in this section.

5.4.2.1 *Performance under balanced linear load*

In the figure 5.14, experimental results, for V_{grid}, I_{grid}, I_{load}, and current provided by inverter (I_{inv}) are presented. Performance, under load of 0.43 kVA, 0.91 pf lag, has been evaluated. According to figure 5.14 (b), the grid side's reactive power and power factor are 0.19 kVAR and 0.91 pf lagging, respectively, before the compensation. According to figure 5.14 (c), power factor at the grid side is unity (approximately i.e., 0.99 pf lagging), after compensation. After compensation, the reactive power supplied by grid is almost zero, and the grid is maintained at UPF, as shown in figure 5.14 (c), which shows UPF operation with the proposed control. The VSC meets the load reactive demand after compensation which was supplied by grid before compensation. Figures 5.14 (b), (c) depict the grid's power and power factor before and after correction. As may be observed in figure 5.14(c), the grid's power factor is kept close to UPF after compensation. By correcting the reactive power, the grid power factor is considerably enhanced and kept around UPF (0.99 lagging) using the proposed control.

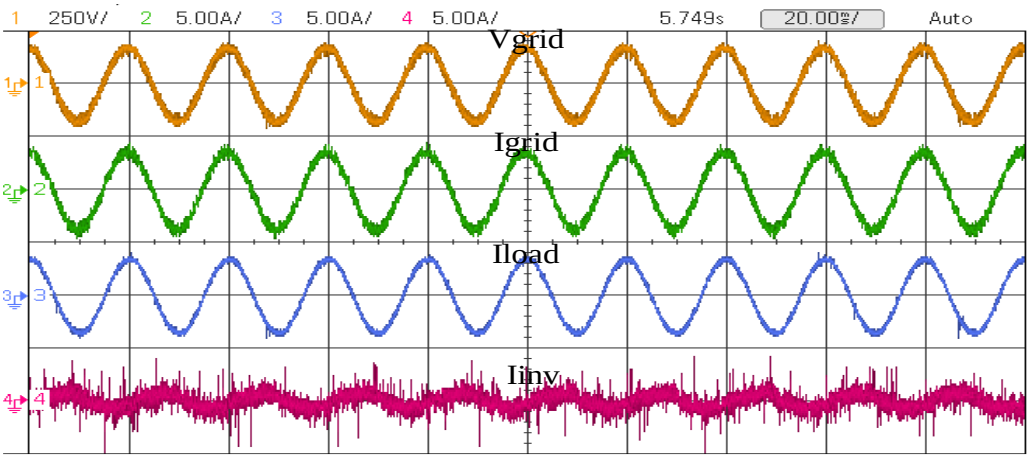

(a)

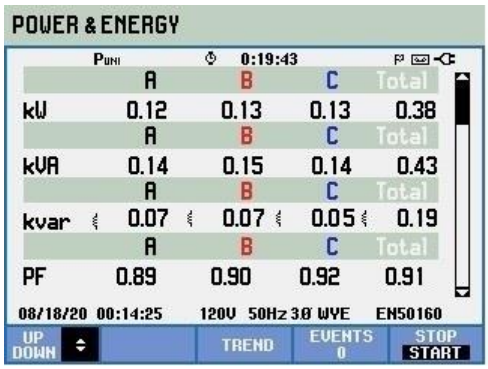

(b)

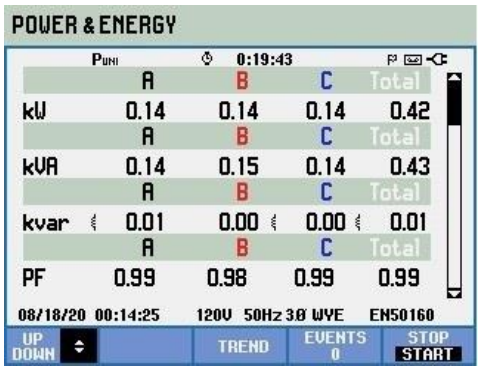

(c)

Fig.5.14. Experimental result: (a) waveform; (b) power factor, before compensation (c) power factor, after compensation

5.4.2.2 *Performance under balanced nonlinear load*

The performance under nonlinear load, V_{grid}, I_{grid}, I_{load}, and current supplied by inverter (I_{inv}) of are shown in figure 5.15 (a), and 5.15(b) illustrates the load resistance fluctuation from 65 to 40. By correcting the harmonics of local loads, the inverter acts as a harmonic compensator. As indicated in figure 5.15 (c) and (d), THD in I_{grid} is 2.8 %, which are under the limit of IEEE standard 519-2014, while THD in nonlinear load current is 27.7%. I_{grid} is considerably improved in terms of THD using the proposed scheme by eliminating the harmonics.

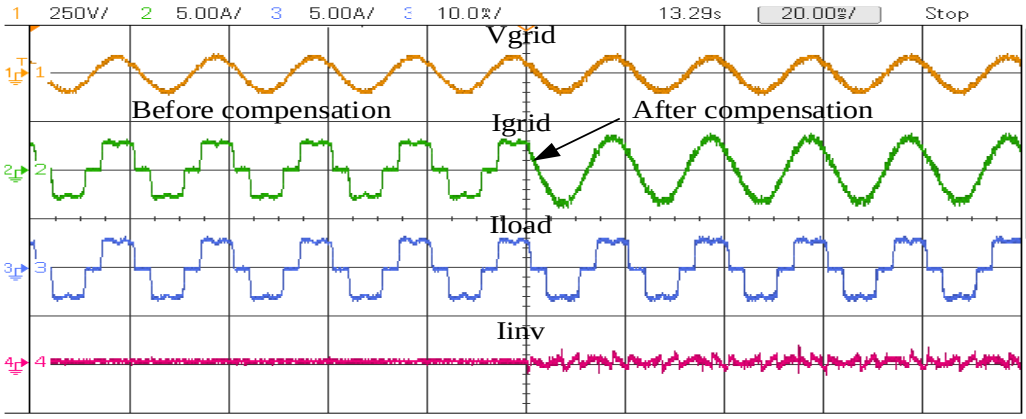

(a)

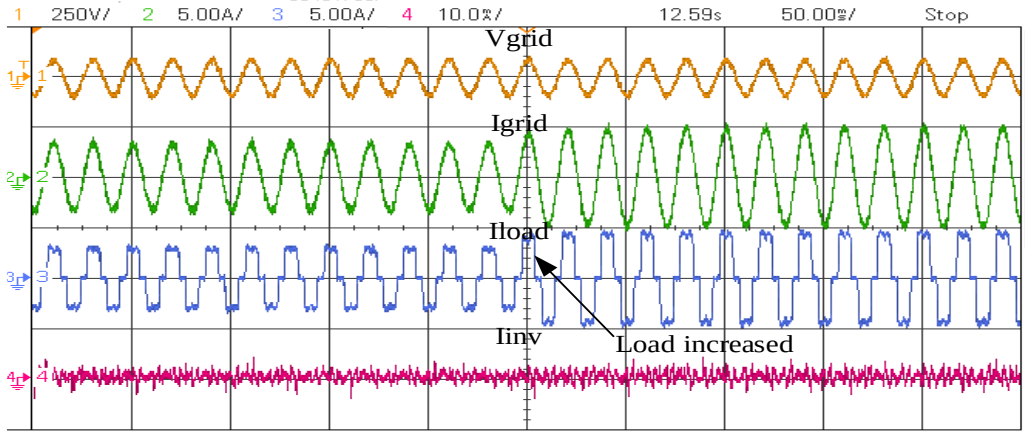

(b)

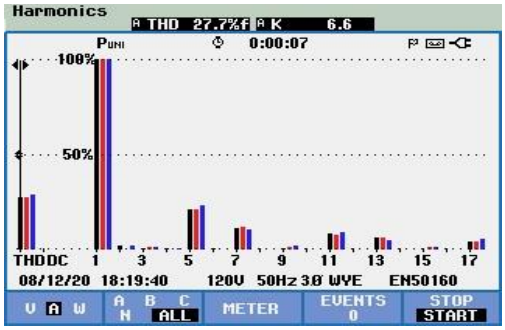

(c)

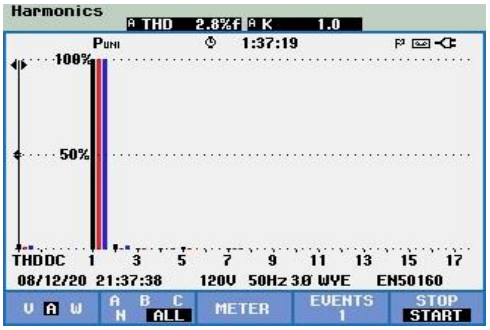

(d)

Fig.5.15. System parameter (a)waveform under nonlinear load; (b) waveform: load increment; (c) THD (%) of I_{load} (d) THD (%) of I_{grid}

5.4.2.3 *Performance under nonlinear unbalanced load*

Control scheme is also evaluated and tested with a nonlinear unbalance load (R= 65Ω, L=20mH). Unbalance is achieved by disconnecting one phase for a few cycles and then reconnecting it, as seen in figure 5.16, by the circled area. The system's various experimental parameters, including Iload, Wps, Vdc, and Iinv, are displayed in figure 5.16. The proposed control's performance is found to be efficient even when the load is unbalanced.

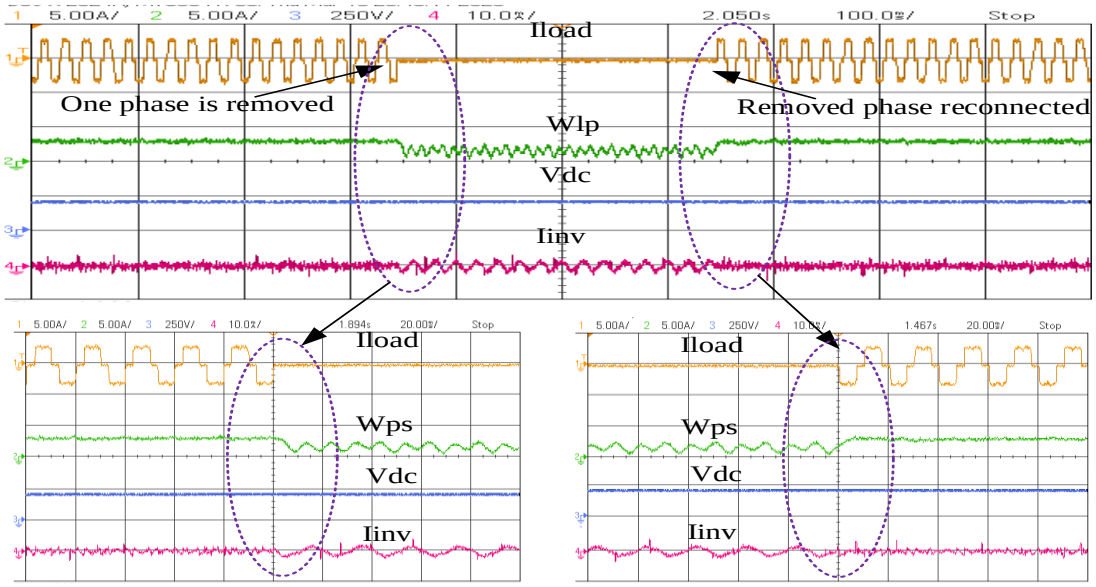

Fig .5.16. Experimental result under unbalance nonlinear load

5.4.2.4 *Performance under unbalanced voltage of grid*

The proposed control's performance is also analyzed for nonlinear and unbalanced loads under unbalanced grid voltage. Figure 5.17(a) shows that the control scheme is efficient in keeping, I_{grid} free of harmonics while the grid voltage is unbalanced by 21% (increased) in phase 'a'. Furthermore, distinct phases of load current are represented in figure 5.17(b), during the unbalance of the load by removing one phase 'b'. It was found that the performance of the proposed control is also efficient under non ideal grid.

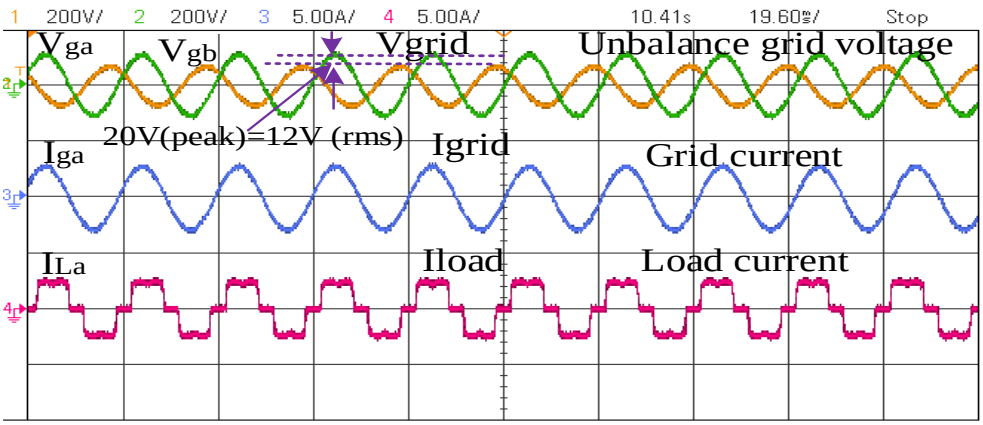

(a)

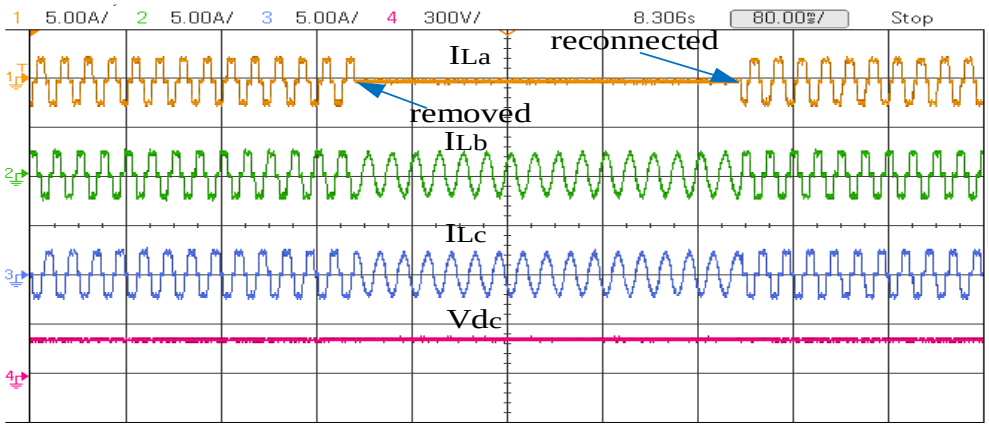

(b)

Figure 5.17. System response under unbalanced grid voltage at: (a) balance load; (b) unbalanced load.

5.5 COMPARISON OF PROPOSED CONTROL ALGORITHMS WITH OTHER CONTROL ALGORITHMS

Performance of proposed VSSLMS, and RLMLS control has been compared with conventional LMS and SRF control separately in terms of active weight convergence. Furthermore, to test the performance under nonlinear load (three phase bridge rectifier with RL load, R=65Ω, L=20mH) has been considered and compared in this section.

5.5.1 Comparison of Proposed VSSLMS And Conventional SRF and LMS Based Control algorithms

Performance of proposed VSSLMS control has been compared with conventional LMS and SRF control and is depicted in figure 5.18. It has been observed that proposed control's performance is efficient over other conventional control and provide comparatively 40msec faster convergence speed with minimum oscillations during dynamic condition viz. unbalanced load. Moreover, proposed control does not require any complex block like phase lock loop (PLL) for the synchronisation, which reduces the additional computational burden and provides faster response in terms of convergence speed compared to the SRF and LMS algorithm to estimate the reference current. Table 5.2, shows the comparative analysis of proposed control with other conventional control.

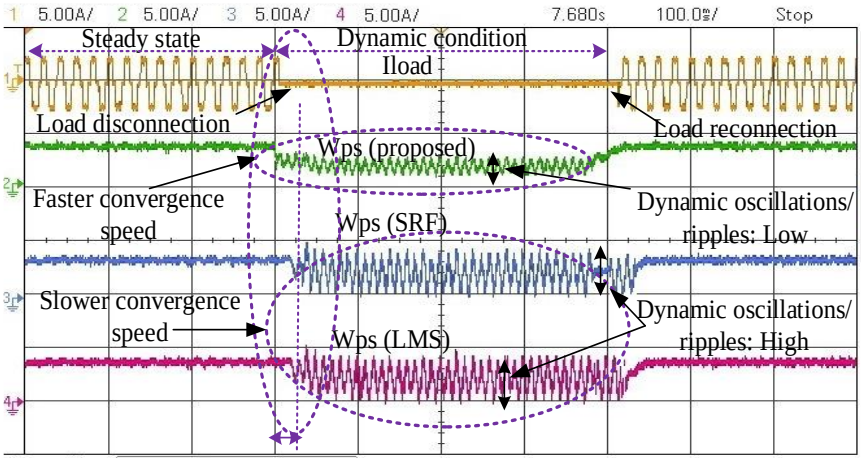

Fig.5.18. Comparison of proposed VSSLMS and conventional SRF and LMS based control

5.5.2 Comparison of Proposed RLMLS And Conventional SRF and LMS Based Control algorithms

Figure 5.19, depicts performance comparison of proposed RLMLS, SRF and LMS algorithm under steady state and dynamic performance. Further, one phase of load, has been removed and reconnected, for dynamic response. As can be observed from the figure 5.19, and table 5.1, that, proposed control has low oscillations during dynamic condition viz. unbalanced load, and shows faster convergence speed while estimating the fundamental active component hence, dynamic performance get improved. Furthermore, proposed control algorithm is less complex due to absence of PLL as in case of SRF therefore, sampling time get reduced thus accuracy is better with the added benefits of faster convergence speed, less complexity thus less sampling time, ease of implementation, and adaptability.

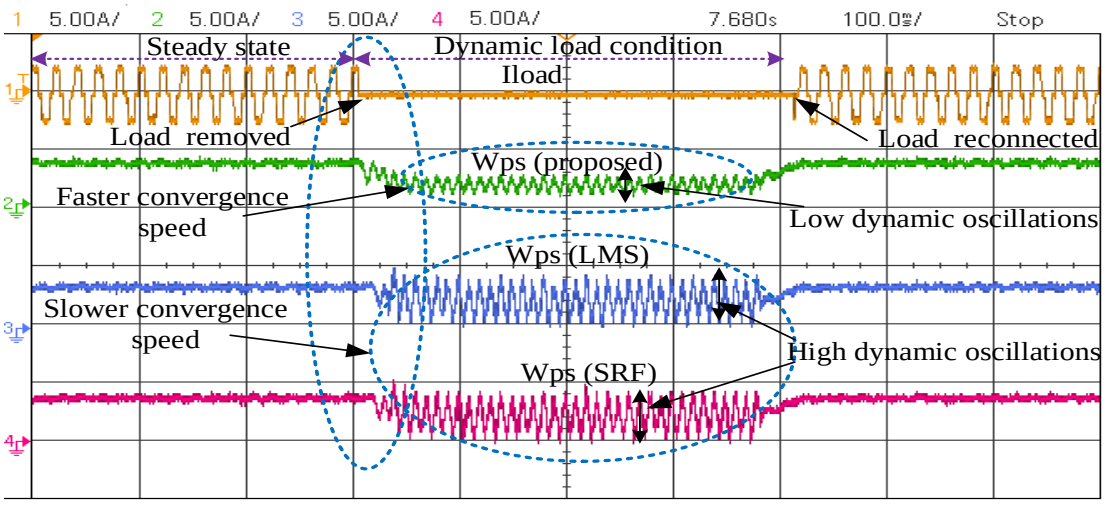

Fig .5.19. Comparison of proposed RLMLS control with conventional SRF and LMS under dynamic load

Table 5.1. Comparison of Proposed VSSLMS and RLMLS algorithm, with conventional SRF and LMS

S.N.	Criteria	SRF	LMS	VSSLMS	RLMLS
1	Convergence	Slow	Moderate	Better	Better
2	Complexity	High	Low	Low	Low
3	dSPACE-1202/ sampling time	50µS	40µS	40µs	40µs
4	Filtering Type	Time Domain	Adaptive	Adaptive	Adaptive
5	Dynamic oscillations in active component	High	High	Low	Low
6	Accuracy of the algorithm	Good	Moderate	Better	Better

5.6 CONCLUSIONS

In this chapter, the three-phase grid connected PV system and its various components are designed and developed for real-time validation/ implementation of the proposed control in the laboratory of the Electrical Engineering Department of DTU. Due to lab resource limitations, VSC control algorithms are tested on prototype hardware set- up of DSTATCOM and real-time results has been presented in this section. Moreover, Micro-Lab box(dSPACE-1202) is employed for real time implementation. Proposed control algorithms viz. Variable Step Size Least Mean Square (VSSLMS), Robust Least Mean Logarithmic Square Control Algorithm (RLMLS) are validated experimentally in the laboratory on prototype hardware set up.

The performance of the proposed adaptive control algorithms has been tested for different condition such as load variation, load unbalancing, nonlinear load, reactive load, grid voltage unbalancing etc. THD (%) in grid current under nonlinear load is observed to be less than 5% which is within the limit of IEEE-519 standard.

Furthermore, proposed control algorithms have better weight convergence capability and better initial transient response in terms of overshoot and undershoot and lesser oscillations in the response during dynamic scenario as compared to SRF algorithm. Performance of the proposed VSC control algorithms VSSLMS, RLMLS has been found to be satisfactory under all test conditions. Experimental investigations justify the efficacy of the proposed algorithms.

CHAPTER-VI
COMPREHENSIVE REVIEW, AND ANALYIS OF ISLANDING DETECTION TECHNIQUES IN MICROGRID

6.1 INTRODUCTION

In the chapter III-IV, design and development of grid connected SPV based microgrid has been carried out. The VSC control algorithms viz. conventional, intelligence and adaptive theory-based control is modelled and simulated for two-stage, three-phase grid integrated SPV system.

The challenges that arise out of grid integrated SPV based microgrid, are reactive power management, synchronisation, power quality, and islanding. One of these problems is islanding detection, which is one of the essential aspects of the PV power generation as distributed generation (DG).

In order to ensure the safety of service personnel and electrical components, the detection of the islanded operations of distributed generators has become very important. Islanding refers to a situation where energized DGs are disconnected from the bulk power grid, providing power only to the local loads for the time being [19]-[20]. Microgrid islanding arises as a consequence of breakers accidentally tripping, resulting in a significant threat to the safety of staff, damage to the equipment of utilities, consumers, loss of control over voltage and frequency, etc.

This chapter provides comprehensive review, analysis and study of the various islanding detection techniques that have been described in the literature. These techniques have been categorised as: remote, passive, active, and signal processing-based techniques. An active islanding identification based on disturbance injection through the quadrature axis controller has been studied and analysed.

In the present work, analysis of different islanding detection scheme along with the advantages, disadvantages and limitations are evaluated and summarised [125].

6.2 ISLANDING OF MICROGRID

Islanding in a microgrid occurs when a section of the utility system, which includes dispersed resources as well as load, keeps running even though it is cut off from the rest of the system [126]. Islanding may occur accidentally or on purpose, both intentional and unintentional islanding are defined by IEEE 929-2000 [126] and IEEE 1547 [127]. In certain circumstances, intentional islanding may be advantageous such as under weather disaster or unplanned outage when microgrid is needed to operate independently.

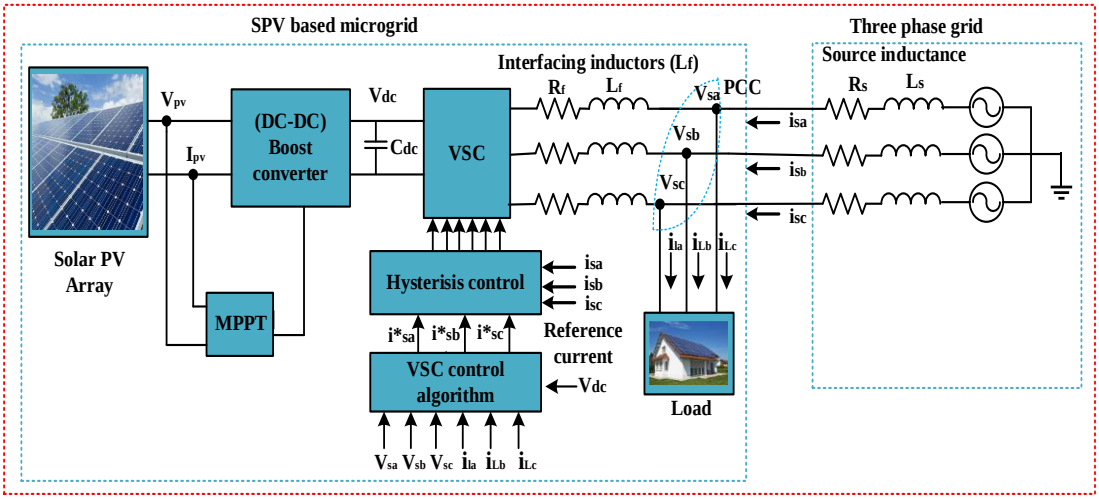

Fig.6.1. Grid integrated PV based microgrid

Unintentional islanding, which occurs when the grid loses control of the electrical parameters of the islanded zone, is not planned and is undesirable. This might lead to voltage or frequency excursions, which could destroy customer equipment or expose staff members to potentially dangerous environments. Thus, islanding must be detected as soon as possible, and the DG device in the islanded zone must be cut off from the rest of the system. Figure 6.1. shows the grid integrated PV based microgrid for the study and analysis of islanding detection schemes.

6.3 ISLANDING DETECTION TECHNIQUES FOR THE MICROGRID

In the present study, to analyse the islanding detection techniques, single line diagram of grid integrated PV based microgrid has been depicted in the figure 6.2, which comprises of one DG (SPV system) and load at PCC is integrated to the grid. To facilitate the islanding identification capability, DG necessitates, the integration with the islanding detection technique. An efficient islanding detection technique has small non-detection zone (NDZ). A NDZ is the operational area when an islanding detection system fails to detect the islanding. The performance of the islanding detection approach will be high when the NDZ is minimum.

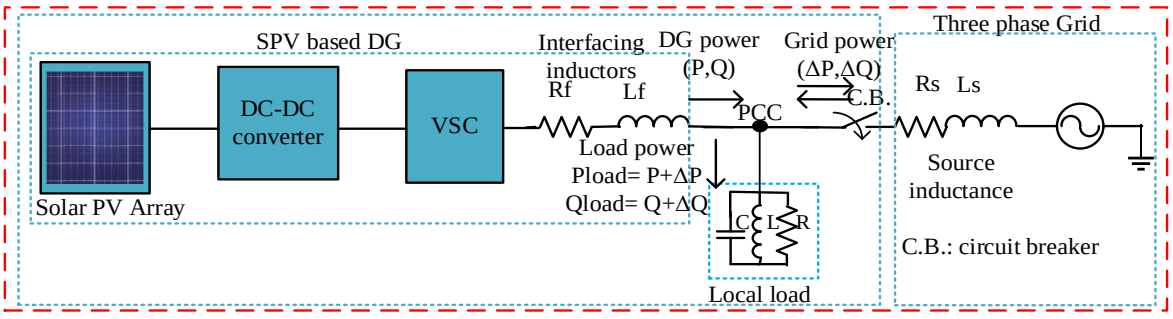

Fig.6.2. Single line diagram of grid integrated PV based microgrid

Power mismatches, (active/reactive) where the frequency and voltage relays fail to detect the islanding, can be used to evaluate NDZ. If there is a minor active and reactive power mismatch at the point of PCC, the changes in the voltage and frequency are not enough to detect the islanding state.

The power balance equation are as follows:

$P_{load} = P_{DG} + \Delta P$ (6.1)

$Q_{load} = Q_{DG} + \Delta Q$ (6.2)

ΔP, ΔQ is active and reactive power shared by grid, and P_{DG}, Q_{DG} are power shared by DG respectively. P_{load} and Q_{load} are active and reactive demand of the load respectively.

Range for the power mismatches can be estimated as follows [128]:

$$\left(\frac{V}{V_{max}}\right)^2 - 1 \leq \left(\frac{\Delta P}{P_{DG}}\right) \leq \left(\frac{V}{V_{max.}}\right)^2 - 1 \quad (6.3)$$

$$Q_f\left(1 - \left(\frac{f}{f_{min}}\right)^2\right) \leq \left(\frac{\Delta Q}{P_{DG}}\right) \leq \left(1 - \left(\frac{f}{f_{max}}\right)^2\right) \quad (6.4)$$

Where Q_f represents the quality factor, and f_{min}, f_{max}, V_{min}, and V_{max} are the minimum and maximum frequencies, and voltages respectively.

6.3.1 Quality Factor and Parallel RLC Load

The load quality factor is a significant measure used to evaluate the robustness and reliability of any islanding detection method (IDMs) [128]. The performance analysis of the IDMs is severely reliant on the load quality factor's value because it influences the size of the NDZ and detection accuracy. The majority of the loads in the power system are inductive, so VSC based DGs often operate at unity power factor condition to generate maximum energy. Detecting islanding is more difficult during a near zero-power mismatch between the DG and connected load. The most difficult RLC load will be one with a high-quality factor (Q_f), as it will have low inductance, high capacitance, and/or high resistance. Both the grid frequency and the resonant frequency are regarded as same. The following mathematical formulas can be used to express the R, L, and C parameters under the unity power factor constraint [128].

$R = V^2 / P_{load}$ (6.5)

$L = V^2 / (2\pi f.P_{load})$ (6.6)

$C = Q_f.P_{load} / (2\pi f. V^2)$ (6.7)

$f = (1/2\pi)\sqrt{(L/C)}$ (6.8)

$Q_f = R\sqrt{(C/L)}$ (6.9)

6.4 ISLANDING CLASSIFICATION

Islanding detection techniques, assist in recognising the islanding situations and the inverter is prompted then to stop energising the loads. As observed in figure 6.3, they may be roughly classified as: remote islanding detection, local islanding detection and signal processing-based islanding detection schemes.

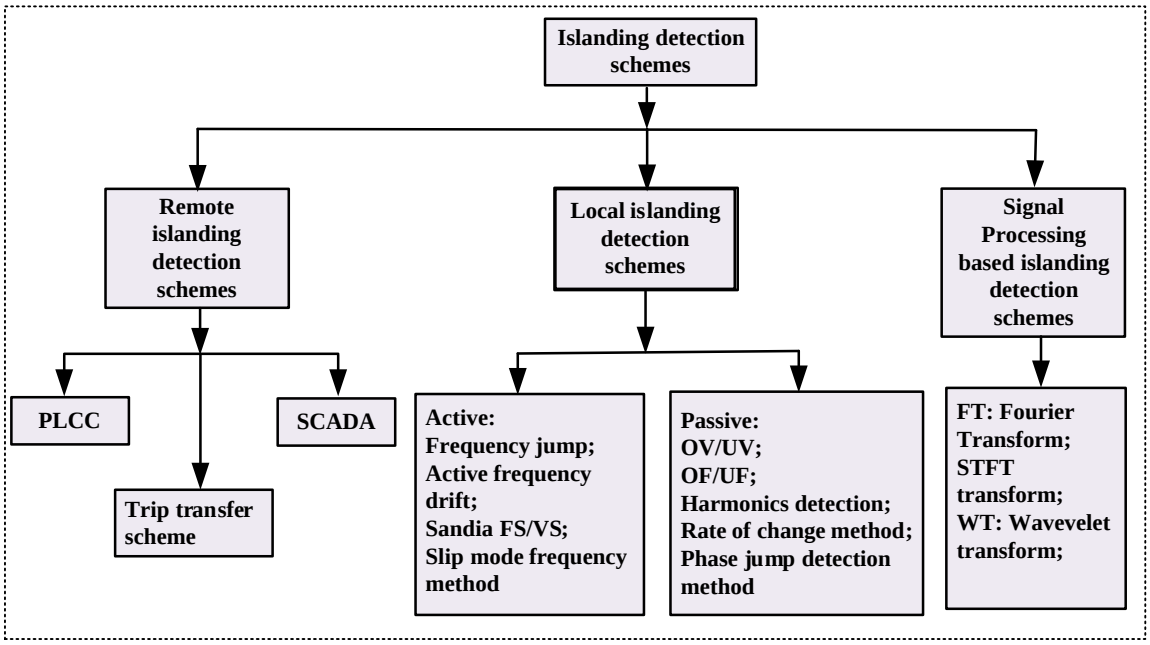

Fig.6.3. Classification of Islanding detection schemes

6.4.1 Remote Islanding Detection

The idea of communication between DERs and utilities is the foundation of remote islanding detection techniques. The DER gets a trip signal from the controller after the islanding occurs. The transfer trip scheme, the power line carrier communication scheme (PLCC), and the supervisory control and data acquisition (SCADA) make up remote islanding detection systems. Zero non-detection zones (NDZ), quicker reaction times, minimal influence on power quality, and efficient use in numerous DG systems are the benefits of remote islanding detection approaches. On the other hand, implementing remote techniques in small-scale systems is quite expensive [91]-[94],[129].

6.4.1.1 *Power line carrier communication*

Using the power line carrier communication (PLCC) technology, the signal is continually delivered via the power line and detected by the receiver at the target DG. The islanding

phenomena is identified and the DGs should be disconnected when the receiver is unable to detect the signal over a set a delay [129].

6.4.1.2 *Supervisory control and data acquisition*

Through the use of a SCADA system, islanding detection is accomplished by continually measuring electrical characteristics like voltage, current, power, and frequency. The utility grid's sudden disengagement will cause a sudden change in the grid's properties. The necessary action is then carried out by the SCADA system by instructing the relays at the relevant DGs to disconnect [130]. The system efficiency is greatly increased by this method as it has very small NDZ. However, it has drawbacks like expensive communication links, and delayed detection.

6.4.1.3 *Transfer trip method*

The basic algorithm of the transfer trip technique monitors the state of the switches. Whenever, the grid is cut off, the algorithm locates the islanded areas and transmits the trip signal to the DGs. This technique is used in conjunction with a SCADA system to monitor the switches' state and to effectively coordinate the microgrid with the utility grid [131]. However, this approach has disadvantage of high cost [132].

6.4.2 Local Islanding Detection

The measurement of changes in the system characteristics like voltage, current, frequency, impedance, phase angle, harmonic distortion, etc. is the basis of local detection techniques. These techniques are further divided into passive and active islanding detection schemes.

6.4.2.1 *Passive islanding detection techniques*

The initial approaches for islanding detection that have been employed are passive ones. The measurement of the local variables at PCC is the key to the success of the conventional passive-based islanding detection method (IDMs).

For analysis, parameters like frequency and voltage that were retrieved from the target DG at PCC are employed. These parameters have established threshold settings, and any variations from those settings will identify the presence of islanding. The flowchart in figure 6.4 outlines the steps involved in passive islanding detection.

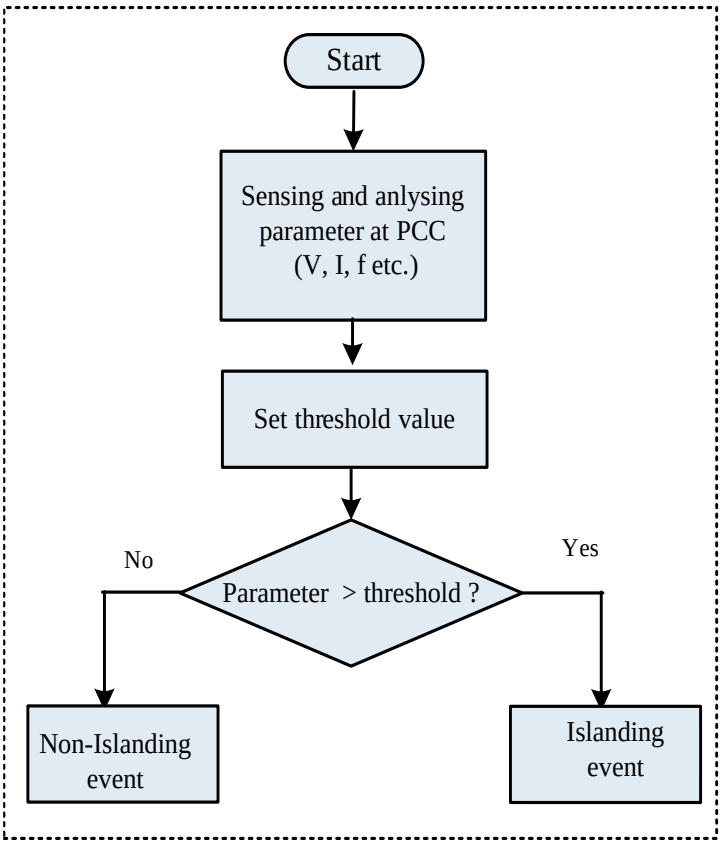

Fig.6.4. Flow chart of passive islanding detection methods

i. *Voltage unbalance method*

During islanding event, a change in the configuration of the system, or small alteration in the load causes the voltage to become unbalanced. Using the positive and negative sequence components, an islanding detection strategy has been proposed in the literature [133].

ii. *Total harmonics distortion method*

This technique for islanding detection has been suggested based on noticing variations in the total harmonic distortion (THD). Changes in the harmonic components of current is monitored in this scheme [133].

iii. *Over/under voltage and over/underfrequency method*

Microgrids that are connected to the grid must have over/under voltage (OV/UV) and over/under frequency (OF/UF) relays, which cut off power to the loads if the frequency or amplitude of the voltage at the PCC goes outside of allowed ranges. The system's behaviour at the moment of grid separation will be determined by ΔP and ΔQ just before the switch opens to create the island. The active and reactive power imbalances (mismatches) at the PCC are shown in the equation (6.1) and (6.2). The ΔP and ΔQ are measured using the over/under voltage (OV/UV) and over/under frequency (OF/UF). If $\Delta P \neq 0$, when the voltage amplitude

changes, the OV/UV relay will switch on. If $\Delta Q \neq 0$, the OF/UF relay will activate, and the DG will trip [134] due to change in frequency.

iv. *Rate of change of power method*

During the islanding state, the load will be directly impacted. In order to detect the islanding event [135], the output power at the DG terminals is employed to further calculate the rate of change of power (ROCOP).

v. *Rate of change of frequency method*

Frequency variations will be caused by the power imbalance caused under the utility grid is cut off [135]. Therefore, the islanding condition has been identified [136] by monitoring the rate of change of frequency (ROCOF) over a few cycles and defining a threshold values.

vi. *Rate of change of frequency over power method*

A method using (df/dP) is proposed [137] to detect the islanding event under a low power mismatch condition because the ROCOF technique will fail to identify the islanding event when the power mismatch is small.

vii. *Phase jump detection method*

The phase difference between the current and voltage obtained at the DG is continually tracked in the phase jump detection (PJD) approach [130]. When everything is working properly, phase-locked loops (PLLs) synchronize the inverter voltage with the PCC voltage. But when islanding happens, the voltage phase angle suddenly increases without any change in the current phase angle as described [138].

Table 6.1: Passive islanding detection methods: summarised [139]

Techniques	Detection time	Description
Voltage unbalance method	53 ms	NDZ is large Error detection rate is low No power quality effect
Harmonic distortion	45 ms	NDZ is large for high-quality factor Error detection rate is high No power quality effect
OV/UV and OF/UF	4 ms -2s	NDZ is large Error detection rate is low No power quality effect
ROCOF	24 ms	NDZ is small

		Error detection rate is high No power quality effect
ROCOP	24-26 ms	NDZ is less than ROCOF Error detection rate is low No power quality effect
Phase jump detection method	10 - 20 ms	NDZ is large Error detection rate is low No power quality effect

6.4.2.2 Active islanding detection techniques

The detection methods for active islanding depend on how the system reacts to disturbances that are either created in the inverter current's or voltage's amplitude, frequency, or phase. The impact of these perturbations experienced at PCC under normal steady-state settings is quite small. The impact of these disturbances experienced at PCC, however, is quite significant once the microgrid is islanded. Reduced NDZ and a decrease in detection rate error are benefits of active detection systems.

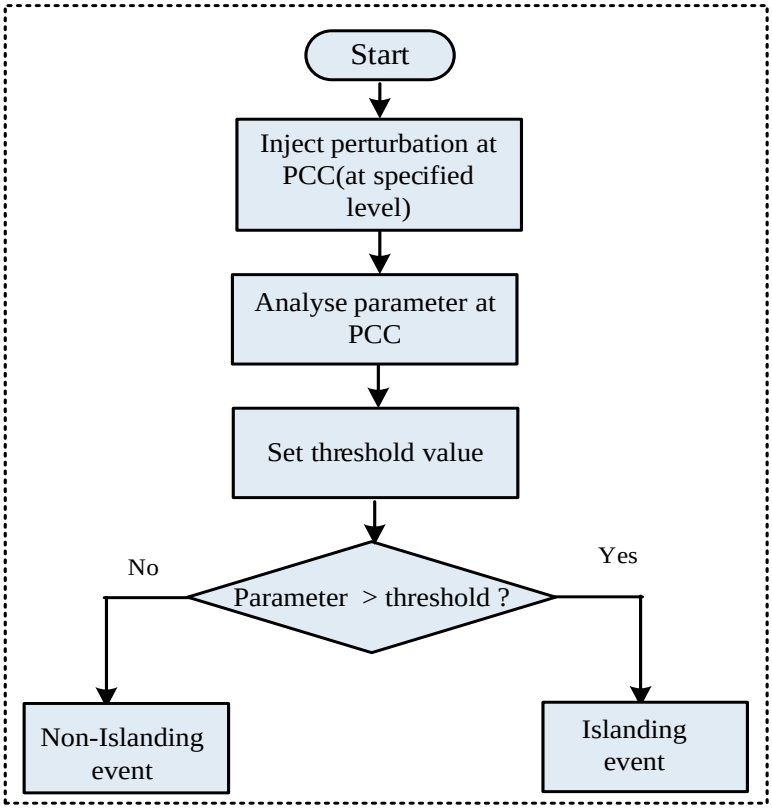

Fig 6.5. Flow chart of active islanding detection methods

Passive scheme detects islanding quickly but they are limited by nuisance tripping because of improper threshold settings, i.e., small threshold values. The slightly large setting may have a large NDZ and make it difficult to detect an islanding condition. Therefore, in active approaches an external disturbance signal is injected to specific parameters in the system.

These changes are utilised with a predetermined threshold setting to determine the islanding event. The flowchart outlines the procedures for active islanding detection as seen in figure 6.5 and different active methods are reported in this section.

i. ***Active frequency drift method (AFD)***

The voltage and currents are constant, in grid synchronised condition, but in a loss of mains situation, the perturbing current signal injection will change the zero crossing of the voltage, which is followed by a change in phase between the voltage and current, and this will start a frequency drift in the current to eliminate the phase error. This drift in the frequency is used to determine the islanding conditions [130]. The AFD distorts the frequency output to produce a persistent trend by in order to "drift" the frequency away from the fundamental. The technique involves changing the frequency by slowly increasing it every half cycle, followed by a "dead time" during which the system waits for the fundamentals to catch up to the biased frequency. To get over the drawbacks of the AFD technique, positive feedback is added [140]. By raising the frequency deviation from the nominal values, it is used to increase the chopping frequency.

ii. ***Frequency jump method (FJ)***

Similar to AFD, the frequency jump (FJ) approach introduces some dead zones into the perturbing current signal. Instead of every cycle, the dead zones are introduced every three cycles [88], with a normal situation, the frequency of the voltage is unaltered; but, with a mains failure, it will vary [130]. FJ and AFD fail in the test system connected with several parallel-connected DGs.

iii. ***Sandia frequency shift method (SFS)***

By adding positive feedback to the frequency of the voltage signal, the Sandia frequency shift (SFS) approach has extended AFD. Then the chopping frequency [88] will be modified as

$$C_f = Cf_0 + K\,(f_{pcc} - f_{grid}) \qquad (6.10)$$

Where, K, f_{PCC}, and f_{grid}, represents the accelerating frequency, voltage signal frequency, and grid frequency respectively. SFS offers the least amount of NDZ in comparison to other active detection schemes [130].

iv. ***Sandia voltage shift method (SVS)***

In order to detect a loss of mains condition, Sandia voltage shift (SVS) additionally applies positive feedback to the voltage at the PCC. When feedback is supplied to the voltage signal during a mains outage, the power and current will change as a result, accelerating the voltage

drift [188]. Although the SVS approach is simple to use and efficient, much like the SFS method, it has some drawbacks include introducing poor power quality and decreases the inverter efficiency [130].

v. *Slip mode frequency shift method*

The positive feedback is applied to the voltage signal's phase in the slip mode frequency shift (SMS) method, which shifts the voltage signal's phase and, as a result, the frequency [138],[141]. For the purpose of islanding detection, a minor modification can be used with ease. In comparison to other active methods, it has a small NDZ. However, it will still result in transient response issues and power quality problems for high feedback loop gains, which are typically present in any schemes with positive feedback.

vi. *Variation of active and reactive power method*

The fluctuations in real power will immediately affect the load when islanding takes place. It has an impact on the PCC's voltage and current. The following formula [142] can be used to determine the variation in the active power injected from the inverter:

$$P_{DG} = P_{load} = V^2/R \quad (6.11)$$

$$\Delta V = \frac{P_{DG}}{2}\sqrt{(R/P_{DG})} \quad (6.12)$$

Similarly, variation in the reactive power and frequency can be estimated using the equation below:

$$dQ = K_f (f_n - f) \quad (6.13)$$

where, where K_f is gain, f is the estimated frequency, and f_n is nominal frequency.

Table 6.2: Active islanding detection methods: summarised [139]

Techniques	Detection time	Description
Active frequency drift method	Within 2 s	NDZ is large for high quality factor Error detection rate is high Power quality degrades
Frequency jump	75 ms	NDZ is small Error detection rate is low Power quality degrades
Active frequency drift	Nearly 1 s	NDZ is smaller than AFD Error detection rate is lower than AFD Power quality slightly degrades
Sandia frequency shift method	0.5 s	NDZ is very small Error detection rate is low Power quality slightly degrades

Sandia voltage shift method	0.5 s	NDZ is very small Error detection rate is low Power quality slightly degrades
Slip mode frequency shift method (SMS)	Nearly 0.4 s	NDZ is small Error detection rate is low Power quality degrades
Variation of active and reactive power	0.3- 0.7 s	NDZ is small Error detection rate is high Power quality degrades

6.4.3 Signal Processing-Based Detection

With the ability to extract hidden features from any signal, signal processing (SP) techniques are introduced into islanding detection to reduce the NDZ of passive technique. The flowchart for the SP-based islanding detection technique is shown in figure 6.6.

i. ***Fourier transform based methods***

A popular frequency-domain method is the Fourier transform (FT). It is the depiction of a signal as the accumulation of several frequency sinusoids.

However, in dynamic circumstances, FT is unable to resolve the transient information [143]. The time frequency analysis is introduced to address the flaw. A modified form of FT called the short-time Fourier transform (STFT) separates the original signal into a series of brief stationary frames. Additionally, a moving window is applied over these frames to examine the signal's time-frequency information [144]. However, STFT is not appropriate for nonstationary signals because of the fixed window [145]. By choosing a smaller window, STFT has been used to identify the transients in the disturbance signal [146].

ii. Wavelet transform based methods

The wavelet transform (WT) is a method for signal analysis [147]. The main difference is that in WT, the information is localized using wavelets in both the temporal and frequency domains. The mother wavelet is used to split the original signal into smaller waves of various frequency, known as wavelets. In order to examine the dynamics and transients in any nonstationary signals, wavelets have longer windows for lower frequencies and narrower windows for higher frequencies. WT is thus helpful for signal analysis in any situation where time-frequency analysis is required [148]. Continuous WT (CWT) and discontinuous WT (DWT) are two types of WT.

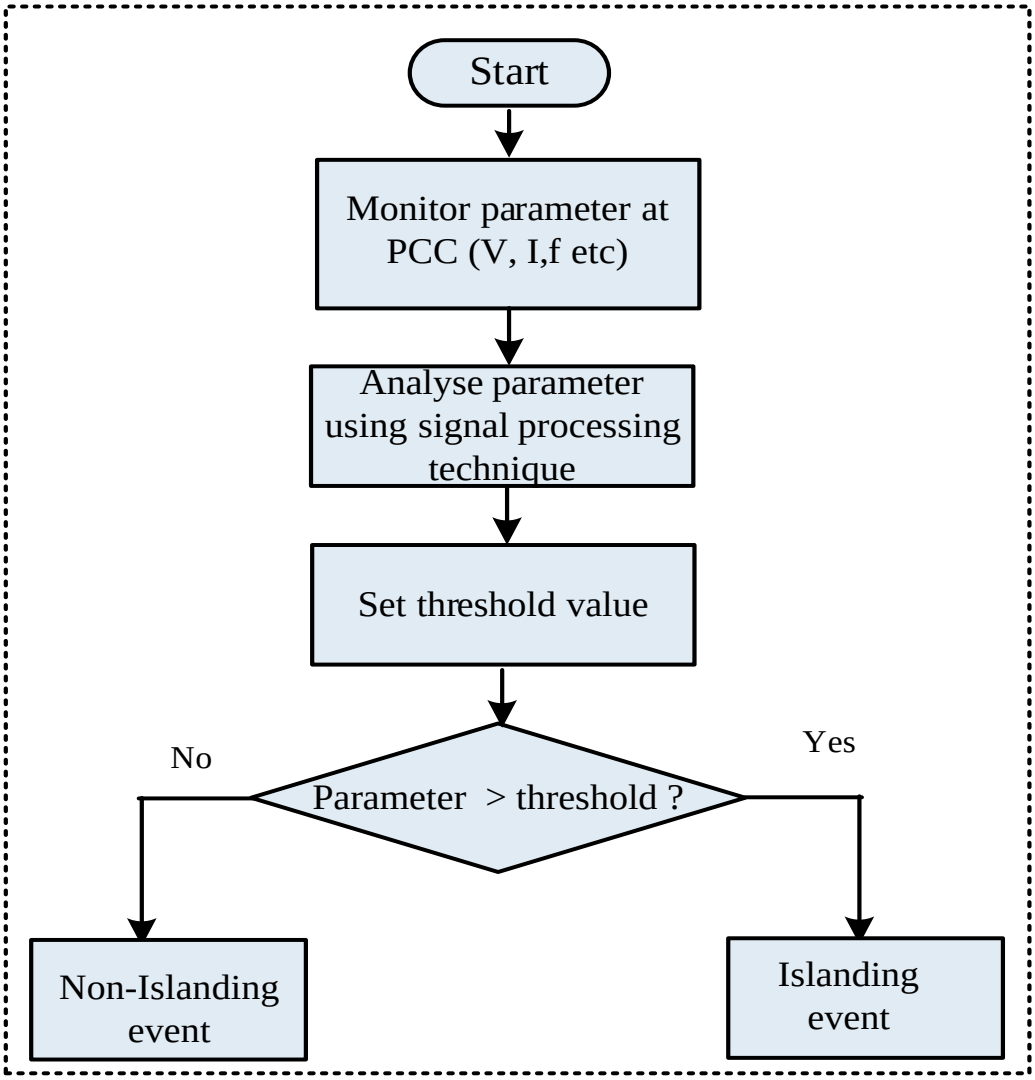

Fig 6.6. Flow chart of signal processing-based islanding detection method

6.5 STUDY OF ISLANDING DETECTION TECHNIQUE USING Q- AXIS CONTROL

In the q-axis current, a disturbance signal is injected into the q-axis current. Figure 6.7 depicts the block diagram for inverter's q-current controllers for islanding detection technique. Q-axes current controllers regulate, real and reactive powers supplied by the VSC [18]. In the present study, an investigation method is presented along with the injection of a sinusoidal waveform working as a disturbance signal at a single frequency via, q-axis controller.

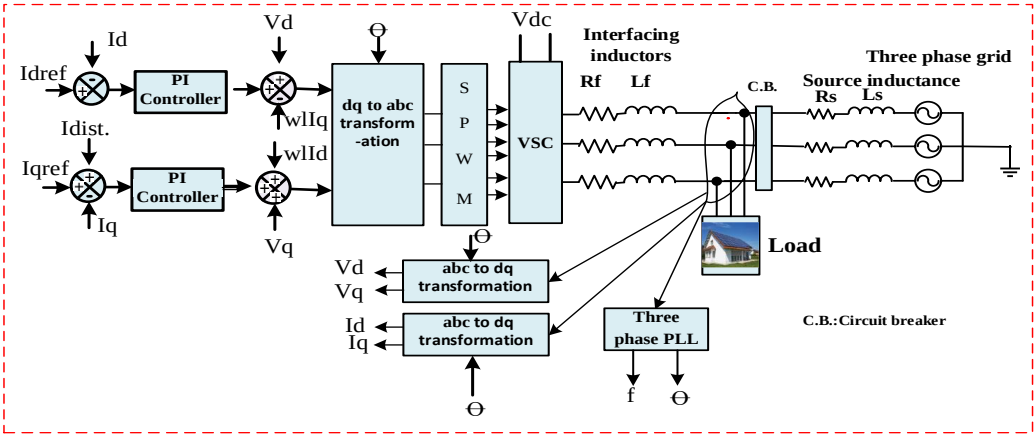

Fig.6.7. Block diagram of q-active control

The power equations are given below:

$$\boldsymbol{p} = \frac{\mathbf{3}}{\mathbf{2}} * (\boldsymbol{v_d} * \boldsymbol{i_d}) \tag{6.14}$$

$$\boldsymbol{q} = -\frac{\mathbf{3}}{\mathbf{2}} * (\boldsymbol{v_d} * \boldsymbol{i_q}) \tag{6.15}$$

The following are the current equations for the inverter output:

$$\begin{bmatrix} i_d \\ i_q \end{bmatrix} = \begin{bmatrix} i_{dref} \\ i_{qref} \end{bmatrix} \tag{6.16}$$

Disturbance signal frequency is injected into the grid, to test for the islanding formation. Furthermore, for an active islanding detection, the equations are reframed as:

$$\begin{bmatrix} i_d \\ i_q \end{bmatrix} = \begin{bmatrix} i_{dref} \\ i_{qref} + i_{dist.} \end{bmatrix} \tag{6.17}$$

$$i_{dist.} = i_{dr} * \sin wdt \tag{6.18}$$

In this investigation, a single 20 Hz signal of magnitude equal to 1% of rated d-axis current is applied to the VSC [149]-[150]. Under perfectly matched power conditions (between the solar PV system and load demand), frequency responses with and without injecting disturbance of current signal via, q-axis, has been observed and analysed when no current disturbance is injected, the frequency variation on post-islanding is negligible. Because of this, the majority of passive islanding detection are inefficient at detecting the island formation. Only in post-islanding conditions, the current disturbance injection significantly change the frequency of the voltage signal [8]. To determine whether the frequency variation is caused by islanded or non-islanded conditions, the frequency is further analysed.

Block diagram of islanding detection schemes for q-axis controller is shown in figure 6.8.

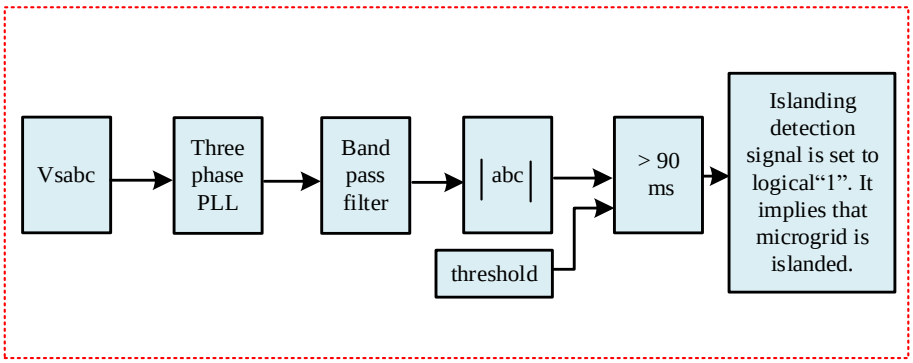

Fig.6.8. Block diagram for islanding detection for q- axis control

6.5.1 Phase-Locked Loop (PLL)

The PLL is used to determine the frequency of the PCC voltage, angular frequency, and the theta needed for transformation from abc to dq0 and vice-versa.

6.5.2 Band-Pass Filter

In the event that the grid frequency deviates more than 0.5 Hz from the nominal system frequency, the active islanding detection technique is projected in [9] and mal-identify, grid integrated mode as islanded operation.

6.5.3 Absolute Frequency Variation (Mean)

Absolute output of BPF is used to calculate AFVmean, which is presented as follows:

$$AFV_{mean} = \left(\frac{1}{T}\right)\left[\int_{t-T}^{t}\left(AFV(t)\right)dt \right. \quad (6.19)$$

T is one period of time, injected sinusoidal wave and t is the time (instantaneous).

6.5.4 Threshold Settings

The AFV and AFVmean are then calculated using equation (6.19). It is important and worthwhile to note that peak frequency deviation. for any well-matched solar PV system and load demand is roughly equal of ($Q_f = 2.5$). As a result, the threshold is set at 95% of the derived AFVmean values. The following generalised expression to estimate peak variation in frequency w.r.t. to Q_f under perfectly matched power state is given below:

$$\text{Deviation in Peak Frequency} = -0.042 \ln(Q_f) + 0.1004. \quad (6.20)$$

The loads of Q_f =2.5, have been recommended for use by several standards and are therefore threshold has been studied in the literature [18]. The presented technique's step-by-step process depicted in the Figure 6.9. The PLL is used to determine the frequency of the Vpcc voltage. Furthermore, estimated frequency is passed through the BPF, and the output is taken as an absolute value. AFVmean is then calculated using equation (6.19). For the purpose of comparing the stable value to the threshold, AFVmean is computed.

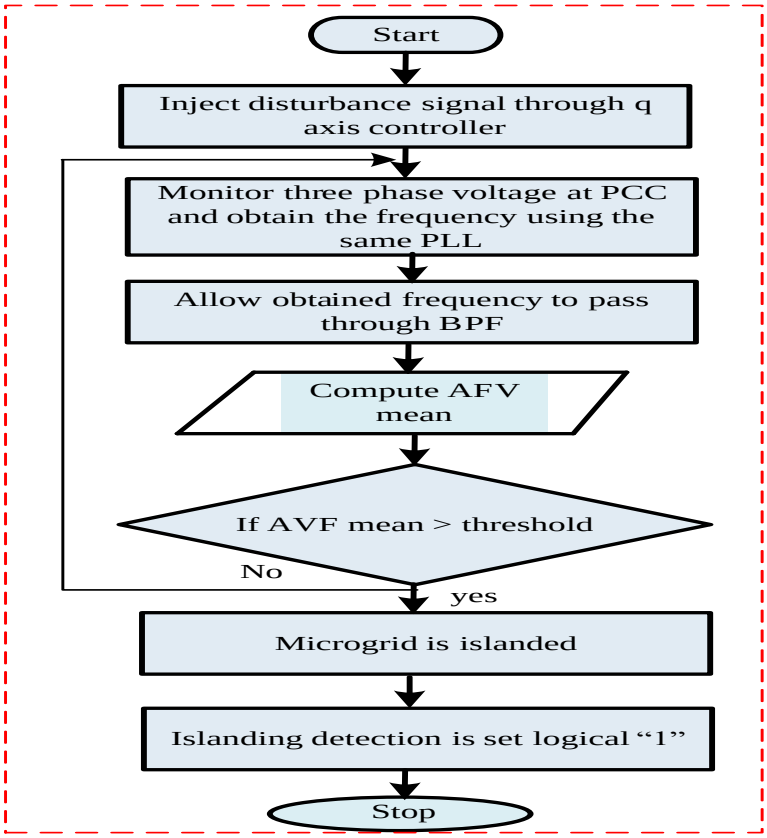

Fig.6.9. Flow chart of islanding detection algorithm

Figure 6.8, depicts, islanding detection system, the deliberate time delay is 90ms, and it is calculated under adverse scenarios [18]. The intentional time delay is required so that the islanding detection technique does not mistakenly identify transients as being on an island.

6.6 CONCLUDING REMARKS

This chapter provides comprehensive review, analysis and study of the many islanding detection techniques that have been described and are divided into the following categories: remote, passive, active, signal processing is presented. An active islanding identification based on disturbance injection through the quadrature axis controller has been studied and analyzed. It offers the several contributions/benefits viz. the islanding identification time is 180 milliseconds (which is better than several other techniques in the literature), correctly distinguishes between non-islanding and islanding scenarios, compatible with all international standards.

CHAPTER-VII
CONCLUSIONS AND SUGGESTION FOR FURTHER WORK

7.1 INTRODUCTION

Renewable energy sources can meet the world's rising demand for energy and environmental concerns. As per present developments, one of the most significant green energy source is a solar photovoltaic generation system.

The major objective of this research work is to design and develop a three-phase, two-stage, grid-connected SPV-based microgrid for efficient and improved performance. In the grid-connected SPV-based microgrid, SPV system is connected to VSC via dc-dc converter (boost converter). To track the maximum power that can be extracted by the SPV array, the P&O MPPT algorithm is used to control the switching pulses of the dc-dc converter. Furthermore, for grid integration of VSC, various conventional control algorithm viz. SRF, IRPT and unit template methods are employed to generate switching pulses for VSC. Proposed system of grid integrated PV based microgrid is designed and simulated in the MATLAB environment utilising the Simulink and SPS tool boxes.

The proposed grid integrated PV based microgrid, provides several functions including compensation of harmonic current, reactive power and load unbalance. Furthermore, novel intelligent based SRF theory based VSC control algorithm has been developed for grid integration of microgrid. The proposed control method of VSC has been examined for the various operating conditions of the load. Control and performance of system with novel developed has been analysed.

Furthermore, Adaptive theory based VSC control algorithms viz. conventional LMS, and novel Variable Step Size Least Mean Square (VSSLMS), Robust Least Mean Logarithmic Square Control Algorithm (RLMLS), for two-stage, three-phase grid interfaced SPV system have been developed and presented. The efficiency of the proposed control algorithms has been tested under different input/output condition such as insolation variation, load variation, load unbalancing, nonlinear load, reactive load, grid voltage unbalancing, and distorted grid voltage etc. Furthermore, the performance of the proposed algorithms is compared with conventional SRF and LMS control in terms of THD (%) in grid current and weight convergence. The performance of the proposed control algorithms is verified on MATLAB/ Simulink.

To test the validity of the proposed algorithms, the prototype hardware for the grid connected PV system and its various components has been presented. Furthermore, due to non-availability

of solar PV array/PV simulator in the laboratory, developed VSC control algorithms are tested on the DSTATCOM in the laboratory. Proposed control algorithms viz. Variable Step Size Least Mean Square (VSSLMS), Robust Least Mean Logarithmic Square Control Algorithm (RLMLS) are validated experimentally in the laboratory on prototype hardware set up.

The performance of the proposed adaptive control algorithms has been tested for different condition such as load variation, load unbalancing, nonlinear load, reactive load, grid voltage unbalancing etc. THD (%) in grid current under nonlinear load is observed to be less than 5% which is within the limit of IEEE-519 standard.

Furthermore, comprehensive review, analysis and study of the various islanding detection techniques have been carried out. Islanding detection techniques are categorised into the following categories: remote, passive, active, and signal processing. An active islanding identification based on disturbance injection through the quadrature axis controller has been studied and analysed. the analysis and study of all the aforementioned techniques have been discussed in details.

7.2 MAIN CONCLUSIONS

The following are the main key conclusions of the research study that is being presented:

- In this present work, design, and development of three phase, two-stage grid integrated solar PV based microgrid has been carried out. The efficiency of a solar PV system is affected because of the changes in the output in response to changing weather conditions. Maximum power point approaches, have been studied and analysed. P&O MPPT has been used in order to extract the maximum power.
- The design and development of conventional control viz. SRFT, IRPT and unit template algorithms has been carried for grid integration and control and performance has been analysed.
- In a grid connected microgrid system, PV inverter control (VSC), is very essential part of the system. The inverter (VSC) should include features like active filtering and preserve the grid's power quality along-with supplying power to the load at the defined voltage and frequency.
- A novel, IT-2 FLC based modified SRFT control algorithm has been developed. It has been tested under different operating condition such as insolation variation, load variation, load unbalancing, nonlinear load, reactive load etc, Simulation results under different operating scenarios have been analysed and presented to demonstrate the viability of the developed control technique. Under all test conditions, the proposed IT-2 FLC based modified SRFT

algorithms' performance is found to be efficient and satisfactory. It has been observed that the developed control algorithm ensures power balance and compensates for the load's reactive power and nonlinearity. The THD (%) in grid current is observed to be less than 5% which is within IEEE-519 standard.

- Furthermore, adaptive theory based VSC control algorithms for grid integration viz. variable step size least mean square (VSSLMS) and robust least mean logarithmic square (RLMLS) are developed and presented. The performance of the proposed control algorithms is verified on MATLAB/ Simulink.
- The efficiency of the proposed adaptive control algorithms has been tested under different operating condition such as insolation variation, load variation, load unbalancing, nonlinear load, reactive load, grid voltage unbalancing, and distorted grid voltage etc. and it is found to be efficient and satisfactory under all the conditions.
- The developed control algorithms also maintain power balance, compensates reactive power, and harmonics.
- Furthermore, the performance of the proposed algorithms is compared with conventional SRF and LMS control in terms of THD (%) in grid current and weight convergence. Furthermore, proposed control has better weight convergence capability and better initial transient response in terms of overshoot and undershoot and lesser oscillations in the response during dynamic scenario.
- THD (%) in grid current under nonlinear load is observed to be less than 5% which is within the limit of IEEE-519 standard.
- Furthermore, proposed control algorithms are also tested on prototype hardware set up of DSTATCOM, developed in laboratory under different load and adverse scenario of grid viz. unbalanced voltage of grid condition. Performance of the proposed VSC control algorithms has been found to be satisfactory under all test conditions and THD (%) in grid current is within the 5% under nonlinear loads.
- Analysis of different islanding detection scheme along with the advantages, disadvantages and limitations are evaluated and summarized.

7.3. SUGGESTIONS FOR FURTHER WORK

There are a number of critical issues that needs to be examined in the present work.

- These algorithms can be extended to mitigate power quality issues in three phases, four wire DSTATCOM systems, in addition to neutral current compensation.

- The present research focuses on the design and management of solar-powered photovoltaic microgrids under stable grid conditions. It is possible to evaluate the performance of proposed control, under the fault conditions.
- Due to laboratory limitations the developed algorithms have been tested on DSTATCOM. It can be extended for experimental verification on a SPV based system.

REFERENCES

[1] S. Strache, R. Wunderlich, and S. Heinen, "A Comprehensive, quantitative comparison of inverter architectures for various PV Systems, PV cells, and irradiance profiles," *IEEE Trans. Sustain. Energy*, vol. 5, no. 3, pp. 813–822, 2014, doi: 10.1109/TSTE.2014.2304740.

[2] C. Lupangu and R. C. Bansal, "A review of technical issues on the development of solar photovoltaic systems," *Renew. Sustain. Energy Rev.*, vol. 73, no. February 2016, pp. 950–965, 2017, doi: 10.1016/j.rser.2017.02.003.

[3] P. Shukl and B. Singh, "Grid Integration of Three-Phase Single-Stage PV System Using Adaptive Laguerre Filter Based Control Algorithm under Nonideal Distribution System," *IEEE Trans. Ind. Appl.*, vol. 55, no. 6, pp. 6193–6202, 2019, doi: 10.1109/TIA.2019.2931504.

[4] P. Verma, R. Garg, and P. Mahajan, "Asymmetrical interval type-2 fuzzy logic control based MPPT tuning for PV system under partial shading condition," *ISA Trans.*, no. January, 2020, doi: 10.1016/j.isatra.2020.01.009.

[5] M. Singh and A. Chandra, "Real-time implementation of ANFIS control for renewable interfacing inverter in 3P4W distribution network," *IEEE Trans. Ind. Electron.*, vol. 60, no. 1, pp. 121–128, 2013, doi: 10.1109/TIE.2012.2186103.

[6] A. Q. Al-Shetwi and M. Z. Sujod, "Grid-connected photovoltaic power plants: A review of the recent integration requirements in modern grid codes," *Int. J. Energy Res.*, vol. 42, no. 5, pp. 1849–1865, 2018, doi: 10.1002/er.3983.

[7] P. Paniyil, V. Powar, R. Singh , B. Hennigan, P. Lule, M. Allison, J Kimsey, A. Carambia, D. Patel, D.Carrillo, Z. Shriber, T. Bazer, J. Farnum, K. Jadhav and D. Pumputis, "Photovoltaics- And battery-based power network as sustainable source of electric power," Energies, vol. 13, no. 19, pp. 1–22, 2020.

[8] A. Mohanty, M. Viswavandya, D. K. Mishra, P. K. Ray, and S. Pragyan, "Modelling & Simulation of a PV Based Micro Grid for Enhanced Stability," *Energy Procedia*, vol. 109, pp. 94–101, 2017.

[9] M. Gaayathri and K. Ranjith Kumar, “Modelling and Simulation of PV-BES based Microgrid System Operating In Standalone Mode,” IOP Conf. Ser. Mater. Sci. Eng., vol. Vol. 1084, pp. 1-8, 2021.

[10] X. Xiong and Y. Yang, “A photovoltaic-based DC microgrid system: Analysis, design and experimental results,” *Electronics*, vol. 9, no. 6, pp. 1–17, 2020. https://doi.org/10.3390/electronics9060941.

[11] P. Sharma and V. Agarwal, “Exact maximum power point tracking of grid-connected partially shaded PV source using current compensation concept,” *IEEE Transactions on Power Electronics*, vol. 29, no. 9, pp. 4684–4692, Sep. 2014. doi:10.1109/TPEL.2013.2285075.

[12] K. Kurokawa, et al., “Sophisticated verification of simple monitored data for Japanese field program,” *2nd World Conference and Exhibition on Photovoltaic Solar Energy Conversion, Vienna, Austria*, 1998, pp. 1941–1946.

[13] X. Zhang, D. Gamage, B. Wang, and A. Ukil, “Hybrid maximum power point tracking method based on iterative learning control and perturb & observe method,” *IEEE Trans. Sustain. Energy*, vol. 12, no. 1, pp. 659–670, 2021, doi: 10.1109/TSTE.2020.3015255.

[14] S. Chauhan and B. Singh, “Control of Solar PV Arrays Based Microgrid Intertied to a 3-Phase 4-Wire Distribution Network,” *IEEE Transactions on Industry Applications*, vol. 58, no. 4, pp. 5365-5382, July-Aug. 2022, doi: 10.1109/TIA.2022.3171529.

[15] B. Singh, P. Jayaprakash, D. P. Kothari, A. Chandra, and K. Al Haddad, “Comprehensive study of dstatcom configurations,” *IEEE Trans. Ind. Informatics*, vol. 10, no. 2, pp. 854–870, 2014, doi: 10.1109/TII.2014.2308437.

[16] S. Srita and S. Somkun, "Implementation of Harmonic Compensation for Three-Phase Grid-Connected Voltage-Source Converter Under Grid Voltage Distortio*n,”,19th International Conference on Electrical Engineering/Electronics, Computer, Telecommunications and Information Technology* (ECTI-CON)*, Prachuap Khiri Khan, Thailand, 2022, pp. 1-5, doi: 10.1109/ECTI-CON54298.2022.9795533.*

[17] S. R. Arya, B. Singh, R. Niwas, A. Chandra, and K. Al-Haddad, “Power Quality Enhancement Using DSTATCOM in Distributed Power Generation System,” *IEEE Trans. Ind. Appl.*, vol. 52, no. 6, pp. 5203–5212, 2016, doi: 10.1109/TIA.2016.2600644.

[18] S. Murugesan, V. Murali, and S. A. Daniel, “Hybrid Analyzing Technique for Active Islanding Detection Based on d-Axis Current Injection,” *IEEE Systems Journal*, vol. 12, no. 4, pp. 3608–3617, 2018, doi: 10.1109/JSYST.2017.2730364.

[19] M. Mahdi and V. M. Istemihan Genc, “A real-time self-healing methodology using

model- And measurement-based islanding algorithms," *IEEE Trans. Smart Grid*, vol. 10, no. 2, pp. 1195–1204, 2019, doi: 10.1109/TSG.2017.2760698.

[20] M. R. Alam, K. M. Muttaqi, and A. Bouzerdoum, "Characterization of Voltage Dips and Swells in a DG-Embedded Distribution Network during and Subsequent to Islanding Process and Grid Reconnection," *IEEE Trans. Ind. Appl*., vol. 54, no. 5, pp. 4028–4038, 2018, doi: 10.1109/TIA.2018.2833056.

[21] N. Beniwal, I. Hussain, and B. Singh, "Second-order volterra-filter-based control of a solar PV-DSTATCOM system to achieve lyapunov's stability," *IEEE Trans. Ind. Appl.*, vol. 55, no. 1, pp. 670–679, 2019, doi: 10.1109/TIA.2018.2867324.

[22] M. Karimi, H. Mokhlis, K. Naidu, S. Uddin, and A. H. A. Bakar, "Photovoltaic penetration issues and impacts in distribution network - A review," *Renew. Sustain. Energy Rev.*, vol. 53, pp. 594–605, 2016, doi: 10.1016/j.rser.2015.08.042.

[23] X. Liang, "Emerging Power Quality Challenges Due to Integration of Renewable Energy Sources," *IEEE Trans. Ind. Appl.*, vol. 53, no. 2, pp. 855–866, 2017, doi: 10.1109/TIA.2016.2626253.

[24] P. Kumar, "Simulation of custom power electronic device D-STATCOM -a case study," *India Int. Conf. Power Electron. IICPE 2010*, pp. 1–4, 2011, doi: 10.1109/IICPE.2011.5728057.

[25] X. Liang and C. Andalib-Bin-Karim, "Harmonics and Mitigation Techniques Through Advanced Control in Grid-Connected Renewable Energy Sources: A Review," *IEEE Trans. Ind. Appl*., vol. 54, no. 4, pp. 3100–3111, 2018, doi: 10.1109/TIA.2018.2823680.

[26] N. Patel, N. Gupta, and B. C. Babu, "Design, development, and implementation of grid-connected solar photovoltaic power conversion system," *Energy Sources, Part A Recovery, Utilization, and Environmental Effects*, Vol. 43, no.22, pp.915-2934, 2019. https://doi.org/10.1080/15567036.2019.1668506.

[27] B. Singh, C. Jain, S. Goel, R. Gogia, and U. Subramaniam, "A Sustainable Solar Photovoltaic Energy System Interfaced with Grid-Tied Voltage Source Converter for Power Quality Improvement," *Electric Power Components and Systems*, vol. 45, no. 2, pp.171–183, 2017. https://doi.org/10.1080/15325008.2016.1233298.

[28] IEEE. IEEE Recommended Practices and Requirements for Harmonic Control in Electrical Power Systems. Vol. 1992, IEEE Std 519-1992. 1–112, (1993).

[29] B. Singh and S. Kumar, "Grid Interactive Residential Photovoltaic-Battery Based Microgrid for Rural Electrification," *IEEE Trans. Ind. Appl.,* vol. 56, no. 4, pp. 4114–4123, 2020.

[30] N. Kumar, B. Singh, and B. K. Panigrahi, "ANOVA Kernel Kalman Filter for Multi-Objective Grid Integrated Solar Photovoltaic-Distribution Static Compensator," *IEEE Transactions on Circuits and Systems I: Regular Papers*, vol. 66, no. 11, pp. 4256–4264, 2019, doi: 10.1109/TCSI.2019.2922405.

[31] C. Lupangu and R. C. Bansal, "A review of technical issues on the development of solar photovoltaic systems," *Renew. Sustain. Energy Rev.*, vol. 73, no. February 2016, pp. 950–965, 2017, doi: 10.1016/j.rser.2017.02.003.

[32] R. Panigrahi, S. K. Mishra, S. C. Srivastava, A. K. Srivastava and N. N. Schulz, "Grid Integration of Small-Scale Photovoltaic Systems in Secondary Distribution Network—A Review,", *IEEE Transactions on Industry Applications*, vol. 56, no. 3, pp. 3178-3195, May-June 2020, doi: 10.1109/TIA.2020.2979789.

[33] P. Shukl and B. Singh, "Grid Integration of Three-Phase Single-Stage PV System using Adaptive Laguerre Filter Based Control Algorithm under Non-Ideal Distribution System," *IEEE Trans. Ind. Appl.*, vol. PP, no. c, pp. 1–1, 2019, doi: 10.1109/tia.2019.2931504.

[34] Rohten; Matías N. Garbarino; Javier A. Muñoz; José J. Silva; Esteban S. Pulido; Jose R, "A Novel Global Maximum Power Point Tracking Method Based on Measurement Cells," *IEEE Access*, vol. 10, pp. 97481-97494, 2022, doi: 10.1109/ACCESS.2022.3205163.

[35] Mukhtiar Singh, Vinod Khadkikar, Ambrish Chandra, and Rajiv K Varma, "Grid Interconnection of Renewable Energy Sources at the Distribution Level with Power-Quality Improvement Features", *Transaction on power delivery*, 26(1), 307-315, (2011).

[36] K. Arulkumar, K. Palanisamy, and D. Vijayakumar, "Recent advances and control techniques in grid connected PV system – A review," *International Journal of Renewable Energy Research*, vol. 6, no. 3, pp. 1037–1049, 2016. https://doi.org/10.20508/ijrer.v6i3.4075.g6886.

[37] M. Karimi, H. Mokhlis, K. Naidu, S. Uddin, and A. H. A. Bakar, "Photovoltaic penetration issues and impacts in distribution network - A review," *Renew. Sustain. Energy Rev.*, vol. 53, pp. 594–605, 2016, doi: 10.1016/j.rser.2015.08.042.

[38] N. Tak, S. K. Chattopadhyay and C. Chakraborty, "Single-Sourced Double-Stage Multilevel Inverter for Grid-Connected Solar PV Systems," IEEE *Open Journal of the Industrial Electronics Society*, vol. 3, pp. 561-581, 2022, doi: 10.1109/OJIES.2022.3206352.

[39] P. Paniyil, V. Powar, R. Singh, B. Hennigan, P. Lule, M. Allison, J Kimsey, A. Carambia, D. Patel, D.Carrillo, Z. Shriber, T. Bazer, J. Farnum, K. Jadhav and D. Pumputis, "Photovoltaics- And battery-based power network as sustainable source of electric power," *Energies*, vol. 13, no. 19, pp. 1–22, 2020.

[40] A. Mohanty, M. Viswavandya, D. K. Mishra, P. K. Ray, and S. Pragyan, "Modelling & Simulation of a PV Based Micro Grid for Enhanced Stability," *Energy Procedia*, vol. 109, pp. 94–101, 2017.

[41] R. Meenakshi and K. Selvi, "Controller design for a Single-Stage Single-Phase Grid-Connected Solar PV Microgrid,"*2023 Second International Conference on Electrical, Electronics, Information and Communication Technologies (ICEEICT)*, Trichirappalli, India, 2023, pp. 01-04, doi: 10.1109/ICEEICT56924.2023.10157251.

[42] A. Rolán, S. Bogarra and M. Bakkar, "Integration of Distributed Energy Resources to Unbalanced Grids Under Voltage Sags with Grid Code Compliance," *IEEE Transactions on Smart Grid*, vol. 13, no. 1, pp. 355-366, Jan. 2022, doi: 10.1109/TSG.2021.3107984.

[43] P. Sharma and V. Agarwal, "Exact maximum power point tracking of grid-connected partially shaded PV source using current compensation concept," *IEEE Transactions on Power Electronics*, vol. 29, no. 9, pp. 4684–4692, Sep. 2014.

[44] B. Subudhi and R. Pradhan, "A comparative study on maximum power point tracking techniques for photovoltaic power systems," *IEEE Transactions on Sustainable Energy*, vol. 4, no. 1, pp. 89–98, Jan. 2013.

[45] D. Verma, S. Nema, A. M. Shandilya, and S. K. Dash, "Maximum power point tracking (MPPT) techniques: Recapitulation in solar photovoltaic systems," *Renewable and Sustainable Energy Reviews*, vol. 54, pp. 1018–1034, Feb. 2016.

[46] M. A. S. Masoum, H. Dehbonei, and E. F. Fuchs, "Theoretical and experimental analyses of photovoltaic systems with voltage and current-based maximum power-point tracking," *IEEE Transactions on Energy Conversion*, vol. 17, no. 4, pp. 514–522, Dec. 2002.

[47] Trishan, E.; Patrick, L. C., "Comparison of Photovoltaic Array Maximum Power Point Tracking Techniques", IEEE Trans. Energy Convers, 22(2), 439-449 (2007). doi: 10.1109/TEC.2006.874230.

[48] Y. Jiang, J. A. Abu Qahouq, and T. A. Haskew, "Adaptive step size with adaptive-perturbation-frequency digital MPPT controller for a single-sensor photovoltaic solar system," *IEEE Trans. Power Electron.*, vol. 28, no. 7, pp. 3195–3205, 2013, doi:

10.1109/TPEL.2012.2220158.

[49] M. Killi and S. Samanta, "Modified perturb and observe MPPT algorithm for drift avoidance in photovoltaic systems," *IEEE Trans. Ind. Electron.*, vol. 62, no. 9, pp. 5549–5559, 2015, doi: 10.1109/TIE.2015.2407854.

[50] M. A. Elgendy, D. J. Atkinson, and B. Zahawi, "Experimental investigation of the incremental conductance maximum power point tracking algorithm at high perturbation rates," *IET Renew. Power Gener.*, vol. 10, no. 2, pp. 133–139, 2016, doi: 10.1049/iet-rpg.2015.0132.

[51] M. A. G. de Brito, L. Galotto, L. P. Sampaio, G. D. A. e Melo, and C. A. Canesin, "Evaluation of the main MPPT techniques for photovoltaic applications," *IEEE Transactions on Industrial Electronics*, vol. 60, no. 3, pp. 1156–1167, Mar. 2013.

[52] R. B. Bollipo, S. Mikkili, and P. K. Bonthagorla, "Hybrid, optimal, intelligent and classical PV MPPT techniques: A review," *CSEE Journal of Power and Energy Systems*, vol. 7, no. 1, pp. 9–33, 2021, doi: 10.17775/CSEEJPES.2019.02720.

[53] R. Ahmad, A. F. Murtaza, and H. A. Sher, "Power tracking techniques for efficient operation of photovoltaic array in solar applications- A review," *Renewable and Sustainable Energy Reviews*, vol. 101, pp. 82– 102, Mar. 2019.

[54] N. Femia, G. Petrone, G. Spagnuolo, and M. Vitelli, "Optimization of perturb and observe maximum power point tracking method," *IEEE Trans. Power Electron.*, vol. 20, no. 4, pp. 963–973, 2005, doi: 10.1109/TPEL.2005.850975.

[55] B. Singh, A. Chandra, K. Al-Haddad, "Power Quality Problems and Mitigation Techniques", Wiley (2015). http://onlinelibrary.wiley.com/book/10.1002/ 978111 8922064, ISBN: 978-1-118-92205-7

[56] P. R. Kasari, M. Paul, B. Das and A. Chakraborti, "Analysis of D-STATCOM for power quality enhancement in distribution network," *TENCON 2017 - 2017 IEEE Region 10 Conference, Penang, Malaysia*, 2017, pp. 1421-1426, doi: 10.1109/TENCON.2017.8228081.

[57] B. Singh, P. Jayaprakash, D. P. Kothari, A. Chandra, and K. Al Haddad, "Comprehensive study of dstatcom configurations," *IEEE Trans. Ind. Informatics*, vol. 10, no. 2, pp. 854–870, 2014, doi: 10.1109/TII.2014.2308437.

[58] B. Singh, D. T. Shahani, and A. K. Verma, "Power balance theory based control of grid interfaced solar photovoltaic power generating system with improved power quality," *PEDES 2012 - IEEE Int. Conf. Power Electron. Drives Energy Syst.*, 2012, doi: 10.1109/PEDES.2012.6484359.

[59] S. B. Pandu, Sundarabalan, Srinath, T Santhana Krishnan, Soorya Priya , Balasundar , Jayant Sharma, Soundarya, Pierlugi Siano, Hassan Haes Alhelou "Power Quality Enhancement in Sensitive Local Distribution Grid Using Interval Type-II Fuzzy Logic Controlled DSTATCOM," *IEEE Access*, vol. 9, pp. 59888–59899, 2021, doi: 10.1109/ACCESS.2021.3072865.

[60] P. K. Barik, G. Shankar, and P. K. Sahoo, "Power quality assessment of microgrid using fuzzy controller aided modified SRF based designed SAPF", *International Transactions on Electrical Energy Systems* . Apr2020, Vol. 30 Issue 4, p1-24. 24p. (2019). doi: 10.1002/2050-7038.12289.

[61] P. Karuppanan, KK. Mahapatra, "PI and fuzzy logic controllers for shunt active power filter A report", *ISA Transactions*,Vol. 51, no.1, January 2012, Pages 163-169. https://doi.org/10.1016/j.isatra.2011.09.004.

[62] H. K. Yada and M. S. R. Murthy, "An improved control algorithm for DSTATCOM based on single-phase SOGI-PLL under varying load conditions and adverse grid conditions," *IEEE Int. Conf. Power Electron. Drives Energy Syst. PEDES 2016*, vol. 2016-January, pp. 1–6, 2017, doi: 10.1109/PEDES.2016.7914564.

[63] F. Xiao, L. Dong, L. Li, and X. Lia, "A Frequency-Fixed SOGI Based PLL for Single-Phase Grid-Connected Converters", *IEEE Transactions on Power Electronics*, 32(3) 1713 - 1719, (2017). DOI: 10.1109/TPEL.2016.2606623.

[64] F. Wu, L. Zhang, and J. Duan, "A new two-phase stationary-frame-based enhanced PLL for three-phase grid synchronization," *IEEE Trans. Circuits Syst. II Express Briefs*, vol. 62, no. 3, pp. 251–255, 2015, doi: 10.1109/TCSII.2014.2368257.

[65] T. A. Youssef and O. Mohammed, "Adaptive SRF-PLL with reconfigurable controller for Microgrid in grid-connected and stand-alone modes," *IEEE Power Energy Soc. Gen. Meet.*, pp. 1–5, 2013, doi: 10.1109/PESMG.2013.6673028.

[66] S. Deo, C. Jain, and B. Singh, "A PLL-less scheme for single-phase grid interfaced load compensating solar PV generation system," *IEEE Trans. Ind. Inform*., vol. 11, no. 3, pp. 692–699, Jun. 2015.

[67] N. Beniwal, I. Hussain, and B. Singh, "A second-order volterra filter based control of SPV-DSTATCOM system to achieve Lyapunov's stability," *2016 IEEE 7th Power India Int. Conf.*, pp. 1–5, 2016, doi: 10.1109/POWERI.2016.8077292.

[68] P. Ray, P. K. Ray and S. K. Dash, "Power Quality Enhancement and Power Flow Analysis of a PV Integrated UPQC System in a Distribution Network," *IEEE Transactions on Industry Applications*, vol. 58, no. 1, pp. 201-211, Jan.-Feb. 2022, doi:

10.1109/TIA.2021.3131404.

[69] D. Pullaguram, S. Bhattacharya, S. Mishra, and N. Senroy, "A Fuzzy Assisted Enhanced Control for Utility Connected Rooftop PV," *IFAC-PapersOnLine*, vol. 50, no. 1, pp. 7693–7698, 2017, doi: 10.1016/j.ifacol.2017.08.1144.

[70] M. Farhat, M. Hussein, AM. Atallah, "Enhancement performance of a three phase grid connected photovoltaic system based on pi-genetic algorithm (pi-ga) controller", *2017 19th Int Middle-East Power Syst Conf. MEPCON 2017* - Proc.;2018-February(December):145–51,(2018).

[71] N. Gupta, R. Garg and P. Kumar, "Asymmetrical fuzzy logic control to PV module connected micro-grid,"*2015 Annual IEEE India Conference (INDICON)*, New Delhi, India, 2015, pp. 1-6, doi: 10.1109/INDICON.2015.7443356.

[72] N. Gupta and R. Garg, "Tuning of asymmetrical fuzzy logic control algorithm for SPV system connected to grid," *Int. J. Hydrogen Energy*, vol. 42, no. 26, pp. 16375–16385, 2017, doi: 10.1016/j.ijhydene.2017.05.103.

[73] X. Li, H. Wen, Y. Hu, and L. Jiang, " A novel beta parameter based fuzzy-logic controller for photovoltaic MPPT application", *Renewable Energy*,130,pp:416–27. https://doi.org/10.1016/j.renene.2018.06.071.

[74] H. Suryanarayana and M. K. Mishra, "Fuzzy logic based supervision of DC link PI control in a DSTATCOM," *2008 Annual IEEE India Conference,* Kanpur, India, 2008, pp. 453-458, doi: 10.1109/INDCON.2008.4768766.

[75] A.H. Sayed , Fundamentals of Adaptive Filtering, John Wiley & Sons, New York, 2003.

[76] K. Zeb , Waqar Uddina, Muhammad Adil Khana, Zunaib Alic, Muhammad Umair Alia, Nicholas Christofidesc, and H.J. Kima, "A comprehensive review on inverter topologies and control strategies for grid connected photovoltaic system," *Renew. Sustain. Energy Rev.*, vol. 94, no. November 2017, pp. 1120–1141, 2018, doi: 10.1016/j.rser.2018.06.053.

[77] S. K. Patel, S. R. Arya, and R. Maurya, "Harmonic mitigation technique for DSTATCOM using continuous time LMS adaptive filter," *2016 IEEE Uttar Pradesh Sect. Int. Conf. Electr. Comput. Electron. Eng. UPCON 2016*, pp. 19–24, 2017, doi: 10.1109/UPCON.2016.7894617.

[78] R. K. Agarwal, I. Hussain, and B. Singh, "LMF-based control algorithm for single stage three-phase grid integrated solar PV system," *IEEE Trans. Sustain. Energy*, vol. 7, no. 4, pp. 1379–1387, 2016, doi: 10.1109/TSTE.2016.2553181.

[79] Z. Li, D. Li, X. Xu, and J. Zhang, "New normalized LMS adaptive filter with a variable

regularization factor," *Journal of Systems Engineering and Electronics*, vol. 30, no. 2, pp. 259–269, 2019, doi: 10.21629/JSEE.2019.02.05.

[80] M. O. Sayin, N. D. Vanli, and S. S. Kozat, "A Novel Family of Adaptive Filtering Algorithms Based on the Logarithmic Cost," *IEEE Trans. Signal Process.*, vol. 62, no. 17, pp. 4411–4424, 2014, doi: 10.1109/TSP.2014.2333559.

[81] Y. Tsuda and T. Shimamura, "An improved NLMS algorithm for channel equalization," Proceedings - *IEEE International Symposium on Circuits and Systems,* vol.5, no. 2, pp. 353–356, 2002, doi: 10.1109/iscas.2002.1010713.

[82] A. Chaturvedi, K. Raj, and A. Kumar, "A comparative analysis of LMS and NLMS algorithms for adaptive filtration of compressed ECG signal," *ICPCES 2012 - 2012 2nd Int. Conf. Power, Control Embed. Syst.*, pp. 1–6, 2012, doi: 10.1109/ICPCES.2012.6508051.

[83] J. Dhiman, S. Ahmad, and K. Gulia, "Comparison between Adaptive filter Algorithms (LMS, NLMS and RLS)," *Int. J. Sci. Eng. Technol. Res.*, vol. 2, no. 5, pp. 2278–7798, 2013.

[84] K. Xiong and S. Wang, "Robust least mean logarithmic square adaptive filtering algorithms," *J. Franklin Inst.*, vol. 356, no. 1, pp. 654–674, 2019, doi: 10.1016/j.jfranklin.2018.10.019.

[85] Z. Yuan and X. Songtao, "New LMS adaptive filtering algorithm with variable step size," *Proc. - 2017 Int. Conf. Vision, Image Signal Process. ICVISP 2017*, vol. 2017-Novem, pp. 1–4, 2017, doi: 10.1109/ICVISP.2017.11.

[86] B. Fan and X. Wang, "A Lyapunov-Based Nonlinear Power Control Algorithm for Grid-Connected VSCs," in IEEE Transactions on Industrial Electronics, vol. 69, no. 3, pp. 2916-2926, March 2022, doi: 10.1109/TIE.2021.3065614.

[87] A. A. S. Mohamed, H. Metwally, A. El-Sayed, and S. I. Selem, "Predictive neural network based adaptive controller for grid-connected PV systems supplying pulse-load," *Sol. Energy*, vol. 193, no. September, pp. 139–147, 2019, doi: 10.1016/j.solener.2019.09.018.

[88] Canbing Li, Chi Cao, Yijia Cao, Yonghong Kuang, Long Zeng, Baling Fang, "A review of islanding detection methods for microgrid", renewable and sustainable energy Review. Volume 35, Pages 211-220 35 (2014). https://doi.org/10.1016/j.rser.2014.04.026

[89] M. Mahdi and V. M. Istemihan Genc, "A real-time self-healing methodology using model- And measurement-based islanding algorithms*," IEEE Trans. Smart Grid*, vol.

10, no. 2, pp. 1195–1204, 2019, doi: 10.1109/TSG.2017.2760698.

[90] M. R. Alam, K. M. Muttaqi, and A. Bouzerdoum, "Characterization of Voltage Dips and Swells in a DG-Embedded Distribution Network during and Subsequent to Islanding Process and Grid Reconnection," *IEEE Trans. Ind. Appl*., vol. 54, no. 5, pp. 4028–4038, 2018, doi: 10.1109/TIA.2018.2833056.

[91] Z. Lin, Tao Xia; Yanzhu Ye; Ye Zhang, Lang Chen, Kevin Tomsovic, Terry Bilke, Fushuan Wen "Application of wide area measurement systems to islanding detection of bulk power systems," *IEEE Transactions on Power Systems*, vol. 28, no. 2, pp. 2006-2015, May 2013, doi: 10.1109/TPWRS.2013.2250531.

[92] R. Sun and V. A. Centeno, "Wide area system islanding contingency detecting and warning scheme," *IEEE Trans. Power Syst.*, vol. 29, no. 6, pp. 2581–2589, Nov. 2014.

[93] G. Bayrak, "A remote islanding detection and control strategy for photovoltaic-based distributed generation systems," *Energy Conversion and Management*, vol. 96, pp. 228–241, 2015. https://doi.org/10.1016/j.enconman.2015.03.004.

[94] G. Bayrak and E. Kabalci, "Implementation of a new remote islanding detection method for wind–solar hybrid power plants," *Renewable Sustain. Energy Rev*., vol. 58, pp. 1–15, 2016.

[95] N. Liu, C. Diduch, L. Chang, and J. Su, "A reference impedance-based passive islanding detection method for inverter-based distributed generation system," *IEEE Journal of Emerging and Selected Topics in Power Electronics,* vol. 3, no. 4, pp. 1205–1217, Dec. 2015, doi: 10.1109/JESTPE.2015.2457671.

[96] B. Guha, R. J. Haddad, and Y. Kalaani, "Voltage ripple-based passive islanding detection technique for grid-connected photovoltaic inverters," *IEEE Power and Energy Technology Systems Journal*, vol. 3, no. 4, pp. 143–154, Dec. 2016. doi: 10.1109/JPETS.2016.2586847.

[97] J. Merino, P. Mendoza-Araya, G. Venkataramanan, and M. Baysal, "Islanding detection in microgrids using harmonic signatures," *IEEE Transactions on Power Delivery,* vol. 30, no. 5, pp. 2102–2109, Oct. 2015. doi: 10.1109/TPWRD.2014.2383412.

[98] K. Colombage, J. Wang, C. Gould, and C. Liu, "PWM harmonic signature-based islanding detection for a single-phase inverter with PWM frequency hopping," *IEEE Transactions on Industry Applications*, vol. 53, no. 1, pp. 411–419, Jan. 2017. DOI: 10.1109/TIA.2016.2611671.

[99] D. Reigosa, F. Briz, C. Blanco, and J. M. Guerrero, "Passive islanding detection using inverter nonlinear effects," IEEE Transactions on Power Electronics, vol. 32, no. 11, pp.

8434–8445, Nov. 2017. doi: 10.1109/TPEL.2016.2646751.

[100] Y. M. Makwana and B. R. Bhalja, "Experimental performance of an islanding detection scheme based on modal components," *IEEE Transactions on Smart Grid*, vol. 10, no. 1, pp. 1025–1035, Jan. 2019. doi: 10.1109/TSG.2017.2757599

[101] R. Haider, Ch. Hwan Kim, T. Ghanbari, S. B. A. Bukhari, M. S. Zaman, Sh. Baloch, and Y. Sik Oh, "Passive islanding detection scheme based on autocorrelation function of modal current envelope for photovoltaic units," *IET Generation, Transmission & Distribution*, vol. 12, no. 16, pp. 3911–3911, Sep. 2018.

[102] M. Bakhshi, R. Noroozian, and G. B. Gharehpetian, "Novel islanding detection method for multiple DGs based on forced Helmholtz oscillator," *IEEE Trans. on Smart Grid*, vol. 9, no. 6, pp. 6448–6460, Nov. 2018.

[103] H. Pourbabak and A. Kazemi, "A new technique for islanding detection using voltage phase angle of inverter-based DGS," *International Journal of Electrical Power and Energy Systems,* vol. 57, pp. 198–205, 2014. https://doi.org/10.1016/j.ijepes.2013.12.008.

[104] Q. Sun, J. M. Guerrero, T. Jing, J. C. Vasquez, and R. Yang, "An islanding detection method by using frequency positive feedback based on FLL for single-phase microgrid," *IEEE Trans. on Smart Grid*, vol. 8, no. 4, pp. 1821–1830, Jul. 2017.

[105] S. Liu, S. Zhuang, Q. Xu, and J. Xiao, "Improved voltage shift islanding detection method for multi-inverter grid-connected photovoltaic systems," *IET Generation, Transmiss. Distrib.*, vol. 10, no. 13, pp. 3163–3169, Oct. 2016.

[106] J. Laghari, H. Mokhlis, A. Bakar, and M. Karimi, "A new islanding detection technique for multiple mini hydros based on rate of change of reactive power and load connecting strategy," Energy Conversion and Management, vol. 76, pp. 215–224, 2013.

[107] J. Laghari, H. Mokhlis, M. Karimi, A. Bakar, and H. Mohamad, "An islanding detection strategy for distribution network connected with hybrid DG resources," *Renewable Sustain. Energy Rev*., vol. 45, pp. 662–676, 2015.

[108] S. Sumathi, L. Ashok Kumar, and P. Surekha, "Solar PV and Wind Energy Conversion Systems: Introduction to Theory, Modeling with MATLAB/SIMULINK, and the Role of Soft Computing Techniques," *Green Energy and Technology*, 2015, http://link.springer.com/10.1007/978-3-319-14941-7, ISBN 978-3-319-14941-7 (eBook), ISSN:0885-8993, doi: 10.1007/978-3-319-14941-7.

[109] S. Kolsi, H. Samet, M. Ben Amar, "Design Analysis of DC-DC Converters Connected to a Photovoltaic Generator and Controlled by MPPT for Optimal Energy Transfer

throughout a Clear Day," *Journal of Power and Energy Engineering*, 2, 27-34. doi: 10.4236/jpee.2014.21004.

[110] B. Singh, S. Dwivedi, I. Hussain, and A. K. Verma, "Grid integration of solar PV power generating system using QPLL based control algorithm," *Proc. 6th IEEE Power India Int. Conf. PIICON 2014*, no. 1, pp. 0–5, 2014, doi: 10.1109/34084POWERI.2014.7117785.

[111] S. Chatterjee and S. Chatterjee, "Simulation of synchronous reference frame PLL based grid connected inverter for photovoltaic application,"*2015 1st Conference on Power, Dielectric and Energy Management at NERIST (ICPDEN)*, Itanagar, India, 2015, pp. 1-6, doi: 10.1109/ICPDEN.2015.7084493.

[112] M. F. Schonardie and D. C. Martins, "Application of the dq0 transformation in the three-phase grid-connected PV systems with active and reactive power control,"*2008 IEEE International Conference on Sustainable Energy Technologies*, Singapore, 2008, pp. 18-23, doi: 10.1109/ICSET.2008.4746965.

[113] N. Gupta, R. Garg and P. Kumar, "Characterization study of PV module connected to microgrid,"*2015 Annual IEEE India Conference (INDICON)*, New Delhi, India, 2015, pp. 1-6, doi: 10.1109/INDICON.2015.7443360.

[114] X.-Q. Guo, W.-Y. Wu, and H.-R. Gu, "Phase locked loop and synchronization methods for grid-interfaced converters: a review," Przegląd Elektrotechniczny (Electrical review), vol. 4, pp.184-187, 2011.

[115] S. K. Khadem, M. Basu, and M. F. Conlon, "Power Quality in Grid connected Renewable Energy Systems: Role of Custom Power Devices", *Proc. for the International Conference on Renewable Energies and Power Quality* (ICREPQ'10), 23 - 35 March, 2010, Granada, Spain.

[116] Z. Li, D. Li, X. Xu, and J. Zhang, "New normalized LMS adaptive filter with a variable regularization factor," *J. Syst. Eng. Electron.*, vol. 30, no. 2, pp. 259–269, 2019, doi: 10.21629/JSEE.2019.02.05.

[117] A. Chaturvedi, K. Raj, and A. Kumar, "A comparative analysis of LMS and NLMS algorithms for adaptive filtration of compressed ECG signal," *ICPCES 2012 - 2012 2nd Int. Conf. Power, Control Embed. Syst.*, pp. 1–6, 2012, doi: 10.1109/ICPCES.2012.6508051.

[118] Z. Yuan and X. Songtao, "New LMS adaptive filtering algorithm with variable step size," P*roc. - 2017 Int. Conf. Vision, Image Signal Process. (ICVISP* 2017), vol. 2017-

Novem, pp. 1–4, 2017, doi: 10.1109/ICVISP.2017.11.

[119] N. Femia, G. Petrone, G. Spagnuolo, and M. Vitelli, "A technique for improving P&O MPPT performances of double-stage grid-connected photovoltaic systems," *IEEE Transactions on Industrial Electronics*, vol. 56, no. 11, pp. 4473–4482, 2009, doi: 10.1109/TIE.2009.2029589.

[120] H. C. Huang and J. Lee, "A new variable step-size NLMS algorithm and its performance analysis," *IEEE Trans. Signal Process*., vol. 60, no. 4, pp. 2055–2060, 2012, doi: 10.1109/TSP.2011.2181505.

[121] Datasheet of Semikron converter stack, SKM150GB12V, SEMIKRON Electronics Private Limited, Navi Mumbai, India.

[122] B. Singh, D. T. Shahani and A. K. Verma, "Power balance theory-based control of grid interfaced solar photovoltaic power generating system with improved power quality," *2012 IEEE International Conference on Power Electronics, Drives and Energy Systems (PEDES)*, Bengaluru, India, 2012, pp. 1-7, doi: 10.1109/PEDES.2012.6484359.

[123] P.G Barbosa, L.G Rolim, E.H Watanabe and R. Hamish, "Control Strategy for grid connected DC-AC Converter with load power factor correction", *Proceedings - Generation, Transmission and Distribution*. vol.145, no.5, Sept. 1998, pp. 487 – 492 DOI: 10.1049/ip-gtd:19982174.

[124] Datasheet and application note of voltage sensor, LEM LV 25-P. (http://www.lem.com/docs/products/lv%2025-p.pdf).

[125] G. Song, B. Cao and L. Chang, "A Passive Islanding Detection Method for Distribution Power Systems with Multiple Inverters," *IEEE Journal of Emerging and Selected Topics in Power Electronics*, vol. 10, no. 5, pp. 5727-5737, Oct. 2022, doi: 10.1109/JESTPE.2022.3165631.

[126] IEEE standard conformance test procedures for equipment interconnecting distributed resources with electric power systems, IEEE Std. 1547.1–2005, 2005, pp. 1–62.

[127] IEEE recommended practice for utility interface of PV system, IEEE standard 929-2000, 2000.

[128] M. Kim, R. Haider, G. Cho, C. Kim, and C. Won, "Comprehensive Review of Islanding Detection Methods for Distributed Generation Systems," Energies 12(5):837,pp:1-21, doi: 10.3390/en12050837.

[129] W. Xu, G. Zhang, C. Li, W. Wang, G. Wang and J. Kliber, "A Power Line Signaling Based Technique for Anti-Islanding Protection of Distributed Generators—Part I: Scheme and Analysis," *IEEE Transactions on Power Delivery*, vol. 22, no. 3, pp. 1758-1766, July 2007, doi: 10.1109/TPWRD.2007.899618.

[130] W. Bower, M. ROPP, "Evaluation Of Islanding Detection Methods For Photovoltaic Utility-Interactive Power System," *Int. Energy Agency Implement. Agreem. Photovolt. Power Syst.*, pp.1- 59, 2002, https://iea-pvps.org/wp-content/uploads/2020/01/rep5_09.pdf.

[131] A. Etxegarai, P. Eguía, and I. Zamora, "Analysis of remote islanding detection methods for distributed resources," *Renewable Energies and Power Quality*, vol. 1, no. 9, pp. 1142–1147, 2011, doi: 10.24084/repqj09.580.

[132] R. A. Walling, "Application of direct transfer trip for prevention of DG islanding," *2011 IEEE Power and Energy Society General Meeting*, Detroit, MI, USA, 2011, pp. 1-3, doi: 10.1109/PES.2011.6039727.

[133] S.I. Jang, K.H. Kim, "An islanding detection method for distributed generations using voltage unbalance and total harmonic distortion of current," *IEEE Transactions on Power Delivery*, vol. 19, no. 2, pp. 745-752, April 2004, doi: 10.1109/TPWRD.2003.822964.

[134] F. De Mango, M. Liserre, A. Dell' Aquila and A. Pigazo, "Overview of Anti-Islanding Algorithms for PV Systems. Part I: Passive Methods," *12th International Power Electronics and Motion Control Conference*, Portoroz, Slovenia, 2006, pp. 1878-1883, doi: 10.1109/EPEPEMC.2006.4778679.

[135] M. A. Redfern, O. Usta and G. Fielding, "Protection against loss of utility grid supply for a dispersed storage and generation unit," *IEEE Transactions on Power Delivery*, vol. 8, no. 3, pp. 948-954, July 1993, doi: 10.1109/61.252622.

[136] W. Freitas, Wilsun Xu, C. M. Affonso and Zhenyu Huang, "Comparative analysis between ROCOF and vector surge relays for distributed generation applications," *IEEE Transactions on Power Delivery*, vol. 20, no. 2, pp. 1315-1324, April 2005, doi: 10.1109/TPWRD.2004.834869.

[137] Fu-Sheng Pai and Shyh-Jier Huang, "A detection algorithm for islanding-prevention of dispersed consumer-owned storage and generating units," in IEEE Transactions on Energy Conversion, vol. 16, no. 4, pp. 346-351, Dec. 2001, doi: 10.1109/60.969474.

[138] F. Liu, Y. Kang, Y. Zhang, “Improved SMS islanding detection method for grid connected converters,” *IET Renewable Power Generation, vol.* 4,no.1,pp.36-42, February 2010, doi:10.1049/iet-rpg.2009.0019.

[139] B.K. Chaitanya, Anamika Yadav, Mohammad Pazoki, Almoataz Y. Abdelaziz, “Chapter 8 –A comprehensive review of islanding detection methods,” *Uncertainties in Modern Power Systems, Academic Press*, 2021, Pages: 211-256, ISBN:9780128204917. https://doi.org/10.1016/B978-0-12-820491-7.00008-6.

[140] M. E. Ropp, M. Begovic and A. Rohatgi, "Analysis and performance assessment of the active frequency drift method of islanding prevention," in IEEE Transactions on Energy Conversion, vol. 14, no. 3, pp. 810-816, Sept. 1999, doi: 10.1109/60.790956.

[141] L. A. C. Lopes and Huili Sun, “Performance assessment of active frequency drifting islanding detection methods,” *IEEE Transactions on Energy Conversion*, vol. 21, no. 1, pp. 171-180, March 2006, doi: 10.1109/TEC.2005.859981.

[142] F. De Mango, M. Liserre and A. Dell'Aquila, “Overview of Anti-Islanding Algorithms for PV Systems. Part II: Active Methods,” *12th International Power Electronics and Motion Control Conference*, Portoroz, Slovenia, 2006, pp. 1884-1889, doi: 10.1109/EPEPEMC.2006.4778680.

[143] M. Karimi, H. Mokhtari, M.R. Iravani, Wavelet based on-line disturbance detection for power quality applications, IEEE Trans. Power Deliv. 15 (4) (2000), pp. 1212-1220.

[144] P.K. Dash, B.K. Panigrahi, D.K. Sahoo, Power quality disturbance data compression, detection, and classification using integrated spline wavelet and S-transform, IEEE Trans. Power Deliv. 18 (2) (2003) 595-600.

[145] C. Zhao, M. He, X. Zhao, Analysis of transient waveform based on combined short time Fourier transform and wavelet transform, in: Int. Conf. Power System Technology Power Con. 2004, Singapore, Singapore, 2004, pp. 1122-1126.

[146] Y.H. Gu, M.H.J. Bollen, Timeefrequency and time-scale domain analysis of voltage disturbances, IEEE Trans. Power Deliv. 15 (4) (2000) 1279-1284.

[147] R. Polikar, The story of wavelets I, in: Physics and Modern Topics in Mechanical and Electrical Engineering, World Scientific and Engineering, Society, USA, 1999, pp. 192-197.

[148] A. Graps, An introduction to wavelets, IEEE Comput. Sci. Eng. 2 (2) (1995) 50-61.

[149] S. Murugesan and V. Murali, "Disturbance Injection Based Decentralized Identification of Accidental Islanding," in IEEE Transactions on Industrial Electronics, vol. 67, no. 5, pp. 3767-3775, May 2020, doi: 10.1109/TIE.2019.2917361.

[150] G. Hernandez-Gonzalez and R. Iravani, "Current injection for active islanding detection of electronically-interfaced distributed resources," IEEE Transactions on power delivery, vol. 21, no. 3, pp. 1698–1705,2006.

APPENDICES

APPENDIX-A

Parameters: Simulation of grid integrated SPV system		Attributes
Solar PV array	Power	10.25 kW
(SunPower SPR-205-BLK-U)	Array Short circuit voltage	478 V
	Array Open circuit current	27.65 A
	Array current at MPP	25.65 A
	Array voltage at MPP	400 V
Boost Converter	Duty Ratio	0.46
	Inductor	3.58 mH
	Capacitor	1000 μF
	Switching frequency	10 kHz
Inverter	DC link voltage (reference)	750 V
	DC link Capacitor	1000 μF
	Interfacing inductor	4 mH
	Line-to-line voltage	415 V
	Line-to-neutral voltage	239.6 V
Grid	Grid frequency	50 Hz
	Source impedances (Rs, Ls)	0.01 Ω, 0.1mH
	Line-to-line voltage	415 V
	Line-to-neutral	239.6 V
Load	linear load (balanced/unbalanced)	5 kVA, 0.8 pf lag.
	linear varying load	10 kVA, 0.8 pf lag.
	Non-Linear Load	Three phase bridge rectifier with RL load, R= 100Ω, L= 20mH

PI Gains	DC PI gain Kpd, Kid	Kpd = 0.2, Kid = 20
Matlab/Simulink model	Sampling time	5.5 μs

APPENDIX-B

Development of prototype hardware		**Attributes**
Three phase AC mains (grid)	Input voltage Auto-transformer	415 V
	Output voltage Auto-transformer	110 V
	Grid voltage (Line-to-line)	110 V
	Grid frequency	50 Hz
Inverter	DC link voltage	200 V
	DC link Capacitor (C_{dc})	1650 μF
	Interfacing Inductance	3 mH
Load	Linear Load	0-0.5 kVA, 0.9 p.f. lagging
	Non-Linear Load	Three phase bridge rectifier with RL load, R= 0-100Ω, L= 20mH
PI Gains	DC PI gain Kpd, Kid	0.5,0.1
Real -time hardware model	Sampling time	40 μs

LIST OF PUBLICATIONS

Journal Papers (SCIE)

1. A. Kumar, R. Garg, and P. Mahajan, "Modified Synchronous Reference Frame Control of Solar Photovoltaic-Based Microgrid for Power Quality Improvement," Arab. J. Sci. Eng., vol. no.46, pp. 1001–1018 (2021). https://doi.org/10.1007/s13369-020-04789-9. Indexing: Science Citation Index Expanded (SCIE), Impact Factor: 2.807.

2. A. kumar, R. Garg, and P. Mahajan, “Control of Grid Integrated Photovoltaic system using new Variable Step Size Least Mean Square adaptive filter,” Electrical Engineering, vol no. 103, pp.2945–2959 (2021). https://doi.org/10.1007/s00202-021-01273-x. Indexing: Science Citation Index Expanded (SCIE), Impact Factor: 1.630.
3. A. Kumar, R. Garg, and P. Mahajan, “Performance improvement of grid-integrated PV system using novel robust least mean logarithmic square control algorithm”, Electrical Engineering, vol. no.104, pp. 3207–3224 (2022). https://doi.org/10.1007/s00202-022-01552-1. Indexing: Science Citation Index Expanded (SCIE), Impact Factor: 1.630.
4. P. Verma, A. Kumar, R. Garg, and P. Mahajan, "Reweighted L0 norm variable step size continuous mixed p-norm control scheme for mitigating power quality problems of grid coupled solar PV system," CSEE Journal of Power and Energy Systems (2022), VOL. 9, NO. 4, pp.1-11. doi: 10.17775/CSEEJPES.2021.07310. Indexing: Science Citation Index Expanded (SCIE), Impact Factor: 7.1.

Proceedings Papers- International

5. A. Kumar, R. Garg, and P. Mahajan, “Harmonics Mitigation Techniques in Grid Integrated PV based Microgrid: A Comparative Analysis,” 2021 International Conference on Advances in Electrical, Computing, Communication and Sustainable Technologies (ICAECT), February, pp. 1–6, 2021. doi: 10.1109/icaect49130.2021.9392631.
6. A. Kumar, R. Garg, and P. Mahajan, “Performance Analysis of Grid Integrated PV System using SRF and IRPT Control,” 2019 1st Int. Conf. Signal Processing and VLSI Communication Engineering, (ICSPVCE-2019), 2019. doi: 10.1109/ICSPVCE46182.2019.9092869.
7. Avdhesh Kumar, “Performance Analysis of Perturb and Observe and Incremental Conductance Method of Maximum Power Point Tracking in Solar PV-Based Power Generation”, Renewable Power for Sustainable Growth. Lecture Notes in Electrical Engineering. Springer, Singapore. 2nd International Conference on Renewable Power (ICRP-2023), Haryana, India, Mar 28-29, 2023. https://doi.org/ 10.1007/978-981-99-6749-0-10.
8. Avdhesh Kumar, “Control and Performance Analysis for Active Islanding Detection Using q-Axis Control in Renewable Energy Sources Based Microgrid: A Review”, Renewable Power for Sustainable Growth. Lecture Notes in Electrical Engineering. Springer, Singapore. 2nd International Conference on Renewable Power (ICRP-2023), Haryana, India, Mar 28-29, 2023. https://doi.org/10.1007/978-981-99-6749-0-39.